Fabrication and Energetic Characterization of Al/Cu_2O Nano-Laminate Thermite

by

Victoria Ann Kerr

A thesis

presented to the University of Waterloo

in fulfilment of the

thesis requirements for the degree of

Master of Applied Science

in

Mechanical and Mechatronics Engineering

Waterloo, Ontario, Canada, 2020

Author's Declaration

I hereby declare that I am the sole author of this thesis. This is a true copy of the thesis, including any required final revisions, as accepted by my examiners.

I understand that my thesis may be made electronically available to the public.

Abstract

Thermites are a class of material which utilizes the oxidation/reduction reaction of the metal fuel and metal/non-metal oxide to produce heat. Thermite materials are used in a variety of applications including welding, metal refining, propulsion and, as technology has progressed, micro-applications including MEMs. Nano-laminate thermite materials have been developed to offer specialized controllability of ignition and reaction characteristics, and also provide significant improvements in reaction rates, sensitivity, and activation energy than traditional thermite.

This thesis provides an in-depth examination of the Al/Cu_2O nano-laminate thermite system using DSC bulk heating, laser-ignition, and microwave-ignition sources. This system has been largely overlooked due to its low heat of reaction, however this characteristic may be advantageous in certain micro-scale applications to avoid damage to sensitive components. It is critical to understand the range of energetic characteristics that can be achieved in this system by varying the structural properties.

The effects of the structural properties including number of layers, layer thickness ratio and substrate use on the ignition and reaction characteristics were studied. This examination provides insight into the reaction mechanism(s) present in the samples, filling a critical research gap. With the knowledge of how the structural characteristics can be tailored to achieve certain ignition and reaction characteristics, it is shown that the Al/Cu_2O nano-laminate thermite structure can be applicable in a wide range of applications with varying energetic requirements and ignition sources.

There is a major source of error in this work that must be assessed in order to ensure the accuracy of the results. Due to the removal procedure of the substrate-free flakes, it is critical that further investigation occur to ensure that there is no contamination of the samples from the applied photoresist coating. This assessment is expected to improve the reliability of the results presented in this thesis.

Acknowledgements

I would like to thank Professor John Z. Wen and Professor Carolyn Ren for their support and guidance throughout this process. Your dedication to the success of your students is truly inspiring. I appreciate the time and patience you have taken to expand my perceptions of what research should be.

I would also like to thank my readers, Professor Jean-Pierre Hickey and Professor Yimin Wu. I appreciate your insight and critical evaluation of my manuscript to help me improve.

I have had the opportunity of being surrounded by helpful and motivating colleagues in both the Laboratory of Emerging Energy Research (LEER) and the Waterloo Microfluidics Laboratory. I am grateful for the feedback and insight provided by all of the members of these laboratories. Thank you Lauren LeSergent, Yiqi Zhang, Florin Saceleanu, Anqi Yang, Weijia Cui, Matt Courtney and Pei Zhao for all of your valuable insight and advice. Thank you Shina Maini for spending hours with me calibrating the DSC machine, and being a source of joy, friendship and support in and out of the lab. I would also like to extend my thanks to Richard Barber and Czang-Ho Lee in the Giga-to-Nanoelectronics (G2N) Laboratory. Without your help, this thesis would not be possible.

Finally, I would like to thank my parents and sisters for being a source of unwavering love and support. Thank you to my boyfriend Devon, for celebrating with me on the good days and helping me through the bad. I would not have gotten this far without you all. Special thanks to my best friends Jackson, Ella and Flash.

Dedication

Dedicated to my family, given and chosen.

Table of Contents

List of Figures

List of Tables

Nomenclature

ALD – Atomic Layer Deposition

DSC – Differential Scanning Calorimetry

DFT – Density Functional Theory

DTA – Differential Thermal Analysis

EDX – Energy Dispersive X-ray Spectroscopy

EPD – Electrophoretic Deposition

EPT – Exothermic Peak Temperature

FIB – Focused Ion Beam

FTIR – Fourier-Transform Infrared Spectroscopy

HR-TEM – High Resolution Transmission Electron Microscopy

IOT – Ignition Onset Temperature

IR – Infrared

MEMs – Micro-electro-mechanical system

MICs – Metastable Intermetallic Composites

SEM – Scanning Electron Microscopy

TEM – Transmission Electron Microscopy

TGA – Thermogravimetric Analysis

TMD – Theoretical Maximum Density

XPS – X-ray Photoelectron Spectroscopy

XRD – X-ray Diffraction

1. Introduction

1.1 Motivation and Problem Statement

Thermites are energetic materials which produce heat through an exothermic oxidation-reduction reaction between a metal fuel and an oxidizer (metal or non-metal oxide). The most common metal fuel for use in thermite applications is aluminum, however other metals can also be used including magnesium, boron, silicon, zinc, and titanium [1]. Aluminum is most commonly used in combination with CuO, Fe_2O_3, and NiO, but other common oxidizers include MoO_3, WO_3, and Bi_2O_3 [2].

Due to their high heat release, thermites have many applications including low-oxygen welding [3-5], metal refining [6], propulsion [7, 8] and actuation [9-13]. As technology has developed, the applications of thermites have expanded to include initiators in micro-electro-mechanical systems (MEMs) [14,15], microjoining [16-18], and micropropulsion [19-23]. Due to the sensitive nature and small size of these applications, a need has arisen to develop the ability to tailor specific aspects of thermite reactions to suit these applications including ignition temperature, ignition delay, heat release, thermite stability, burn rate, flame temperature, flame velocity, and gas generation [24].

Nano-thermites are generally defined as thermites with at least one dimension that is at the nano-scale (less than 1 μm) in size, and show improved reaction characteristics over traditional thermites. Various fabrication methods and structural configurations create opportunities to develop nano-scale thermite materials with a

range of ignition and reaction characteristics which can be tailored for a variety of sensitive applications.

1.2 Research Objectives

The objectives of this thesis are to synthesize Al-Cu_2O nano-laminate thermite materials and investigate the structural factors contributing to their varying ignition and reaction characteristics. The most significant characteristics to be examined include ignition onset and exothermic peak temperatures, ignition speed and average heat release. The structural characteristics to be examined include number of layers, layer thicknesses, layer configuration, and the effect of substrates on ignition and reaction performance. Effects of varying ignition methods are also studied. Through the investigations performed in this study, conclusions will be drawn regarding how the structural characteristics of nano-laminate thermite can be tailored to suit specific applications.

1.3 Thesis Organization

This thesis will begin with a literature review in chapter two including background information on thermite and nano-thermite materials, as well as various fabrication methods and methods of material and reaction classification methods. Chapter three will include a summary of the fabrication and characterization methods used in this thesis to create and characterize Al/Cu_2O nano-laminate thermite. Chapter four will examine the experimental procedures and results of differential scanning calorimetry (DSC) and thermogravimetric analysis (TGA) to determine how the structural characteristics affect the ignition and reaction performance. Chapter five will investigate

the use of various ignition sources and their ability to successfully ignite nano-laminate thermite materials. Lastly, Chapter six will summarize the results and contributions of this thesis, as well as discuss recommendations for future work.

2. Literature Review

2.1 Introduction to Energetic Materials

Energetic materials can be broadly characterized into two main material types: monomolecular compounds and metal-based energetic materials. Monomolecular compounds include TNT (Trinitrotoluene), RDX (cyclotrimethylenetrinitramine), HMX (cyclotetramethylene tetranitramine), and CL-20 (Hexanitrohexaazaisowurtzitane) [25], which can perform exothermic reactions at high-speed reaction rates. In comparison to metal-based fuels, however, monomolecular compounds have relatively low energy densities. Metal-based fuels are therefore favoured for applications where a high energy density (by mass or by volume) is required. Figure 2.1 shows the differing energy densities of various metal-based and monomolecular energetic materials.

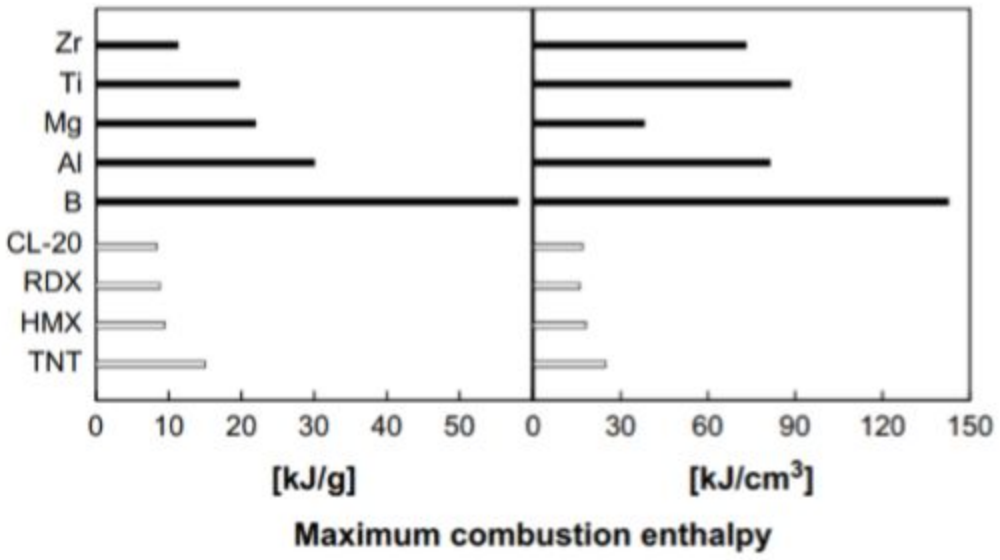

Figure 2.1 Reaction enthalpy of monomolecular energetic materials and metal fuels [25]

Metal fuels can consist of a variety of metals including Zr, Ti, Mg, Al, and B, and are commonly formed with powder morphologies which result in slower and more controllable reaction rates compared to monomolecular compounds. Within the last two decades, metal-based fuels have gained academic and industrial attention due to their attractive capacity of producing localized gas, heat, and power [26]. Figure 2.2 displays the literature available for “Nano-thermite” and “Nano-laminate, Application, AND Ignition” from 2005 - 2019. It is clear that there is a significant increase in interest in both nano-thermite and nano-laminate structures, including their applications and a growing interest in their ignition behaviour.

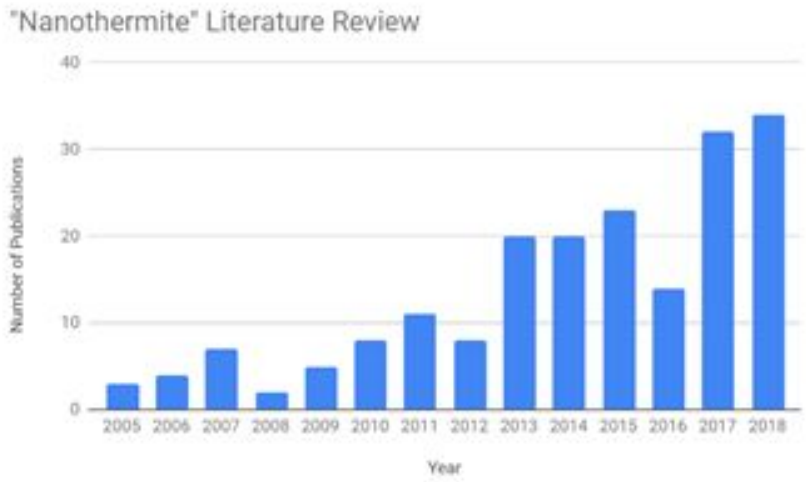

Figure 2.2 Literature review search terms ‘Nanothermite’ and ‘Nanothermite, Application and Ignition’ from 2005 to 2018

2.2 Thermite Composites and Applications

Goldschmidt first defined a thermite reaction in 1908 as the exothermic oxidation/reduction reaction between aluminum and a metal-oxide which rapidly produces a large amount of heat [27]. The definition was later expanded to include any metal (or alloy) and metallic- or non-metallic-oxides. In this type of reaction, the metal

fuel is oxidized due to the strong attraction between the oxygen and metal atoms. The typical thermite reaction is shown in Equation 2.1 below,

$$M + AO \rightarrow MO + A + \Delta H \qquad \textit{(Eq. 2.1)}$$

where M and AO are the metal (fuel) and oxidizer, respectively, MO and A refer to the newly produced oxidized and reduced product, respectively, and ΔH is the enthalpy of the reaction.

In order for the thermite reaction to initiate, two conditions must be met. The first condition is that a sufficient amount of energy must be transferred to and absorbed by the thermite from the energy source to overcome the initial activation energy barriers of the thermite. The second condition is that there must be sufficient mass transport of active components (oxygen) to the metal and oxide interface, through any protective layers. Because these two reaction characteristics are limiting, the thermite ignition and subsequent reaction can be discussed in terms of heat and mass transfer, and improvements to the ignition and reaction performance can be made by altering these characteristics.

The most beneficial aspect of thermite composite ignition is the high enthalpies of reaction and high energy density with respect to both mass and volume. Due to the significant amount of heat produced during these reactions, thermite reactions are typically of a self-sustaining nature, meaning that after the ignition source has terminated the reaction will continue until the thermite has fully reacted. Thermite

composites also produce a substantial amount of gas per gram of reactants. Table 2.1 outlines the unique thermochemical properties of various Al-oxide thermite systems.

Table 2.1 Thermochemical properties of various Al-oxide thermite systems [28]

Reactants		*Adiabatic Reaction Temperature*		*State of Products*		*Gas Production*		*Heat of Reaction*	
Constituents	TMD [g/cm^3]	W/O Phase Changes [K]	W/ Phase Changes [K]	State of Oxide	State of Metal	Moles of Gas per 100 g	g of Gas per g	-Q [cal/g]	-Q [cal/cm^3]
2 Al + Bi_2O_3	7.188	3995	3253	liquid-gas	liquid	0.4731	0.8941	506.1	3638
2 Al + 3 CuO	5.109	5718	2843	liquid	liquid	0.54	0.3413	974.1	4976
2 Al + 3 Cu_2O	5.28	4132	2843	liquid	liquid-gas	0.1221	0.0776	575.5	3039
2 Al + Fe_2O_3	4.175	4382	3135	liquid	liquid-gas	0.1404	0.0784	945.4	3947
4 Al + 3MnO_2	4.014	4829	2918	liquid	gas	0.8136	0.447	1159	4651
2 Al + 3 NiO	5.214	3968	3187	liquid	liquid-gas	0.0108	0.0063	822.3	4288
2 Al + WO_3	5.458	5544	3253	liquid-gas	liquid	0.1434	0.1463	696.4	3801

Thermite composites have many applications that utilize the previously discussed four distinct advantages of thermites over other energetic materials: high heat release, high energy density, high specific gas production, and the self-sustaining nature of thermite reactions. Specific thermite metal fuels and oxides are chosen for use in specific applications because of their favourable thermochemical properties. Examples

of these tailored material choices are outlined in the following sections: Applications in Welding, Applications in Metal Refining, Applications in Propulsion and Thrust, and Applications in Micro-electro-mechanical systems (MEMs).

2.2.1 Applications in Welding

One of the first major applications of thermite composites was welding, due to the high heat release during reaction. Welding using thermites can be achieved by initiating the thermite reaction and injecting the molten metal thermite reaction products to create a weld [29]. Thermites can uniquely be used for welding in low-oxygen or vacuum-type environments because the reaction does not require oxygen from the environment to sustain it. This expands the possibilities for welding applications using thermites to include underwater [3] and outer space applications [4]. Al/CuO and Al/Fe_2O_3 are commonly used thermite systems for welding applications due to their high heat release and liquid-based phases.

2.2.2 Applications in Metal Refining

Thermite composites can also be used for metal refining applications. During the thermite reaction the fuel is oxidized to produce a metal-oxide product and the oxide reactant is reduced to form the desired metal product. This process allows for the refinement of the metal product from the original oxide reactant. This method has been utilized by Bodsworth et al. to refine chromium (Cr) from an iron-chromium alloy [6]. To successfully refine Cr, sodium-chromate is first formed by heating the Fe-Cr core with sodium carbonate, which is then heated further and sulfur is added to form sodium sulfate and chromium oxide. A thermite reaction is then initiated to reduce the chromium

oxide to pure chromium. The largest disadvantage of this application of thermite materials is that it is often difficult to separate the metal and oxide products. When choosing a thermite material to use for metal refining applications, the metal-oxide material choice will clearly correspond with the desired metal product. Although this application is useful, it can be very costly. Additionally, it is important to achieve a complete, stoichiometric reaction in order to fully refine the desired product and avoid wasting thermite material.

2.2.3 Applications in Propulsion and Thrust

There are many thermite applications that capitalize on the high specific energy density and gas production of the reaction to produce propulsion and thrust. Specifically, in a study by Galfetti et al. Al micro- and nano-sized powders were used as the metal fuel with ammonium perchlorate (AP) as the oxidizer and hydroxyl-terminated polybutadiene (HTPB) as a binder in order to achieve steady burn rates in propellants [30]. The use of nano-Al particles increases the propellant density and the specific rocket impulse, which leads to improved performance over micro-sized particles.

Thermites have also been utilized for outer space and underwater propulsion, taking advantage of their unique ability to ignite and sustain their reaction with little to no oxygen in the environment. Due to the high heat release, the reactions are not greatly affected by the environment in which they are used. Apperson et al. investigated the use of CuO nano-rod and Al nanoparticle thermite for use as solid-propellant microthrusters in space [23], while Hacker et al. studied the use of thermites for high-speed propulsion of underwater vehicles [31]. There are many applications for

layered themites structures including a layered propellant with a tailored burn rate [44]. Thermite choice for applications in propulsions and thrust often depend on the high energy density and high gas production of the reaction (as this propels the object forward). The gas production of a thermite can be upwards of 0.89 grams of gas per gram of thermite for the Al/Bi_2O_3 system.

2.2.4 Applications in MEMs

Due to the small size of micro-electro-mechanical-systems (MEMs), an energy source of small stature, high energy density, and often high gas release are required for applications including micro-thrust and micro-actuation. Rossi et al. validated the applications of pyrotechnical thrusters in MEMs with a composite propellant of zirconium perchlorate potassium (ZPP) [19], while Choi et al. investigated the use of solid chemical propellant to function as a pressure source to control movement of fluids of disposable lab-on-a-chip, biochemical analysis or drug delivery systems [13]. In both of these cases, nano-thermite composites were utilized to achieve specific reaction characteristics required for these applications. The challenge of this particular application is that the rate of reaction for thermite materials are generally uncontrolled in terms of reaction rate. The amount of energy release, however, is controllable based on the chemical and structural characteristics selected.The sensitivity of many MEMs components and structures often require strict control over the thermite reaction to avoid damages. An example of this is demonstrated by Youngner et al. who developed a thruster array for the stationkeeping of small satellites which contained 250,000 thrusters within very close proximity to each other [20]. Very small, highly controlled

reactions were required to create impulses and correct the course of the satellite as it progressed along its course. These reactions must be highly controlled in order to effectively correct the course and avoid unintentional detonation of nearby thrusters. In this case, a thermite material with high reliability and low heat release may be advantageous.

2.2.5 Summary

The potential applications of thermite composites continues to expand as a better understanding of their ignition and reaction characteristics is achieved. As devices become smaller the need for precise control over these energy sources increases. Sections 2.2.1 - 2.2.4 outlined many potential applications for thermite materials, and highlighted the importance of tailoring the thermite composition and structure to appropriately suit the needs of the applications. Table 2.2 summarizes the most commonly used reactants for a variety of thermite applications.

Table 2.2 Commonly used reactants for specific thermite applications

Desired Attributes	*Applications*	*Commonly Used Reactants*
Heat Release	Micro Welding Micro Ignition and Rapid Initiation Materials Processing Micro Power Generation	Al/MnO_2 Al/CuO Al/Fe_2O_3
Gas Generation	Micro Actuation Propulsion and Thrust	Al/Bi_2O_3 Al/Fe_2O_3
Reaction Products	Metal Refining Material Synthesis	Product Dependent

2.3 Drawbacks of Traditional Thermite Composites

Traditional thermite composites are composed of microscale metal and oxide powders which have lower reaction rates and longer ignition delays compared to monomolecular compounds [32]. Because the reaction depends on the diffusion of oxygen through the material to the interface, the micro-sized particles with a longer diffusion distance will result in a slower reaction rate than required for many applications. In the case of aluminum fuels specifically, during the reaction as oxygen is transported from the metal-oxide to the Al microparticle the outer edge of Al becomes oxidized generating Al_2O_3. This process is known as passivation. This passivation shell of Al_2O_3 surrounds the Al microparticle and as the thermite reaction continues, the Al2O3 shell grows until the entire microparticle has been oxidized from Al to produce Al_2O_3. The reaction kinetics of the micropowders is slowed in part because this passivation shell increases the resistance for oxygen transport to the Al layer. Slower reaction rates will result in significant heat loss. An image showing the passivation of an aluminum microparticle is shown in Figure 2.3.

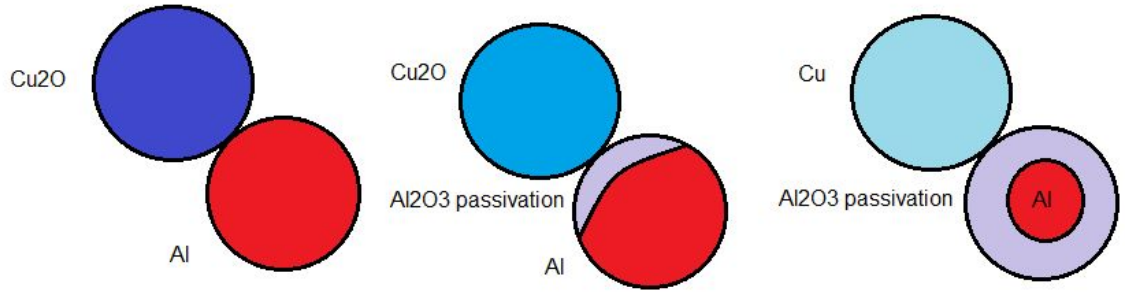

Figure 2.3 Passivation of an aluminum micro-particle due to the reduction of the metal-oxide

Micro-scale particles also have a much lower surface area to volume ratio compared to their nano-scale counterparts, further decreasing their ignition and reaction performance. Additionally, the micro-sized metal fuel particles are often not fully consumed during the reaction, lowering the energy density of the reaction. These factors can be detrimental in many applications. The limitations of microscale thermite composites are such that they are unable to meet the requirements of many microscale applications.

New structural compositions have been developed to combat the limitations of traditional microscale powder thermites. Research has concluded that the relationship between the size and thermal properties of thermites is such that smaller scale thermites with a higher surface area to volume ratio leads to lower activation energy and a higher reaction speed [33]. The reaction speed will further be increased due to the smaller heat and mass diffusion distances between particles. This research has led to the development of nano-scale thermite composites, defined by having at least one dimension less than 1 μm in length.

2.4 Nano-Thermite Composites

Nano-scale thermite composites continue to be developed to improve upon the performance of micro-scale thermite composites. Nano-thermite materials are commonly referred to as metastable intermolecular composites (MICs) due to their improved energetic performance which is similar to that of monomolecular energetic

materials. MICs have improved reaction rates and consequently less heat loss compared to their micro-scale counterparts.

2.5 Nano-Thermite Structures

Many novel structures have been developed in the field of MICs to suit various applications. Different structures have varying ignition and reaction characteristics due to the oxygen diffusion lengths and interfacial surface area between reactive components. Four common structures will be examined in the following sections: loose powders and pellets, monolithic bulk, core-shell particles, and thin films and multilayers.

2.5.1 Loose Powders and Pellets

Loose thermite powders consist of micro- or nano-particle components and are fabricated by physical mixing technologies [34-36]. There are two common configurations of loose powders. The first is physically mixed metal and oxide powders, as shown in Figure 2.4, which result in randomly positioned reactant particles.

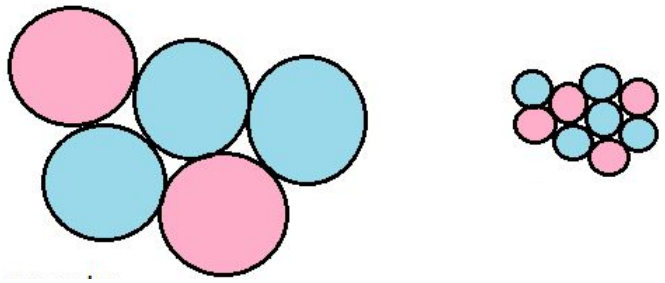

Figure 2.4 Physically mixed loose powders with micro-particles (left) and nano-particles (right) showing higher surface area to volume ratio in the nano-particles

Alternatively, loose powders can be layered with one component resting on top of the other, as shown in Figure 2.5.

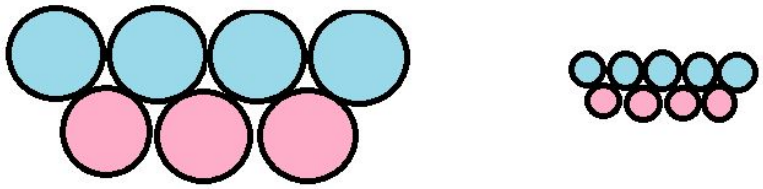

Figure 2.5 Layered loose powders with micro-particles (left) and nano-particles (right) showing improved structural control

The nano-powders in both configurations show clear advantages over micro-powders. Nano-powders create a higher surface area to volume ratio which facilitates faster reaction speeds with lower heat losses. There are, however, some disadvantages to the use of loose powders. One major disadvantage is the agglomeration of particles. Specifically, the increased specific surface area of nano-particles leads to higher surface energy which tends to result in the agglomeration of individual particles [37]. This makes it more difficult to achieve homogeneous mixing, the lack of which will result in less than optimal reaction characteristics.

Loose powders can also be utilized as pellets created using a pellet mold [38]. Pellets can be beneficial for applications which do not require mobile particles, or specifically require the thermite to be stationary. The effects of thermite density on ignition and reaction characteristics can be investigated by varying percentages of the theoretical maximum density (TMD) as studied by Sacleanu et. al [39].

2.5.2 Monolithic Bulk

Monolithic bulk composites have a porous metal-oxide structure created from solution. This structure is favourable due to its more intimate and homogeneous contact between components, which improves ignition and reaction performances due to smaller diffusion distances. The fabrication of monolithic bulk structures are most popularly Sol-Gel and Self Assembly. A variety of structures can be fabricated including monoclinic, tetragonal and helical [26] The drawback of this structure is the introduction of foreign particles into the composite during the fabrication process, which leads to a decrease in purity and therefore energy density [26].

2.5.3 Core-shell structures

Core-shell structures are characterized with a metal-oxide coating over the fuel particle or nano-wire. The metal core component can range from micro- to nano-scale and the thickness of the oxide layer can be varied to achieve a variety of ignition and reaction characteristics [41]. Core-shell structures have higher interfacial surface areas than both loose powders and monolithic bulk structures with improved energetic characteristics, however there are fabrication concerns including the controllability of shell layer thicknesses and the uniformity of the shell coating. The mobility of core-shell particles with improved energetic characteristics are especially beneficial in certain applications in MEMs and microfluidics.

2.5.4 Thin films and multilayers

Nano-thermite composites with layered structures have become an increasingly popular area of investigation within recent decades. The effects of various structural

characteristics can be investigated including layer thickness, number of layers and bilayers, the use of interlayers, substrate effects, and overall multi-layer design and composition. Thin films and multilayer structures can be mobile or immobile, depending on the presence or absence of a substrate. This flexibility makes them favourable for a variety of applications. Layered structures also provide improved structural controllability over all previously discussed structures, which is especially useful when tailoring properties based on specific structural characteristics.

2.5.5 Summary

Table 2.3 shows a summary of various structures for Al-based nanothermite including loose powders, monolithic bulk, core/shell and thin films/multilayers. The aspects of the structures that are summarized include interfacial area, mobility, structure controllability, and the ease of fabrication. In this thesis, a multilayered structure is utilized because of the very high structural controllability and high interfacial areas resulting in favourable ignition and reaction characteristics.

Table 2.3 Summary of Various Nano-Thermite Structures

Structure	*Interfacial Area*	*Mobility*	*Structure Controllability*	*Ease of Fabrication*
Loose Powder	Low	High	Very Low	Very High
Monolithic Bulk	Medium	Low	Low	High
Core/Shell	Very High	Very High	Medium	Low
Thin Films/ Multilayers	High	Flexible	Very High	Low

2.6 Fabrication Methods of Nano-Thermite Composites

The previous section discussed the various structures of nano-thermite composites. This section will expand upon the fabrication methods used to construct these structures including physical mixing, sol-gel, self-assembly, core/shell fabrication methods and thin film methods. The following aspects of each method will be examined: cost, scalability, impurities, safety, nanostructure controllability, and ease of MEMs integration.

2.6.1 Physical mixing

Physical mixing is a simple, low cost method of nano-thermite production with two common methods: sonication (to produce loose powders) and ball milling (to produce monolithic bulk structures). During sonication, fuel and oxidizer micro- or nano-particles are mixed in a solvent and then sonicated in an ultrasonic bath to increase mixing and decrease opportunity for particle agglomeration. After being sufficiently mixed, the particles precipitate to the bottom of the bath and the solvent is evaporated. For the fabrication of Al-based nano-thermite, organic solvents including ethanol and hexane are often used because of their poor reactivity with Al and low evaporation temperature [37]. The largest issue with sonication is that because the metal and oxide particles often have different sizes, they are sonicated at different velocities which decreases the homogeneity of the mixture. A benefit of sonication, in comparison to ball milling, is that sonication does not change the features or size of the particles. Ball milling, however, involves violent interactions between metal and oxide particles in a ball mill, resulting in an uneven decrease in the size of particles. Another

disadvantage is that it is possible for the impact of these particles in the ball mill to produce oxidation or ignition, which decreases the safety of this preparation method.

2.6.2 Sol Gel

The sol-gel process is used to fabricate monolithic bulk structures and produces nano-thermite composites with better interfacial contact between reactants compared to those produced through physical mixing. Sol-gel processing involves multiple steps, as shown in Figure 2.6.

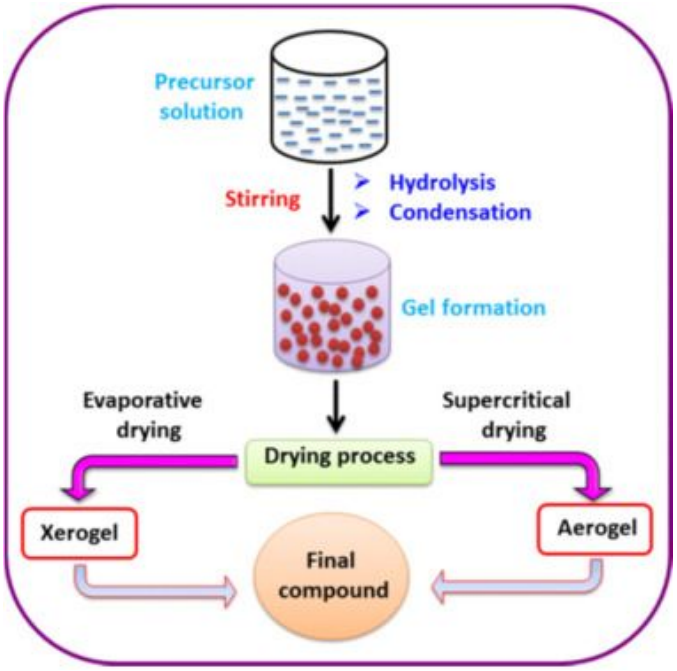

Figure 2.6 The reaction pathway for the production of metal oxide nanostructures in the Sol–Gel method [41]

To begin, the hydrated salts of metal are dissolved in ethanol to form the precursor solution known as sol. Propylene oxide is then added to condense the sol,

forming a porous, three dimensional gel structure. Fuel particles are added and mixed into the solution just before gel formation, which increases the interfacial area between components. The fluid in the pores is then removed by evaporation under various conditions to form xerogel (atmospheric drying) or aerogel (supercritical drying). Aerogel has a porous structure due to the application of CO_2 fluid for evaporation, whereas xerogel has a non-porous structure, as seen in Figure 2.7.

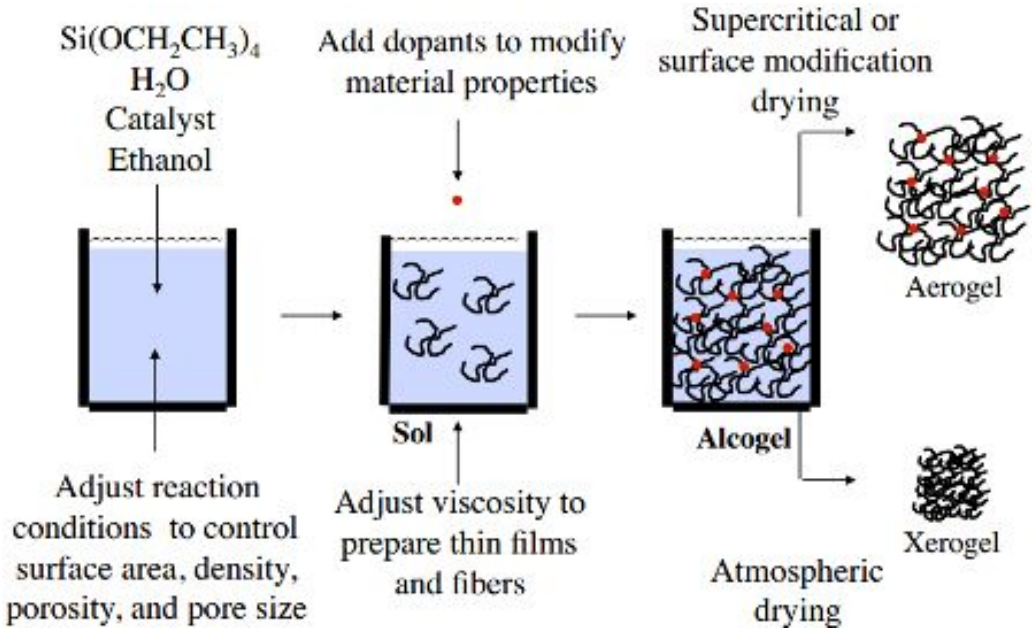

Figure 2.7 Sol, gel, aerogel and xerogel structures [42]

The main disadvantage of the sol gel fabrication method is the exposure of the nano-thermite to foreign materials such as ethanol and propylene oxide during processing. Impurities in the composite will result in a lower energy density. In fact, impurities may represent 10% of the total mass of samples [26]. Another disadvantage

is the high porosity, particularly in aerogel structures, which needlessly increases the diffusion distance between components, creating less than ideal ignition and reaction characteristics.

2.6.3 Self Assembly

Self-Assembly is another alternative for the fabrication of monolithic bulk structures. This method is rooted in the sol-gel method with differences in the functionalization step. The precursor material can be nano-oxidizer rods or hydrated metal salts (as in sol-gel), which are then functionalized by polymers. A critical point for this fabrication method is that modified oxidizers must be used to functionalize properly in order to form the appropriate structures. Without this functionalization step, the structure would not have the desired highly ordered structure. In the case of nano-oxidizer rods, after functionalization the Al nanoparticles surround the nano-rods and adhere to the oxidizer surface, creating direct contact and resulting in a large interfacial area. In the case of hydrated metal salts, polymers act as a gelling agent, similar to their use in sol-gel. Unique to self-assembly, the Al nanoparticles do not need to be added into the solution at a specific time. The functionalization step is unique to self-assembly and results in a more highly ordered structure than sol-gel [43]. The drawback of this method is the costly modified oxidizer, as well as potential contamination lowering the ignition and reaction properties.

2.6.4 Fabrication for Core-Shell Structures

Core-shell structures have many advantages as previously discussed in Section 2.5.2. The disadvantage of this structure, however, is the difficulty of fabrication. Zhang

et al. developed a 2-step innovative method of fabrication involving 1) hydrolysis and 2) thermal decomposition [40]. In order to produce Al/CuO thermite, as-purchased Al micro- or nano-particles are placed in an ethanol solution and stirred to ensure separation. A mixture of $Cu(NO_3)_2 \cdot 2.5H_2O$, aqueous ammonium hydroxide, and ethanol are added to the Al suspension and stirred. A shell consisting of $[Cu(NH_4)]^{2+}$ and OH- is formed on the Al particle through the electrostatic force. The core-shell particles are then collected by vacuum filtration and a sieve is used to break apart aggregated particles. The particles are then heated to 250 °Celsius in air, which oxidizes the shell and results in a CuO shell around the Al particles. Figure 2.8 shows the fabrication process.

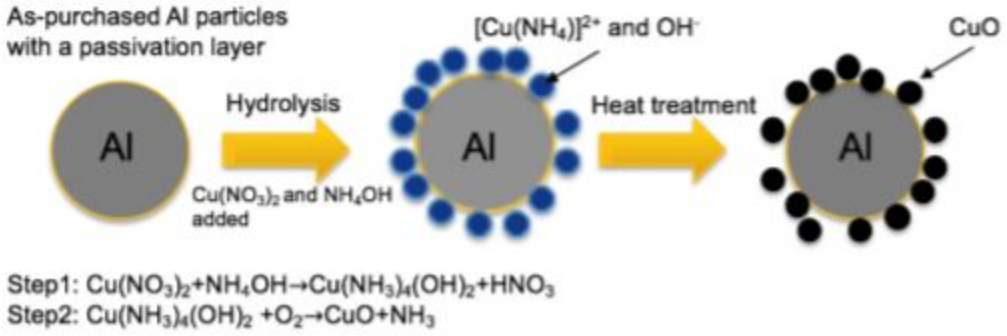

Figure 2.8 Two step fabrication of core-shell particles [40]

The largest disadvantage of this fabrication method is that it is very difficult to control how evenly the shell coating is distributed. Although a sieve is used, there is still the possibility of the agglomeration of particles which greatly affects the reaction

characteristics. Finally, this fabrication method can be difficult to learn and execute properly.

2.6.5 Fabrication for Layered Structures

Layered structures are gaining interest because of their ability to precisely control layer thicknesses and design. There are two main methods used for the formation of layered thermite structures, the first using colloidal particles including electrophoretic deposition (EPD) and vacuum filtration (VF), while the second method is vapour deposition (VD).

EPD involves colloidal particles (which are dispersed and suspended in a liquid medium) that migrate and are deposited onto an electrode under the influence of an electric field (electrophoresis) [68]. The surface charge of the particles provides a repulsive force that makes the solution stable and limits the precipitation of particles. Negatively charged particles will deposit on positive electrodes, whereas positively charged particles deposit on negative electrodes. There are many complex parameters that can be adjusted during EPD processing which can tailor the deposition for various applications. The drawbacks of EPD are that only specific oxidizers can be deposited on conductive electrodes during the process. Certain oxidizers also require a surfactant and additives to achieve deposition, which lowers the purity of the structure.

Vacuum filtration (VF) also utilizes the suspension of colloidal particles, however it does not require a stable solution (as in EPD) because the solution is evaporated to leave the particles deposited on the fuel surface [34]. Because of this, the purity is higher than in EPD as it does not require additives for stability purposes. VF also does

not involve the charging of particles, allowing the deposition of any oxide particles to be achieved. Both EPD and VF fabrication methods are inexpensive and easy to scale, however they are unable to create very thin layers (usually limited to micro-scale).

Vapour deposition has two main subcategories: physical vapour deposition (PVD) and chemical vapour deposition (CVD). The advantage of vapour deposition fabrication is that the deposition of nano-sized layers are possible with excellent precision. CVD involves the process of a solid-state material being deposited from a vapour by a chemical reaction occurring at or in the vicinity of a (normally) heated substrate surface [45]. The main disadvantage of CVD is that only certain compounds are able to be produced on certain substrates through this method. A subclass of CVD is Atomic Layer Deposition (ALD). The ALD process involves a gas phase material reacting with the substrate in order for the material to form a thin layer on top of the substrate. ALD produces highly controlled uniform layers with high purity. Nano-laminate structure and layer thicknesses can be controlled by the precursor type and the number of exposures of the precursor to the substrate. A large disadvantage of ALD is that there are often impurities created by the reaction. ALD has previously been reported to fabricate the thin films of metal-oxides including Co_3O_4 [46], WO_3 [47] and NiO [48]. There have been no reports of the successful deposition of Al nano-layers and therefore ALD is not a suitable solution for fabricating Al-based nano-thermite laminates at this time.

A more widely accepted method to fabricate Al-based nano-thermite laminate structures is PVD, which involves the deposition of material on the substrate without any

chemical reactions upon impact. Magnetron sputtering is a commonly used form of PVD because of its high purity, homogeneity, and efficiency. Sputtering utilizes a negatively charged target in a vacuum chamber, which is then bombarded with Ar+ ions, causing the ejection of partially ionized target particles which impact the substrate surface. A diagram of this process is shown in Figure 2.9.

Figure 2.9 Sputtering process [49]

The substrate is rotated throughout the process to improve the quality of the deposition. Layer thicknesses can be controlled with high sensitivity based on the material's deposition rate, and the fabrication of very thin layers with high uniformity are achievable. The disadvantages of the sputtering fabrication process is that it is expensive and the specific conditions it requires make it difficult to perform on a large scale. Finally, sputtering structures result in the sample being directly applied to a substrate. Post-processing of the sample is required to remove the layered sample from the substrate, if desired.

2.6.6 Summary

Table 2.4 summarizes the features of physical mixing, sol gel, self-assembly, core-shell, and layered structure fabrication methods. Although there is a high cost and low scalability, magnetron sputtering is clearly the ideal fabrication method for Al-based nano-laminate thermite structures. This method provides a structure with high purity and uniformity, while providing extreme control over layer thicknesses and chemical composition. Finally, sputtering provides excellent opportunity for integration into MEMS because of its ability to flexibly produce the laminate structure that can be used with or without a substrate in application.

Table 2.4 Comparison of Various Preparation Methods, modified from X. Zhou et al. [33]

Preparation Method	*Cost*	*Scalability*	*Impurities*	*Safety*	*Controllability of Nanostructures*	*Integration for MEMs*
Physical Mixing	Low	Easy	High	Medium Concern	Not Controllable	Difficult
Sol-Gel	Low	Easy	High	Precaution Needed	Somewhat Controllable	Difficult
Self Assembly	Low	Easy	High	Medium Concern	Good Controllability	Difficult
Core-Shell	High	Difficult	Low	Medium Concern	Good Controllability	Difficult
Deposition	High	Method-dependent	Very Low	Very Safe	Excellent Controllability	Easy

2.7 Ignition Methods

A topic of investigation in conjunction with nanothermite applications is the various ignition methods available. A variety of ignition methods have been commonly used including sparklers, magnesium ribbon, conductive heating , convective and radiative heating, as well as less-extensively studied methods including laser ignition of nano-thermite materials [39]. For the purpose of this thesis four main ignition methods will be discussed further: conductive heating, bulk thermal heating, laser ignition, and microwave ignition.

2.7.1 Conductive Heating Ignition

Conductive heating is a very common ignition method for thermites due to the ease of ignition and implementation in applications. Conductive heating ignition involves the use of a heating instrument in direct contact with the thermite. Due to the direct contact required, costly damage often occurs to the heating instrument from the thermite explosion [55]. Although conductive ignition is commonly used in thermite applications, it is difficult to integrate into nano-thermite applications because of the small size requirements. Many nano-applications require precise ignition areas which are difficult to achieve with conductive heating methods.

2.7.2 Bulk Thermal Ignition

Bulk thermal ignition includes convective and radiative heat transfer which will heat the entire sample at once, from a distance. This type of ignition is useful when studying the fundamental aspects of thermite ignition and reaction properties because it is easily controlled and can be modified as required, including adjusting heating rates

(K/min) to ensure accurate results. Bulk thermal heating ignition can be used as a general approach as it does not involve the complexities of other ignition methods. This method is not often used in applications of nano-thermites however, because the entire volume around the nano-thermite is heated which can result in costly damages to other aspects of the applications.

2.7.3 Laser Ignition

The laser ignition method has been seldom studied as an ignition method for nano-thermite [24] but is promising for applications which require a precise ignition area (ie. thermite arrays for propulsion and applications in MEMs). The ability to adjust laser power densities and spot sizes facilitates the delivery of specific amounts of energy to small areas. The main drawback of laser ignition is the complexity required to integrate the laser for use in applications as it requires precise positioning and tuning.

2.7.4 Microwave Ignition

Microwave energy has recently been considered as a possible ignition source for nanothermite applications in MEMs [3]. Unlike convective/radiative heat transfer ignition methods which involve the heating of the entire area, the microwave energy applied can be tuned to ignite only the nanothermite and prevent unwanted heating of surrounding components. Microwave ignition is also favourable over laser ignition because the microwave energy does not have to be focused precisely on one location, which facilitates an easier integration and use in MEMs applications.

2.8 Al/Cu_2O Nano-Thermite Composites

The Al/Cu_2O nano-thermite system was chosen for this thesis because of it's ignition and reaction properties which make it useful for application in MEMs, as well as the large research gap surrounding the study of the system's ignition and reaction properties. This system has been widely overshadowed in literature by the Al/CuO nano-thermite system. As previously shown in Table 2.1, the Al/Cu_2O system has a smaller heat of reaction than CuO/Al (575.5 cal/g compared to 974.1 cal/g), lower adiabatic reaction temperature (4132 K compared to 5718 K), and significantly lower gas production (0.0776 g gas/ g reactant compared to 0.34331 g gas/ g reactant). These characteristics can be explained by the basic reaction equations 2.2 and 2.3:

$$3CuO + 2Al \rightarrow 3Cu + Al_2O_3 + \Delta H \qquad \textit{(Eq. 2.2)}$$

$$3Cu_2O + 2Al \rightarrow 6Cu + Al_2O_3 + \Delta H \qquad \textit{(Eq. 2.3)}$$

In the Cu_2O/Al system, there is double the amount of Cu used in order to create the same amount of Al_2O_3, which accounts for the smaller heat of reaction per gram and lower gas production per gram. These properties are advantageous for many applications in MEMs where smaller and more controlled ignition and reaction characteristics are needed due to the sensitivity of the components in the system.

The Cu_2O/Al and CuO/Al thermite systems are closely related to each other as the reduction of Cu_2O to Cu + O is an intermediate step in the CuO/Al thermite reaction [50]. It is given by Baijot et al. [51] that the following equations 2.4 - 2.12 illustrate the

other possible reactions, decompositions and phase transformations that can occur throughout the Al/CuO and Al/Cu_2O thermite reactions:

$$Cu_2O(s) \leftrightarrow 2Cu(s) + ½\ O_2(g) \quad \text{(Eq. 2.4)}$$

$$2CuO(s) \leftrightarrow Cu_2O(s) + ½\ O_2(g) \quad \text{(Eq. 2.5)}$$

$$Cu_2O(l) \leftrightarrow 2Cu(l) + ½\ O_2(g) \quad \text{(Eq. 2.6)}$$

$$2Al(s) + 3/2\ O_2(g) \leftrightarrow Al_2O_3(s) \quad \text{(Eq. 2.7)}$$

$$Cu_2O(s) \rightarrow Cu_2O(l) \quad \text{(melting 1235°C)} \quad \text{(Eq. 2.8)}$$

$$CuO(s) \leftrightarrow CuO(l) \quad \text{(melting 1202°C)} \quad \text{(Eq. 2.9)}$$

$$Cu(s) \rightarrow Cu(l) \quad \text{(melting 1085°C)} \quad \text{(Eq. 2.10)}$$

$$Cu(l) \leftrightarrow 2Cu(g) \quad \text{(boiling 2562°C)} \quad \text{(Eq. 2.11)}$$

$$Al_2O_3(s) \rightarrow Al_2O_3(l) \quad \text{(melting 2072°C)} \quad \text{(Eq. 2.12)}$$

$$Al(s) \rightarrow Al(l) \quad \text{(melting 660°C)} \quad \text{(Eq. 2.13)}$$

$$Al(l) \leftrightarrow Al(g) \quad \text{(boiling 2470°C)} \quad \text{(Eq. 2.14)}$$

Equation 2.5 shows the reversible decomposition and oxidation of the CuO/Cu_2O solid materials. Equation 2.6 shows the reversible decomposition and oxidation of liquid Cu_2O into liquid Cu and gaseous oxygen. These two equations are critical in understanding the connection between CuO and Cu_2O nanothermite ignition and reaction characteristics. Equation 2.7 displays the critical Al oxidation reaction which is central to both Al/CuO and Al/Cu_2O nanothermite reactions. Because the Al oxidation can come from the decomposition of both CuO and Cu_2O, it is critical to understand

both processes. Furthermore, understanding of the Cu_2O/Al reaction is critical as it is an intermediate step of the CuO/Al reaction. Finally, the possible phase transformations of various constituents are shown in equations 2.8 - 2.14.

2.9 Classifying Thermite Reactions

It is critical to be able to classify the significant ignition and reaction characteristics of Al/Cu_2O nanothermite laminates in order to fully understand the system and how it can be tailored to suit certain applications. This section aims to outline the parameters and terminology used throughout this thesis to classify thermite reactions. The parameters to be discussed include ignition onset temperature, exothermic peak temperature, reaction speed, and specific exothermic energy release.

2.9.1 Ignition Onset Temperature

In this thesis, the ignition onset temperature is defined by the temperature that is required for the exothermic thermite reaction to begin. This is the temperature at which the energy of the system surpasses the activation energy barrier of the material. In differential scanning calorimetry (DSC) studies, the ignition onset temperature can be evaluated as the temperature at which the exothermic reaction peak begins and can be influenced by heating rates, structural characteristics and gases present in the environment. The understanding and precise control of this characteristic is critical for the process of tailoring the nanothermite laminates to certain applications. A lower onset temperature requires a smaller amount of energy input prior to ignition which can be beneficial, however for many applications it is also critical to have a high enough ignition onset temperature to improve stability and avoid the risk of unintentional ignition. With a

deeper understanding of how the structural characteristics affect the ignition onset temperature, connections can also be made in determining the reaction mechanism.

2.9.2 Exothermic Peak Temperature and Reaction Speed

The exothermic peak temperature is defined as the temperature at which the exothermic peak is maximum for a thermite reaction. It is at this temperature that the highest amount of energy is instantaneously released from the sample. The peak temperature can be compared to the onset temperature in order to determine the reaction speed, which can be defined as the time from ignition onset to the peak temperature. Reaction speed is a critical parameter for many applications including propulsion and propellants where a fast reaction speed is ideal [52]. Generally slower reaction speeds also result in heat loss and consequently lower energy density, as previously discussed.

2.9.3 Specific Energy Release

The specific energy release is an important parameter which indicates the total amount of energy released over the reaction period, normalized by the sample mass and presented in Joules per gram (J/g). In DSC studies the average energy release is evaluated as the integration of the exothermic reaction curve, and represents the energy potential per gram of material (energy density). The specific energy release is critical for applications such as joining, which requires a high energy release in order to reach the melting temperature of one of the materials in the joining area.

2.9.4 Reaction Mechanism

Lastly, the reaction mechanism is a critical aspect of the thermite reaction which requires a deep understanding to draw more accurate conclusions and create models from experimental data. Thermite reactions generally have one of two common reaction mechanisms: condensed phase or heterogeneous. A condensed phase mechanism involves the reaction between two solid components whereas the heterogeneous mechanism involves the decomposition of an oxide to release gaseous oxygen which reacts with the other solid component.

Determining the reaction mechanism of nanothermites can be difficult due to the highly energetic nature of the reaction which involves high heat production, pressure waves, and particle and vapour sprays, limiting the equipment that can be used to investigate these reactions. Previous studies [24], [37], [53], have shown that DSC/TGA can be utilized to investigate the reaction mechanisms of thermites. Unfortunately, the reaction mechanisms of nano-sized thermites are difficult to investigate because those of nanoscale often behave differently than their microscale counterparts. The melting and reaction temperatures often vary depending on particle or layer size, the ability to form alloys, and the formation of oxides. DSC/TGA can provide indirect information about a nanothermite's reaction mechanism by the exothermic and endothermic peaks and mass loss events, however there is a level of uncertainty due to possible errors in interpretation.

2.10 Current Research Gaps and Goals

There is a critical knowledge gap in the nano-thermite space regarding the understanding of Al/Cu_2O systems. Specifically, Al/CuO systems have been quite heavily studied [54-64] and have largely overshadowed Al/Cu_2O systems. As described in section 2.7, it has been proposed that the Al/Cu_2O reaction is an intermediate step in the Al/CuO reaction through the decomposition of CuO to Cu_2O. This intermediate step could have a significant effect on the reaction characteristics of the Al/CuO system. Therefore, it is important to develop a thorough understanding of the Al/Cu_2O reaction to define the Al/CuO reaction at a deeper level. Additionally, the Al/Cu_2O will have different properties than other aluminum/copper-oxide based thermites and should be classified in order to fill that gap [24].

3. Synthesis and Characterization of Al/Cu_2O Nanolaminate Thermites

This chapter will provide an overview of the synthesis method, substrate choice, and characterization methods used in this thesis. The sputtering deposition method is discussed including procedures and parameters used. The challenges of using a substrate is discussed, and the advantages of creating substrate-free films are provided. An overview of the procedures required to produce the substrate-free films is provided. Finally, the various characterization methods and equipment used are presented.

3.1 Sputter Deposition of Nanolaminate Thermites

For the reasons discussed in Section 2.6.5, a magnetron sputtering method was chosen to fabricate the nanolaminate thermite material. An AJA International ATC Orion 5 sputtering machine was used with the assistance of the Giga-to-Nanoelectronics (G2N) Center at the University of Waterloo. To begin the sputtering process, the substrate was prepared (as described in Appendix 1) and loaded into the machine chamber. The machine was then pumped down to a minimum vacuum pressure of 1mTorr. This vacuum ensured that the air was evacuated from the chamber and the sputtering plasma. The use of a Cu_2O target is an improvement on this method because the entire fabrication method can be completed under Ar gas flow, reducing the possibility of O_2 contamination of the Al layers. The flow rates and chamber pressures were carefully calibrated to ensure the correct chemical composition of components was achieved. XPS was used to verify the composition of the components.

The deposition rates of components were determined using a DekTak measurement system (detailed information included in Section 3.3.1). Separate Al and Cu_2O layers were sputtered for 10, 20, and 30 minutes, and the thicknesses were measured in order to determine the deposition rate in nm/second. Thickness measurements were averaged over multiple sections of the sample to ensure an accurate measurement was achieved. The deposition rate for Al was found to be 0.1 nm/second while the Cu_2O deposition rate was 0.12 nm/s. During sample fabrication layer thicknesses were achieved by varying the deposition time according to these rates. Detailed information regarding the sputtering process can be found in Appendix III.

3.2 Substrate Effects

An intrinsic challenge of the sputter deposition process is that the materials must be sputtered onto a substrate. The substrate material is a critical parameter that can affect the reaction characteristics of the sample. When choosing a substrate material, many parameters to be considered include thermal conductivity, reactivity, diffusivity, melting temperature, malleability and optical properties including transmission, reflection and absorption. In this thesis, glass and quartz substrates were tested to determine their effects.

In order to negate substrate effects, a pre-processing procedure was used to allow the removal of the nanolaminate material from the substrate after the sputtering process. The initial silicon substrate was spin-coated with Su8-2005 photoresist, which was then dried on a hot plate. The nanolaminate layers were then sputtered on top of

the photoresist layer. Following the sputtering process, the sample/photoresist/substrate was placed in an acetone bath, which allowed for the separation of the sample from both the dissolved photoresist and the substrate. This allowed for the collection of nanolaminate thermite material absent of substrate, also referred to as the substrate-free sample. A detailed procedure for the preparation and procedures required to fabricate the substrate-free samples are included in Appendix IV.

The use of photoresist introduces a potential source of error in the DSC/TGA measurements of the substrate-free samples. If the photoresist does not completely dissolve from the nano-laminate material following the acetone bath, contamination will occur. This contamination would greatly affect the DSC/TGA results because the decomposition of Su8 photoresist results in exothermic energy release, as well as significant mass changes [70].

3.3 Characterization Methods

A variety of methods were used to fully define the structural, chemical, and energetic characteristics of the nano-thermite laminates studied in this thesis. The following section will explain some common techniques including DekTak, SEM/EDS, XPS, XRD, DSC and TGA.

3.3.1 DekTak

DekTak is a 3D stylus profilometer with high resolution to provide detailed information on a sample's surface profile. In this thesis, DekTak was used to determine the deposition rate of AL and Cu_2O sputtering deposition, by measuring the thickness of a Cu_2O or Al layer that had been sputtered for a specific amount of time to determine a

deposition rate of nm/second, as mentioned in section 3.1. A Veeco Dektak 8 stylus profilometer from the G2N lab was used for these measurements. When gathering thickness data, multiple measurements were taken and the averaged value was used to account for slight non-uniformities in film thickness.

3.3.2 Scanning Electron Microscopy and Energy Dispersive X-Ray Spectroscopy (SEM/EDS)

Scanning Electron Microscopy (SEM) is an imaging tool used to investigate the surface morphology and elemental contrast of samples. Its excellent resolution provides the opportunity to investigate the nano-laminate thermite with great detail at a nano- or micro-scale. The principle of SEM is that a focused electron beam penetrates the sample and interacts with the atoms resulting in a secondary electrons (SE) and back-scattered electrons (BSE). Secondary electrons are emitted by the atoms excited by the incoming electron beam and are measured using the secondary electron detector. SEs reflect the surface morphology of the sample and because SEs originate from excited atoms, their energies are relatively low. In contrast, back-scattered electrons originate directly from the incoming beam and are a result of elastic scattering interactions with the atoms in the sample. BSEs have much higher energies than SEs. Because heavier (higher atomic number) atoms back-scatter significantly more than lighter atoms and result in brighter images, BSE detection provides excellent composition contrast between elements with widely varying atomic numbers. As shown in Figure 3.1, the SE detector is located at the side of the chamber whereas the BSE detector is located above the sample.

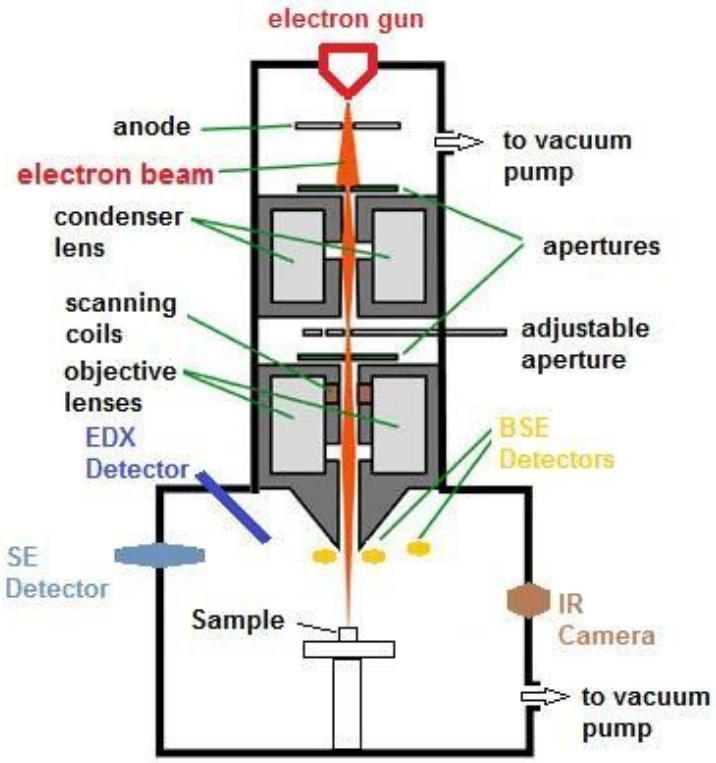

Figure 3.1 Diagram of a typical SEM equipped with EDS [65]

In this thesis, SE and BSE were used in tandem to examine the surface and cross-section morphologies and the elemental contrast of the nano-laminate layers. A Zeiss SEM with EDS from WatLab at the University of Waterloo was used for all characterizations of this type.

Energy Dispersive X-Ray Spectroscopy (EDS) is built into the SEM system and was used for elemental analysis. The EDS detector is located inside the chamber and detects X-rays that are released from excited atoms after the initial electron beam impacts the sample. Because each element has a unique atomic structure, the electromagnetic emission spectrum is unique and allows for elemental characterization

of the sample. A disadvantage of EDS is that it is incapable of determining the oxidation state of compounds in the sample, and the resolution is limited.

3.3.3 X-Ray Photoelectron Spectroscopy (XPS)

X-Ray Photoelectron Spectroscopy (XPS) is a characterization method used to determine the chemical content of the sample surface. In this thesis, XPS is specifically used to confirm the oxidation state of Cu_2O after sputtering. The XPS spectra is used to map the chemical state of the top few nano-meters of the sample being investigated, which provides a unique opportunity to investigate the surface chemical content. Figure 3.2 displays a diagram of a typical XPS setup.

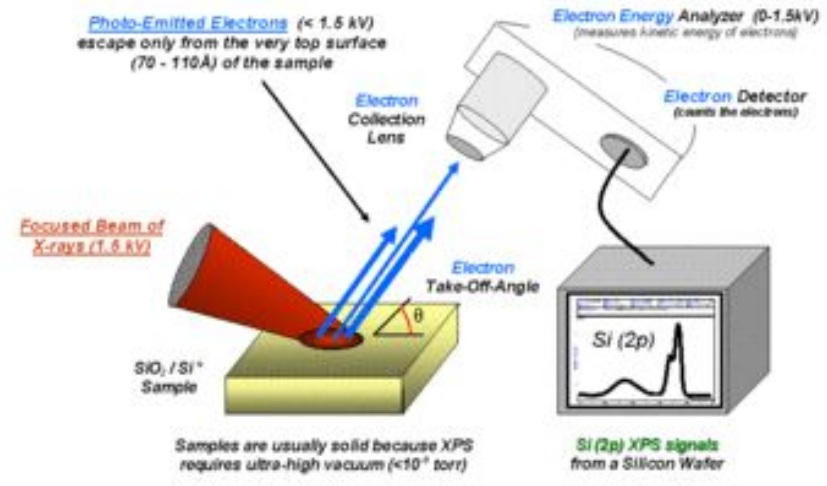

Figure 3.2 XPS Setup [66]

The principle of XPS is that the sample is irradiated with X-rays and a detector measures the kinetic energy and number of electrons ejected from the sample. XPS spectra is plotted as the count of electrons versus the binding energies, as calculated in Equation 3.1:

$$E_{binding} = E_{photon} - (E_{kinetic} + Theta) \qquad Eq.\ 3.1$$

Where $E_{binding}$ is the binding energy, E_{photon} is the energy of the incident X-ray photons being used, $E_{kinetic}$ is the measured kinetic energy of the ejected electrons, and Theta is the work function defined by both the sample material and the instrument being used.

In this thesis, a Thermo Scientific ESCALAB 250 XPS, with a built in Focused Ion Beam (FIB), was used for all analysis, provided by WatLab at the University of Waterloo. The FIB was used to sputter Ar ions on the sample to remove the surface layers and gently expose the bulk material. This enabled the investigation of both the surface and bulk material chemical composition.

3.3.4 X-Ray Diffraction (XRD)

X-Ray Diffraction (XRD) is a technique used to investigate the crystalline phases of samples using X-rays diffracted off of the crystal structure. Incident X-rays experience either constructive or destructive interference based off of Bragg's Law as shown in Equation 3.2:

$$n\lambda = 2dsin(\theta) \qquad Eq.\ 3.2$$

Where λ is the incident X-ray wavelength, d is the planar spacing and θ is the incident angle. Bragg's Law identifies the relationship between the incident X-ray and

the planar distance, which is used to identify specific crystal phases. Generally, the incident X-ray beam is swept along various incident angles and the detector observes the diffracted X-rays. When Bragg's Law is satisfied, constructive interference occurs and the detector receives highly strengthened X-rays, resulting in a peak that indicates that a specific crystal lattice is present. Because λ and θ are known properties of the incident beam, d can be determined, which corresponds to specific compounds. XRD provides detailed information regarding the crystalline structure that is not possible to determine from other methods such as XPS.

3.3.5 Differential Scanning Calorimetry and Thermogravimetric Analysis (DSC/TGA)

Differential Scanning Calorimetry (DSC) and Thermogravimetric Analysis (TGA) are valuable tools used to examine the heat flow and mass changes, respectively, of a sample during heating. The DSC/TGA device uses steady-state heating of a sample within a chamber at a specified heating rate. The sample is placed inside a small ceramic crucible on a stage next to an empty ceramic crucible which acts as the reference to the sample. The sample is heated through a temperature range where the reaction is expected to occur.

When a reaction occurs, generally there is an absorption or release of energy, which corresponds to an exothermic or endothermic peak recorded on the DSC device. The DSC records the heat that is released to or received from the environment, and compares this to the reference sample to provide quantitative information on the thermal characteristics of the sample. Specifically, information can be observed including the

ignition onset temperature, peak temperature, and specific energy released during a reaction. Knowledge of these characteristics are valuable for tailoring samples to suit desired applications.

TGA uses a highly sensitive scale to measure mass changes throughout the test when coupled with the DSC. Throughout a reaction, mass events can occur including the absorption of gas from the environment (such as oxidation), or gas release (such as the decomposition of an oxide). These mass changes can indicate which type of reaction is taking place. In this thesis, a NETZSCH STA 449 F3 Jupiter was used for data collection, in conjunction with the NETZSCH Proteus Thermal Analysis software (version 6.1.0), provided by the Laboratory for Emerging Energy Research (LEER) at the University of Waterloo.

Figure 3.3 DSC/TGA measurement and analysis system [26]

3.4 Summary

In this chapter, an overview of the synthesis and characterization methods for the nano-laminate thermite were discussed. The sputtering deposition fabrication method

was chosen due to its high controllability and low number of impurities. Detailed procedures and settings for the synthesis were given, including the use of Al and Cu_2O targets in an Ar plasma.

The positive and negative effects of substrates were discussed, as well as the advantages of substrate-free films. These free standing films negate the possible substrate effects on the ignition and reaction of the nano-laminate thermite. An overview of the techniques used to produce these substrate-free films were provided.

Finally, the various characterization methods used in this thesis were described. Thickness measurements were performed using DekTak, imaging methods included SEM, chemical characterization methods included XPS with EDS, while heat flow and mass changes were characterized by DSC and TGA. These methods were used in conjunction to fully characterize the ignition and reaction characteristics of the nano-laminate thermite.

4. Effects of Structural Characteristics on the Ignition and Reaction Characteristics of Heated Al/Cu2O Nano-Laminate Thermite

4.1 Motivation

As mentioned in Section 2.7, there are a variety of nano-thermite ignition methods available. Some of these methods, however, can affect the characteristics of the thermite ignition and reaction. In order to determine the base characteristics of the nano-laminate thermite material, it is critical to use a simple, controllable ignition method. In this thesis, a DSC was used to heat samples at a controlled rate (20 K/min) and record any exothermic or endothermic events as they occur. A built-in TGA was used in tandem to record any mass events throughout the ignition and reaction process. These two instruments allowed a full investigation into the thermal properties including ignition onset temperature, exothermic peak temperature, exothermic heat release, reaction speed, and any decomposition, melting, or vaporization events.

4.2 Experimental

Varying the structural characteristics of the nano-laminate thermite samples and performing DSC/TGA testing on each allowed conclusions to be made regarding how the structural characteristics affect the energetic properties of the nano-laminate thermite, as well as provided insight into the reaction mechanism(s). More specifically, the effects of varying the number of layers, layer thickness ratios, and the type of substrate used on the ignition and reaction characteristics will be examined.

Furthermore, evidence will be presented to support the determination of a reaction mechanism for the system. Developing a deeper understanding of how the structural characteristics affect the nano-thermite performance will be beneficial for applications, as previously discussed.

4.2.1 Fabrication Plan

The nano-thermite laminate structures for this chapter were fabricated using magnetron sputtering, as described in Chapter 3. In order to study the effects of the structural characteristics, the total thickness of each nanolaminate with a thickness ratio of 0.6:1.0 Al:Cu2O were kept constant at approximately 355 nm, while nanolaminates with thickness ratios 0.8:1.0 had Al layer thicknesses of 45 nm and Cu2O layer thicknesses of 54 nm (the total thickness was not constant). These ratios were chosen based off of previous work done on the subject [40]. The number of layers varied from two - ten for the 0.6:1.0 ratio case, while the 0.8:1.0 ratio case was only studied in the four, five, and six layer samples. In the case of samples with an odd number of layers, the total ratio of Al:Cu_2O was lower than the constant single bilayer ratio. The top layer was consistently Cu_2O with an Al layer underneath. This pattern repeated until the number of layers required were produced. A full fabrication plan is included in Appendix II.

4.2.2 Material Analysis

It was critical to confirm the structural and chemical composition of the fabricated samples in order to draw accurate conclusions from the results. The chemical

composition was confirmed using XPS while the structural composition was confirmed using SEM imaging.

4.2.2.1 Chemical Composition

It is imperative to know the chemical composition of the sample both on the surface and within the bulk material, to confirm that the sputtering settings resulted in the correct compounds being sputtered, and to identify if any oxidation from the environment had occurred. When exposed to air, Cu_2O will interact with the oxygen in the environment and oxidize to CuO which has higher stability. For this study, it was imperative that Cu_2O was present in both the surface and bulk material to reduce error in the measurements. To reduce the sample's exposure to air, the sample was kept in a vacuum environment from fabrication until testing.

A sample of 100 nm pure Cu_2O was sputtered on glass to test the chemical composition. The sample bulk measurement was taken at a depth of 5 nm below the surface and was achieved by sputtering Ar+ ions within a vacuum inside the XPS system. Ar+ ions are sputtered at a very slow rate in order to gently remove the surface layers and avoid disrupting the composition of the sample. The sample was sputtered for approximately 1 minute.

Figure 4.1 shows the XPS data for the sample surface and the sample bulk. When compared to the NIST XPS database, the XPS results show that both the surface layer and bulk material are consistent with Cu_2O, displaying the 2P1/2 peak at 952.3 eV, the 2P3/2 peak at 932.5 eV, and a very weak satellite peak occurring between the two dominant peaks. In contrast, CuO would display the 2P1/2 peak at 953.7 eV, the 2P3/2

peak at 933.4 eV and the 2P3/2 satellite peak at 943 eV. See Appendix III for a figure presenting the differences in the Cu_2O and CuO binding energy plots.

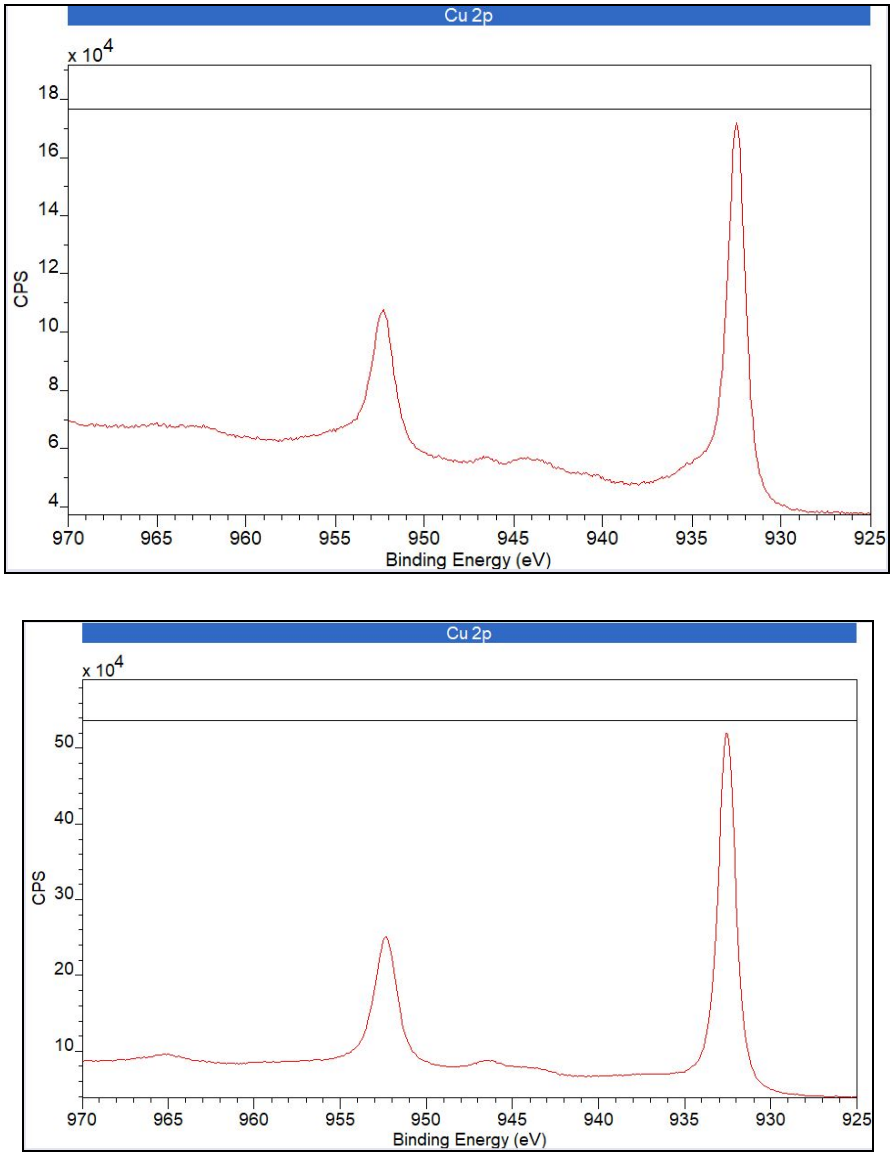

Figure 4.1 XPS results for (a) the sample surface and (b) the sample bulk of 100 nm thick pure Cu_2O on glass substrate

Although there is adequate material characterization in the form of XPS measurements confirming the presence of Cu_2O, there is insufficient characterization of the nano-laminate material for the substrate-free layers after removal from the substrate. Material characterization after nano-laminate separation is critical in order to ensure that the substrate-free flakes do not have any contamination from the acetone or Su-8 photoresist used in processing. In this study, the presence of undissolved photoresist is likely, which could affect the DSC/TGA and laser ignition study results, along with the data interpolation. The requirements for further characterization testing to determine the presence of photoresist post-processing is further explained in Section 6.3.

4.2.2.2 Structural Analysis

SEM images were taken to verify the structure of the samples. Because of the higher atomic weight, Al appears darker and Cu_2O appears lighter in these images. Figure 4.1 displays the four-layer sample on a glass substrate, showing four distinct uniform layers. Unfortunately due to the small thicknesses and the limitations of the SEM system, it was not possible to achieve accurate thickness measurements using SEM.

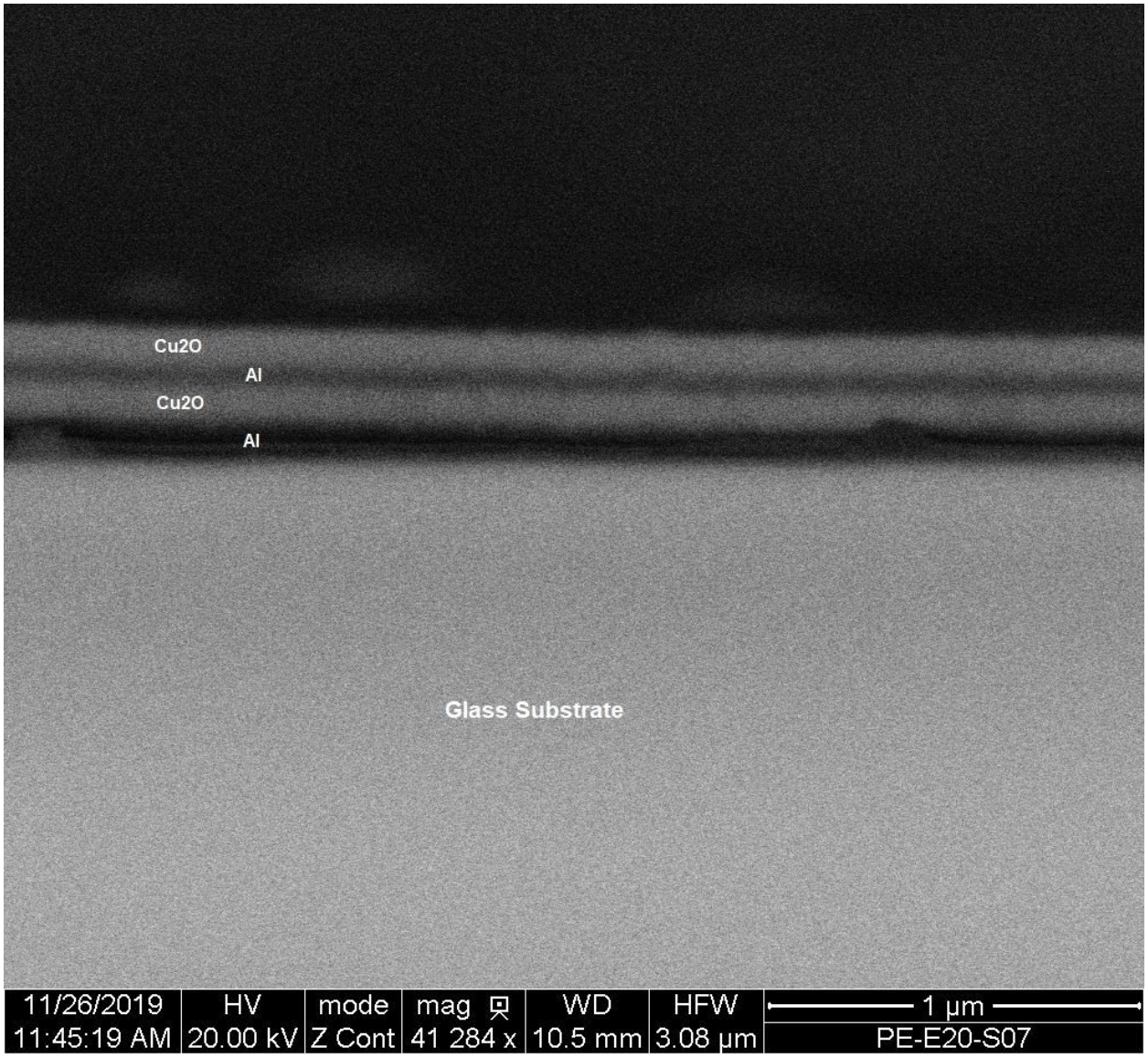

Figure 4.2 SEM of four-layer sample on glass substrate

(Cu_2O thickness of 110 nm, Al thickness of 65 nm)

More imaging challenges were faced when working with the substrate-free samples. When removed from the substrate to create the substrate-free films discussed in this chapter, the free standing films naturally curled up at the edges. Figure 4.3 shows a nanolaminate sample in an acetone bath separating and curling at the edges from the

photoresist and substrate. As previously mentioned, the photoresist may not be fully dissolved in the acetone bath, subsequently affecting the results of this thesis.

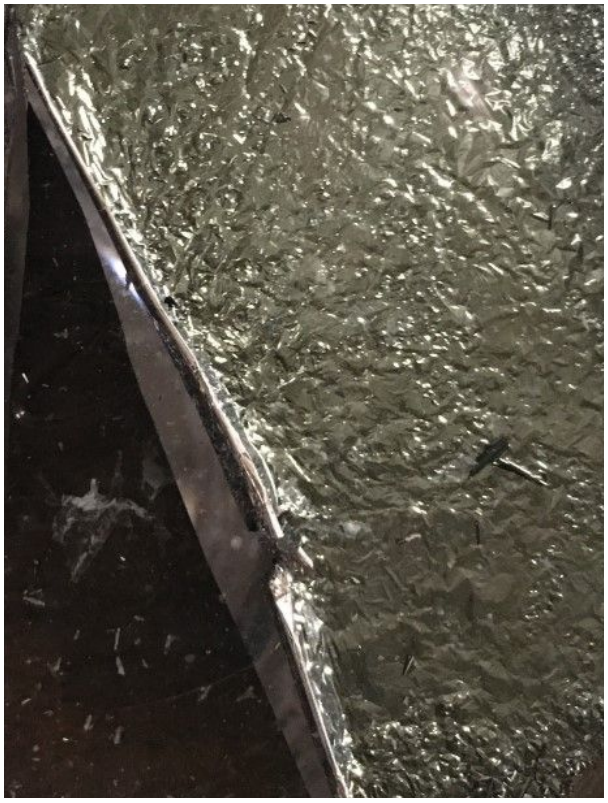

Figure 4.3 Nanolaminate sample separating from photoresist and substrate

Because of the curling nature of the edges of the free-standing flakes, it is very difficult to achieve SEM photos with clearly defined layers (such as those seen in Figure 4.2). Figure 4.4 shows an SEM image of multiple four-layer samples with visible material layering displayed.

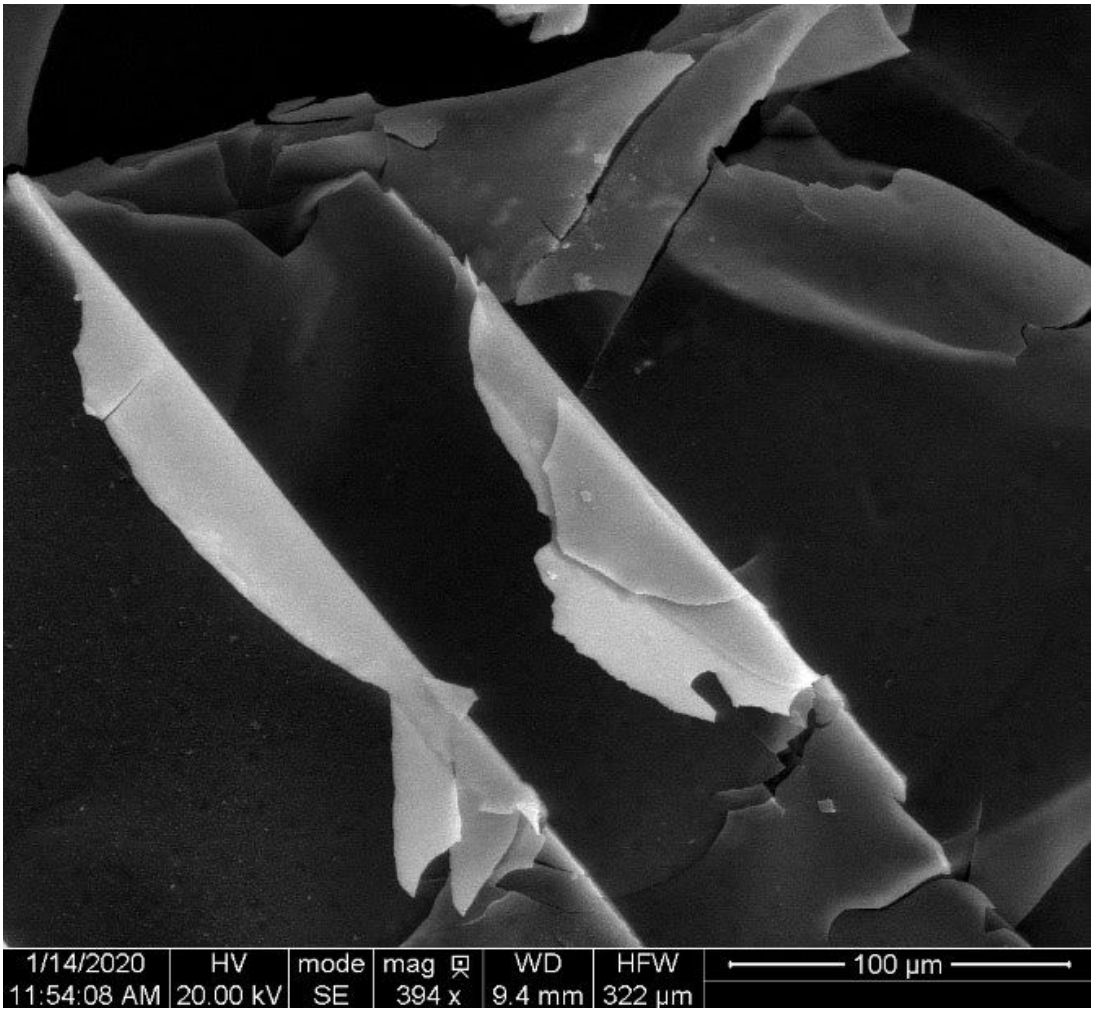

Figure 4.4 SEM image of substrate-free four-layer sample (4a)

4.3 DSC/TGA Machine Calibration

In order to ensure accurate results, the DSC/TGA apparatus was calibrated for both temperature and sensitivity at the specified heating rate (20K/min). Pure materials (In, Sn, Bi, Zn, Al, and Au) were run through three heating and cooling cycles, from approximately 100 degrees above to 100 degrees below their melting temperatures. This allowed the DSC to measure the endothermic melting peak, at a temperature

which was then compared to the known melting temperature. The differences between the theoretical and experimental melting temperatures for all pure materials were then used to calibrate the temperature and sensitivity settings to compensate for any system biases. A thorough explanation of calibration procedures is included in Appendix III.

4.4 Results and Discussion

To examine the effects of the number of layers on the thermite ignition and reaction characteristics, samples were tested with the number of layers varying from two to ten. Samples with Al:Cu_2O bilayer thickness ratios of (a) 0.6:1.0 and (b) 0.8:1.0 were studied in four, five, and six layer structures to determine correlations between layer thickness ratio and ignition and reaction characteristics, hereby referenced as stoichiometric and fuel-rich compositions, respectively. Finally, the effects of a substrate were studied. A full list of samples prepared was presented in section 4.2.1.

Due to the nature of the DSC/TGA instrument, the nano-laminate samples were placed into a small (approximately 5 mm diameter) ceramic crucible, as explained in section 3.3.5. In order for the DSC/TGA to measure the events effectively, a minimum mass of 5.0 mg was required [40]. Due to the very small nature of the flakes, many flakes were required to be placed on top of eachother inside the crucible to meet this mass requirement. In order to preserve the structure of the flakes, they were placed gently and care was taken to not crush them during this process. Figure 4.5 below shows the crucible with flakes before and after reaction. The nano-laminate flakes clearly show a drastic change in both colour and texture before and after the DSC test.

The sample following heating is dull and extremely brittle. The sample is no longer distinct flakes, it becomes a single mass.

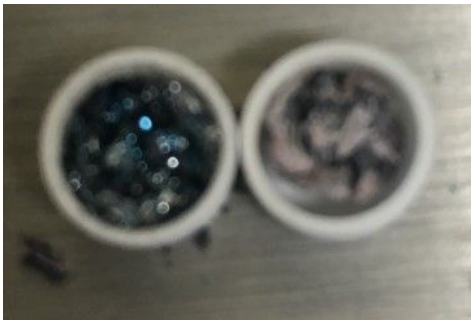

Figure 4.5 Nano-laminate flakes in crucible before (left) and after (right) reaction

The DSC results show that the Al/Cu_2O nanolaminate thermite reactions consist of three significant events. The first event involves the heterogeneous oxidation/reduction reaction previously discussed in section 2.2.8. As the sample is heated from room temperature, the oxide decomposes and releases oxygen which diffuses to the interface where it reacts with Al to produce alumina and heat. A portion of the oxygen is also released into the environment, resulting in significant mass loss recorded by the TGA. This reaction occurs between 250 - 450 °C, depending on the structural characteristics of the thermite.The second thermal event occurs between 550 - 700 °C and involves the melting of aluminum at approximately 660 °C. This melting may cause further exothermic reactions between active components. Finally, the third event occurs during the melting of copper at approximately 1085 °C. Depending on the structural characteristics, there will be an exothermic, endothermic, mixed, or negligible reaction occurring during each of these three events. Figure 4.6 shows the three well-defined thermal events for a 4-layer sample.

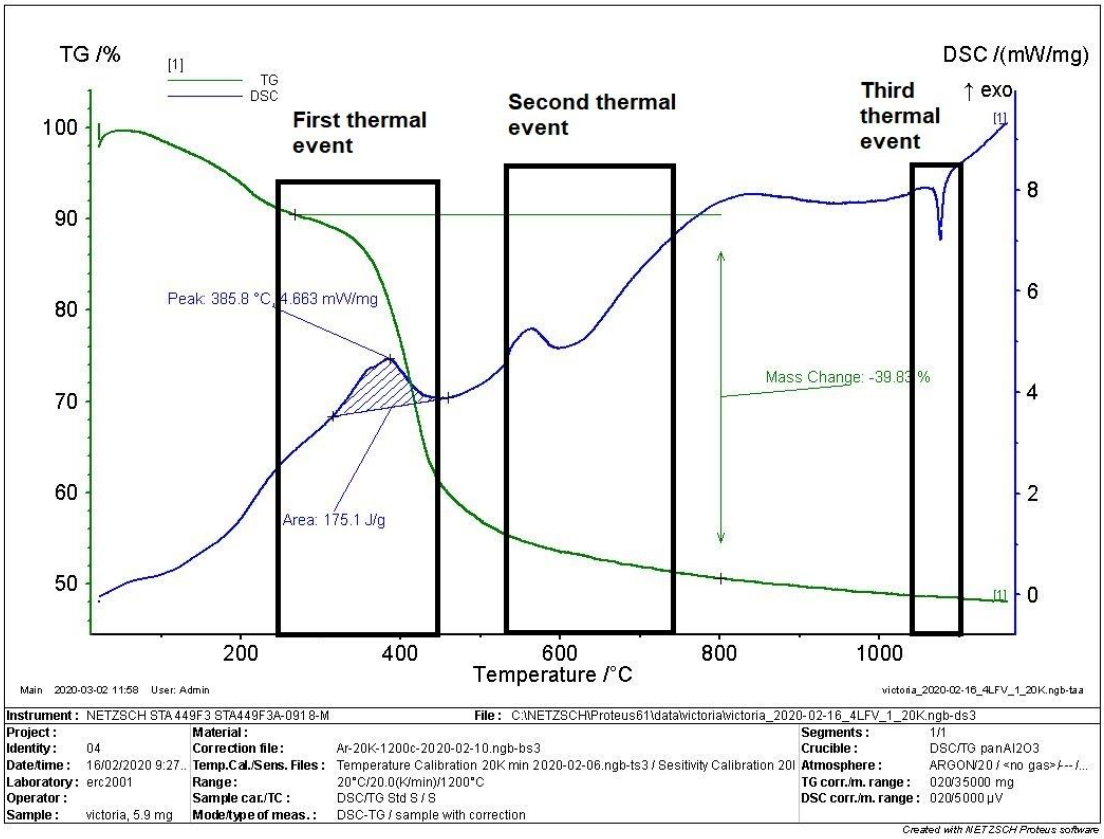

Figure 4.6 Typical DSC/TGA curve of a 4-layer sample, showing three distinct thermal events which vary due to structural characteristics

4.4.1 First Thermal Event

The first thermal event is critical in terms of ignition and energy release for many applications. This event involves the highest energy release of the reaction profile. The initiation of this event presents the Ignition Onset Temperature (IOT) as the temperature at which the exothermic reaction initiates, while the exothermic peak of this event occurs at the Exothermic Peak Temperature (EPT). The amount of energy released from the first thermal event is defined as the Specific Energy Release, which is calculated as the area underneath the DSC exothermic peak, beginning at the IOT and

terminating at the temperature where the slope of the DSC curve becomes equal to the baseline curve. Finally, the reaction time is determined to be the amount of time the reaction takes to progress from the IOT to the EPT. These four dependent variables were determined for each sample using Protezch Analysis Software. Figure 4.7 shows the analysis of a typical DSC peak for the first thermal event.

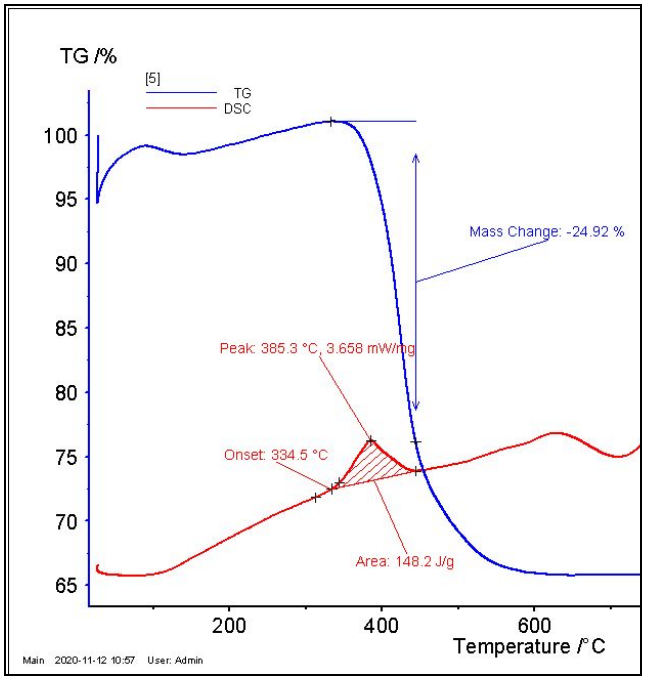

Figure 4.7 DSC Analysis showing ignition onset temperature, exothermic peak temperature, specific energy release and mass change for a typical five-layer sample

An important point of interest is the number of distinct, separate peaks involved in the first thermal event. Uniquely, the three-layer sample displayed two distinct exothermic peaks, while all other samples displayed a single exothermic peak. Figure 4.8 shows the first thermal event for a typical three-layer sample with two distinct peaks.

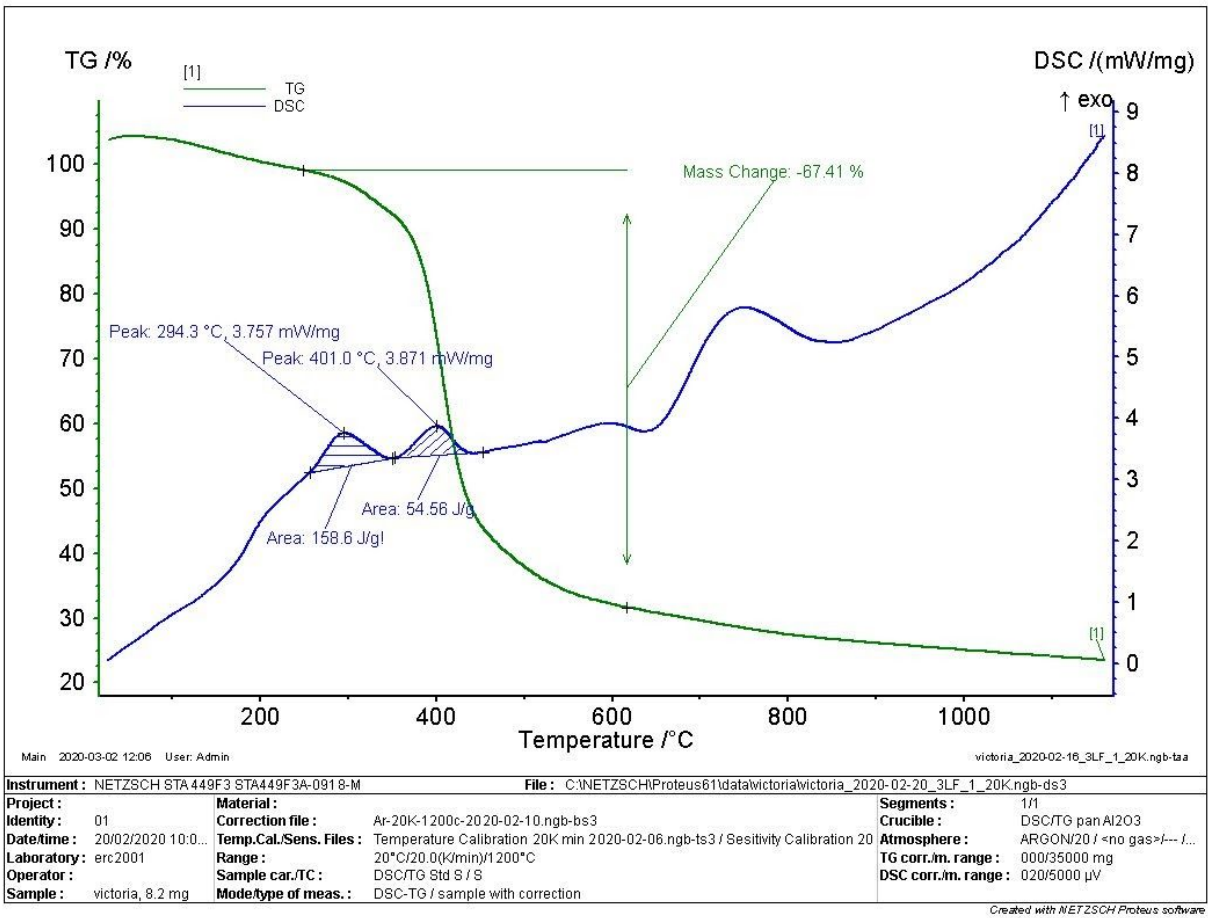

Figure 4.8 Three-layer sample showing two distinct exothermic peaks from 250°C - 450°C

As previously discussed, two conditions must be met to initiate the exothermic reaction. First, there must be a sufficient amount of heat in order for the Cu_2O to decompose and release oxygen, and this oxygen must migrate to the interface and react with Al to release heat. It is believed that the structural characteristics of the nanolaminate will determine which reaction condition is limiting, and this may change as the number of layers increases (and thus layer thicknesses decrease).

The two distinct exothermic peaks in the three-layer sample are due to the large thickness of the individual layers, as well as the unique double interface present. As the

sample is heated from both the top and the bottom, Cu_2O molecules near the Al/Cu_2O interface release its oxygen atoms to the Al, resulting in the first exothermic reaction initiating at approximately 260 °C. As the reaction proceeds, an alumina passivation wall is created, obstructing the motion of the diffusing oxygen atoms to the aluminum layer. The thickness of the Al and developing Al_2O_3 passivation layers slows the heat and mass transfer from the Cu_2O to the Al layer. This obstruction results in a delay before the oxygen atoms can diffuse and react with the remaining Al layer, which then initiates a second exothermic peak. Figure 4.9 demonstrates the suggested reaction dynamics of the three-layer sample.

Figure 4.9 Reaction progress of the three layer sample showing (1) the heating of the sample (2) the first exothermic reaction at the interface (3) the delay caused by the Al_2O_3 passivation layer obstructing O_2 transport and (4) the second exothermic reaction

Further testing is required to fully define the reactions causing these two peaks. It is advised that further DSC tests are performed but are halted at 340 °C and 450 °C; in between the termination of the first peak and the onset of the second peak, and after the completion of the second peak. The material from both cases should be examined using XRD to obtain detailed information regarding the crystalline structure, and how the

structure changes between the pre-test sample, the post-peak one sample, and the post- peak two sample.

The single exothermic peak of all other samples indicates that the reactions between layers are not independent of each other; as the first Al/Cu_2O reaction is initiated at the top and bottom-most interfaces, heat is released and quickly transferred throughout the sample, causing each interface to initiate soon after the first. This rippling effect continues throughout all layers of the sample and results in a single, large exothermic peak with all layers reacting in a short period of time.

The second point of interest involves an endothermic peak directly following the exothermic peak in the first thermal event. This phenomenon is novel and present in samples with more than six layers. Figure 4.10 shows an example of this unique phenomenon in a 10-layer sample.

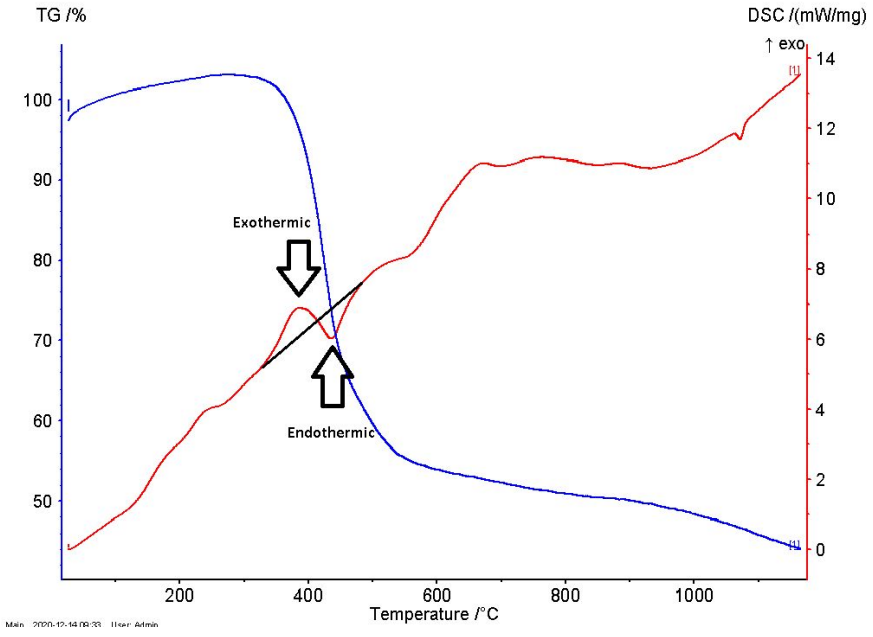

Figure 4.10 Combination exo/endothermic peak in a 10-layer sample

This exothermic/endothermic peak combination suggests that within the small thicknesses of the samples with more than six layers, the exothermic energy release is high enough to raise the temperature significantly within the sample and instigate the melting of Al (approximately 660°C), creating an endothermic peak. This phenomenon decreases the total energy release for these high-layer samples.

4.4.1.1 Effect of Number of Layers

The percentage mass loss, ignition onset temperature, exothermic peak temperature, reaction time, and energy release are all correlated with the number of layers in each sample. As previously discussed in Section 4.2.2, all samples had a standard total thickness of approximately 350 nm. As such, the samples with a small number of layers had larger single layer thicknesses, while those with a larger number of layers had smaller layer thicknesses. To study the effects of the number of layers, the bilayer thickness ratio of 0.6:1.0 Al:Cu_2O was maintained.

Percentage Mass Loss and Number of Layers

The percentage mass loss is a reaction characteristic measured from the beginning of the ignition onset to the termination of the first thermal event. As shown in Figure 4.2, the percentage mass loss for all samples except for the three- and five-layer samples are reasonably constant at approximately 32% mass loss. The three layer sample results in the highest percentage mass loss at 66%, while the five layer sample results in 49% mass loss due to the large Cu_2O layers exposed on both ends of these samples. As discussed in section 2.8, the Cu_2O layers in the sample decompose to

release oxygen as the sample is heated. The large outer layer thicknesses allows the oxygen to escape into the environment instead of reacting with the Al layers, resulting in significant mass losses.

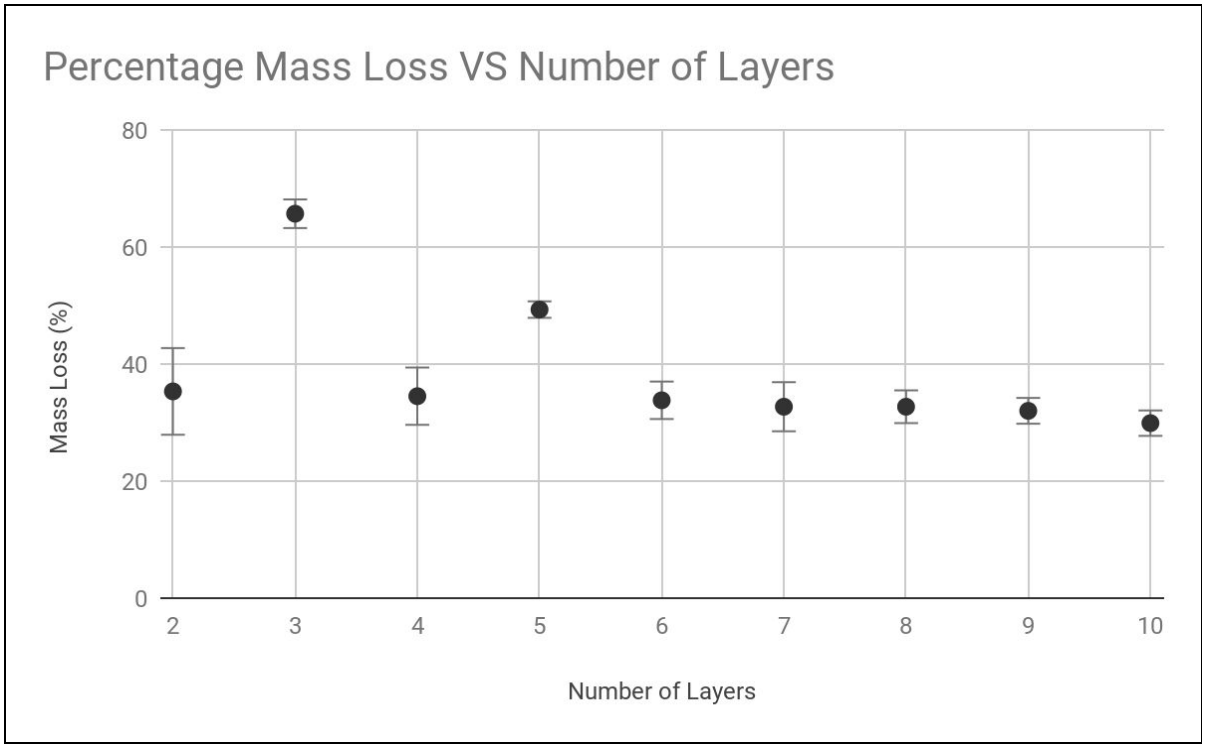

Figure 4.11 Percentage mass loss from ignition onset to the termination of the first thermal event for two - ten layer samples

Although the two- and four-layer samples also have larger layer thicknesses, their structures result in only one Cu_2O layer being exposed to the environment, with Al as the other outer layer. Because the exposure of Cu_2O to the environment is the main contributor to the mass loss, the two- and four-layer mass losses are smaller and more consistent with the other higher-layered samples (6+). Although samples 6, 8, and 10 have two Cu_2O layers exposed, as the increasingly thin layers decompose the majority

of the oxygen atoms migrate to the interfacial area and are involved in the thermite reaction. Thus, there are lower mass losses for these higher-layered samples.

Ignition Onset Temperature and Number of Layers

The ignition onset temperature is an important parameter for the use of thermites in micro- and nano-scale applications. This parameter is critical to understand for applications because in order for the thermite reaction to initiate, this temperature must be reached. A lower onset temperature is often beneficial due to the lower amount of energy input required to initiate ignition.

The increase in the number of layers results in a higher interfacial surface area for which the reaction occurs. It was hypothesized that this increase in interfacial area would increase the ease of heat and mass transfer between components, resulting in a negative linear correlation between IOT and the number of layers. Figure 4.12 shows the results for the ignition onset temperatures measured for layer numbers varying from 2-10.

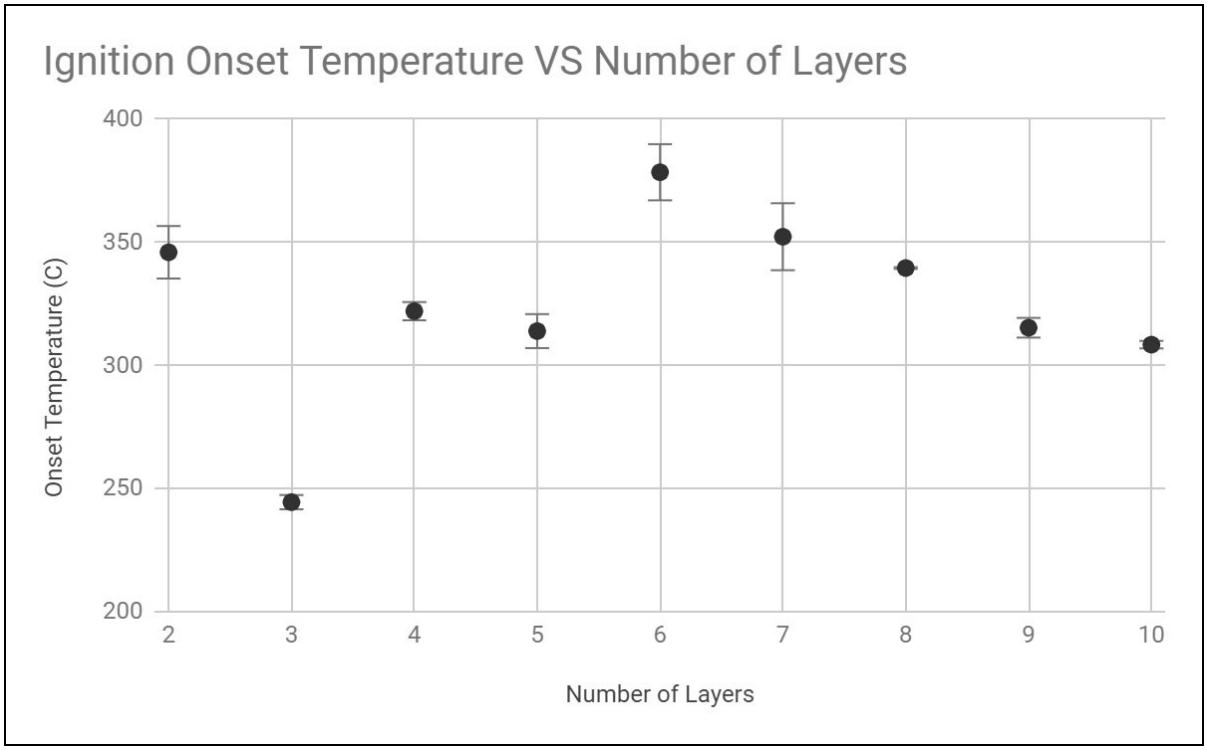

Figure 4.12 IOT for samples with two-ten layers showing two distinct trends for Samples 2, 4, and 5, and 6-10

As previously discussed, the three layer sample had two distinct exothermic peaks present in the first thermal event. The initiation of the first peak is at a significantly lower temperature than all other samples at 244°C, followed by the initiation of its second peak at 345°C. This two-peak phenomenon was discussed in Section 4.3.1. Excepting the three layer sample, samples 2-5 show a linear decrease in OIT from 345°C (two layers) to 313°C (five layers). The six layer sample does not follow this trend and has the highest ignition onset temperature at 378°C and the highest variance with a standard deviation of 11.4°C. As the number of layers increases from 6 - 10, the ignition onset temperatures decrease in a linear fashion (similar to the pattern of samples with 2, 4 and 5 layers).

While this result was not hypothesized, it can be explained by the two requirements needed to initiate the thermite reaction: sufficient heating of Cu_2O to release oxygen, and sufficient mass transport of this oxygen to react with the pure Al particles. It is believed that because of the large layer thicknesses of samples with less than 6 layers, these thermite reactions are limited by the heat transfer within the sample. Due to the geometry of the nanolaminate samples, the outer layers are heated first from the environment, and this heat is then dispersed through the sample. In the 2-layer sample there is bulk heating of the large Cu_2O and Al layers, which requires a higher amount of energy input for the heat to diffuse to the interface in order for the Cu_2O atoms in the middle of the sample to reach the critical temperature and decompose. This large heat diffusion pathway from the outer edges of the sample to the interface results in a high IOT. The three layer sample has a significantly lower IOT than all other samples because the thinner layers allow for the quicker diffusion of heat to the interface, while the unique two-interface structure results in two distinct exothermic peaks. Because the Al layer has a much lower heat conductivity than the copper layer, as the heat is transferred from the outer edges in the interface, the heat builds up quickly and initiates the thermite reaction at the first interface at a lower temperature. The thickness of the Al layer also prevents the diffusion of heat from this initial reaction to travel efficiently to the second interface, resulting in the delay between the first and second exothermic reactions during the first thermal event for this unique sample.

The four- and five-layer samples experience single exothermic peaks and follow the negative linear trend from the 2-layer sample. Like the previously mentioned

samples, the heat diffuses from the environment through the layers to the interfaces. Unlike in sample 3, the smaller layer thicknesses do not create a buildup of heat at the first interface, rather the heat is dispersed throughout the entire sample, delaying its overall ignition. Once ignition is achieved, the entire sample reacts quickly at each interface, resulting in the measurement of a single exothermic peak.

The six-layer sample has the highest ignition onset temperature, and it is at this geometry that the limiting factor is mass, rather than heat transfer. The mass transfer during this reaction is a balance between the incoming oxygen atoms to the interface, and the accumulating Al_2O_3 passivation wall building as these oxygen atoms react with the Al. With the geometry present in the 6-layer structure, it is proposed that the Al_2O_3 passivation interferes with the motion of the oxygen atoms, significantly delaying the ignition of the sample. This prevents an efficient ignition and therefore results in the highest IOT. As the number of layers increases from 7 - 10, the layer thicknesses (and therefore the amount of material) decreases and there is a lower amount of passivation at each interface. This results in the IOT decreasing linearly.

The development of modelling data may provide critical insight for the evaluation of the hypothesis presented in this section. Modelling at a nano-scale, however, comes with challenges. This is further discussed in Section 6.3.

Exothermic Peak Temperature and Number of Layers

The exothermic peak temperature (EPT) of each sample is defined by the temperature at which the highest amount of energy is released. This parameter is useful to understand the length of the reaction. The EPT is correlated to the number of layers

present in each sample. The three layer sample is expected to have the lowest EPT because the EPT for this sample is defined by the peak of the first exothermic reaction, which as discussed involves the quick reaction of only the top interface in the sample. All other samples involve the sum of exothermic reactions occurring at each interface. There may be a small delay between the ignition of the first layer and the ignition of all other layers which is dependent on the thickness and structure of each sample, which results in a variance of peak temperatures. Figure 4.13 shows the correlation between the exothermic peak temperature and the number of layers in each sample.

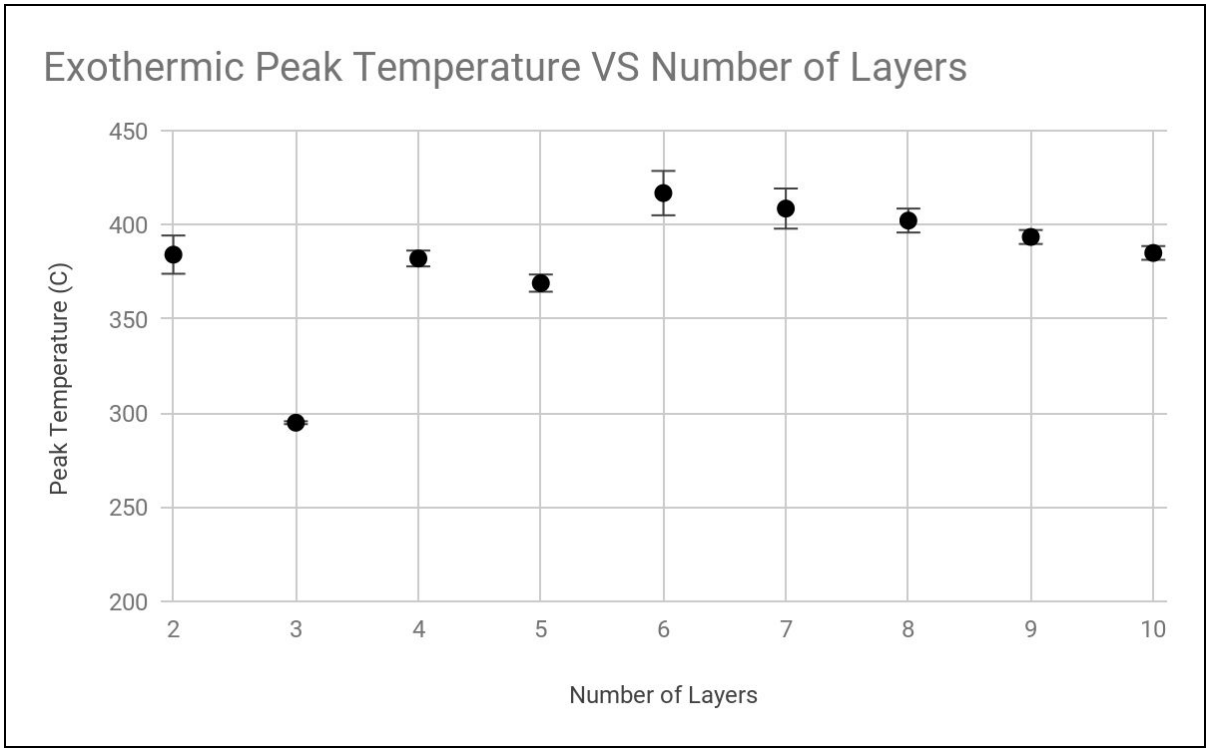

Figure 4.13 EPT for two - ten layers showing two distinct decreasing linear trends

The correlation patterns for the samples of EPT are very similar to the trends examined in the IOT graph. The three layer sample has the lowest initial peak temperature of 295°C for its first peak, followed by a second peak at 402°C. The

presence of similar trends in both IOT and EPT show that all samples experience reactions in similar ways and the processes involved from their ignition to their peak are standard and without exceptionalities.

Reaction Time and Number of Layers

The ignition reaction time is critical because it provides information regarding the speed of the reaction. The reaction time is measured from the onset temperature to the peak exothermic temperature. A shorter reaction time indicates that the onset and peak temperatures are closer together. As the number of layers increases, the reaction time also increases as seen in Figure 4.14.

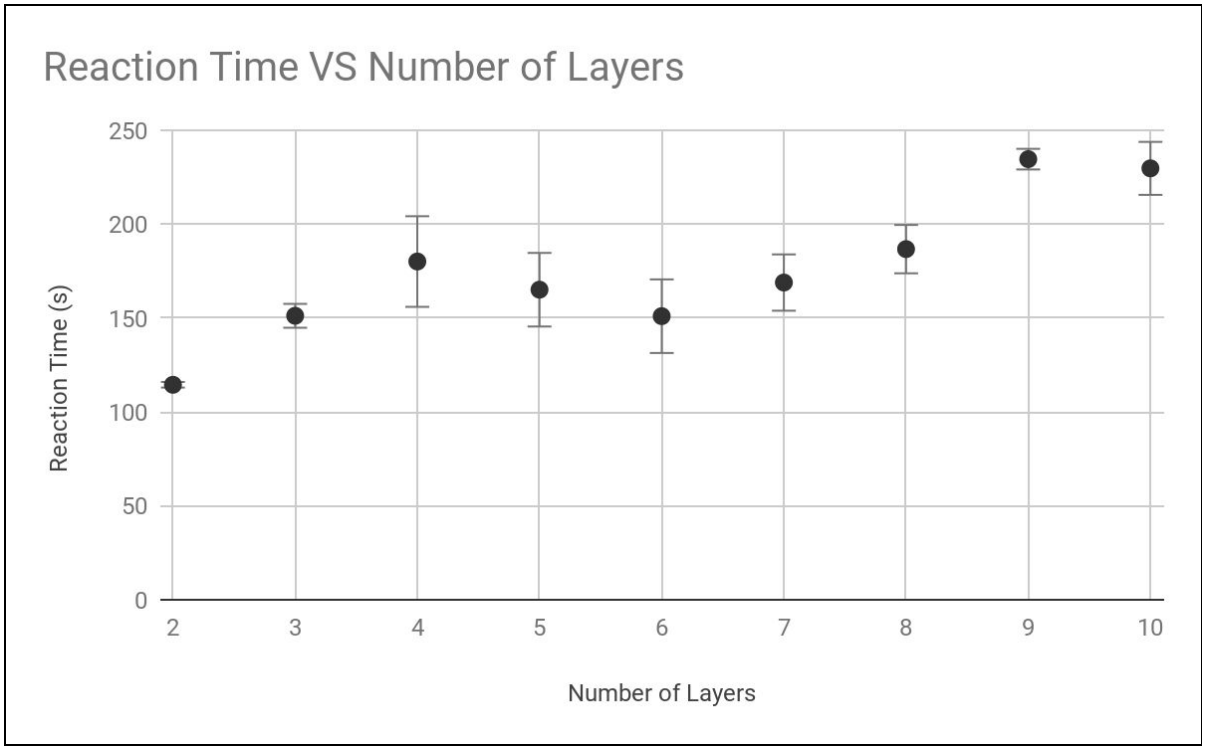

Figure 4.14 Reaction Time for two-ten layers showing an increasing trend

It is assumed that once ignition is initiated, the rate of reaction is constant regardless of structural characteristics. This assumption means that lower reaction times indicate a less complete reaction, whereas the higher-speed reactions indicate a complete reaction. This is corroborated with the findings in the following section regarding specific energy release.

Specific Energy Release and Number of Layers

The last and most difficult reaction characteristic to measure in the first thermal event is the exothermic energy release. This characteristic involves the extraction of the area under the DSC exothermic curve, and is most prone to human error during analysis due to the process of determining the reaction end point. Thus, the standard deviations from the mean are much larger for this characteristic than for other characteristics. In this thesis, the method of determining the end point of the reaction was chosen to be the point where the DSC slope of the curve becomes equal to the slope of the baseline curve, after the reaction peak. This measurement does not take into account the shape of the exothermic peak, it merely measures the bulk exothermic energy released. Figure 4.15 shows the correlation between energy released and number of layers.

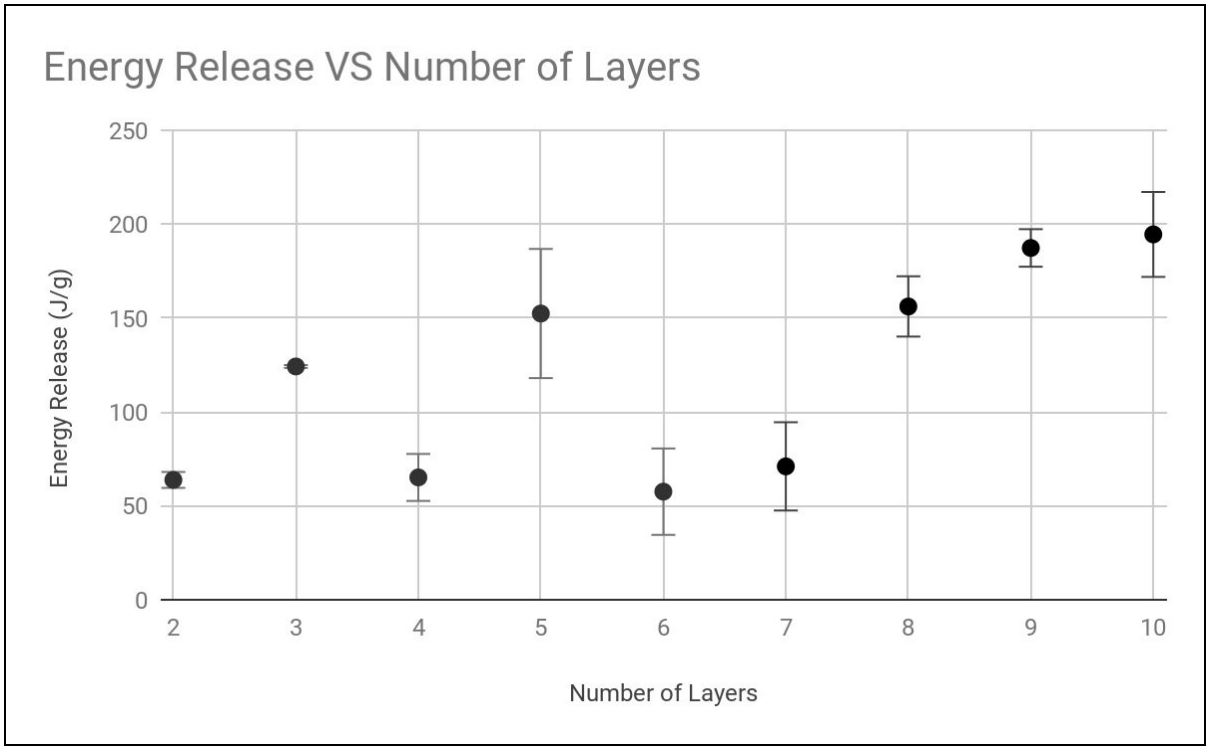

Figure 4.15 Specific Energy Release for two - ten layers showing two distinct increasing trends

There are two distinct trends in regards to energy release. For samples 2-5, the energy release for samples with an even number of layers are low (65 J/g) compared to the energy release from the three and five layer samples (124 J/g and 150J/g, respectively). As previously discussed, the reactions of samples with less than six layers are limited by the heat transfer through the layers. The odd-numbered layer samples have two outer Cu_2O layers, resulting in a higher amount of available oxygen per gram to be reacted in the sample. This results in substantially higher energy released per gram of reactant.

As previously discussed in Section 4.3.1.1.5, for samples with six or more layers the diffusion of oxygen to the Al particles becomes the limiting factor in the reaction due to Al passivation. For samples with six and seven layers, the thicknesses of the Cu_2O

layers prevents the oxygen from diffusing and reacting with Al. This results in the presence of unreacted Al and Cu_2O, significantly decreasing the specific energy release. For samples with more than seven layers, the thicknesses decrease and result in a complete reaction. With no unreacted matter left over, the specific energy release increases drastically.

4.4.1.2. Effect of Layer Thickness Ratio

In order to fully understand how the structural characteristics affect the ignition and reaction characteristics, it is critical to not only examine the number of layers, but also the thicknesses and ratios of Al to Cu_2O availability. The sputtering fabrication process allows for precise control over the individual layer thicknesses, which made it possible to easily and accurately alter the layer thicknesses for two sets of samples: stoichiometric and fuel-rich. The stoichiometric thickness ratio was determined to be 0.6:1.0 (Al:Cu_2O) through previous work (24), while the fuel rich thickness ratio was chosen to be 0.8:1.0 (Al:Cu_2O). Similar to the work completed in Section 4.3.1.1, the effects of these two structural conditions on the reaction's IOT, EPT and specific energy release were examined.

Based on the proposed reaction mechanisms and limiting factors determined in section 4.3.1.1 it is hypothesized that the varying thickness ratios would not significantly affect the structures with less than 6 layers because the limiting factor for these structures is the heat transfer through the layers. Increasing the Al ratio would not significantly affect the heat transfer, and thus the reaction characteristics of these samples. For samples with 6 or more layers, however, it is proposed that the Al-rich

condition would improve the energetic characteristics of these structures, due to the limiting mass transfer condition. An increase in Al thickness and therefore decrease in CU_2O thickness (as the total thickness for the samples remains constant) creates a situation where the Cu_2O layers appear more similarly both in structure and energetic behaviour to the higher-layer stoichiometric samples which have improved ignition and reaction characteristics. If these hypotheses are confirmed, the proposal for two separate limiting factors based on the number of layers will be further supported.

Ignition Onset Temperature and Layer Thickness Ratio

Figure 4.16 examines the relationship between varying thickness ratio and the ignition onset temperature.

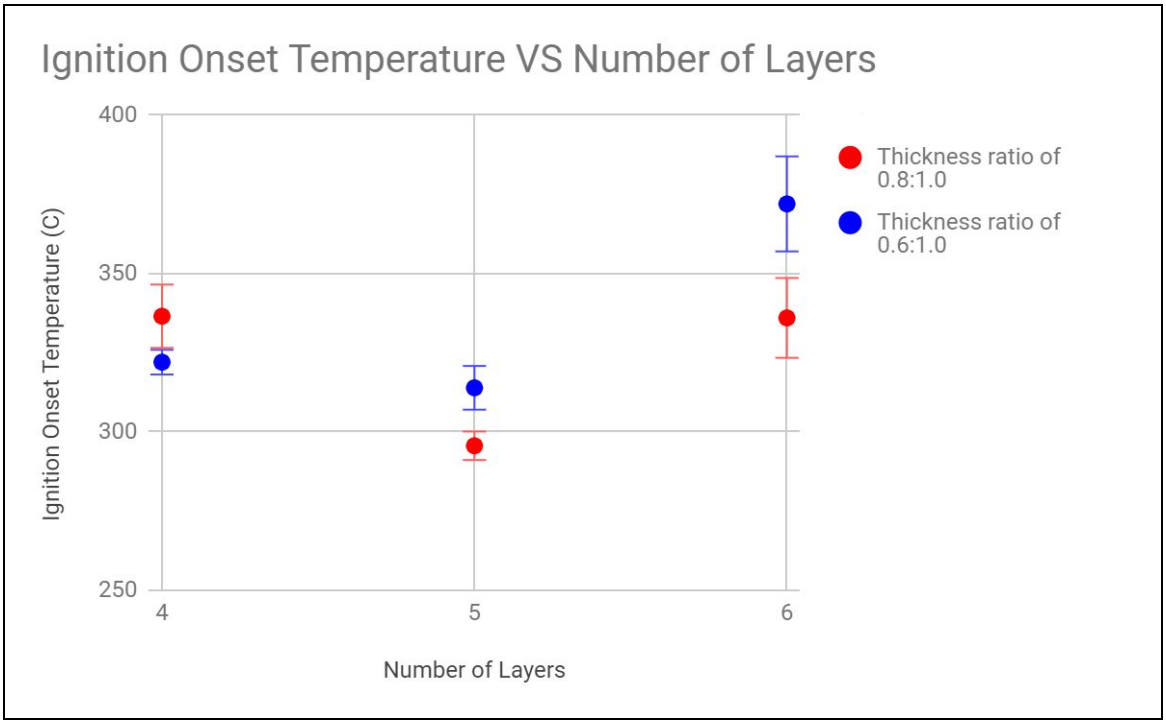

Figure 4.16 IOT for four - six layers with various thickness ratios showing insignificant results

From Figure 4.16 it is clear that there is not a statistically significant or reliable correlation between varying layer thicknesses and the IOT for structures with less than six layers. This result corroborates the results from the previous section, confirming the hypothesis for these structures. The six-layer sample shows that the aluminum-rich (0.8:1.0) thickness ratio results in a lower IOT, further supporting the hypothesis and showing that the IOT for the six-layer sample is delayed in the stoichiometric condition due to the large oxygen diffusion distances.

Exothermic Peak Temperature and Layer Thickness Ratio

Figure 4.17 below shows the correlation between the exothermic peak temperature and the effects of the thickness ratio on the 4, 5, and 6 layer samples. As expected, there are no significant effects of the varying thickness ratios on the EPT. The six-layer sample also does not show a statistically significant difference between the stoichiometric and fuel-rich ratios (416.8 +/- 11.8 °C, 412.0 +/- 4.5 °C). Under the assumption that the Al-rich six-layer sample acts similarly to the seven- or eight-layer stoichiometric samples, it would be expected that the EPT would be within the range of 408.6 +/- 10.7 °C. Therefore, this result is expected and does not disprove the hypothesis presented.

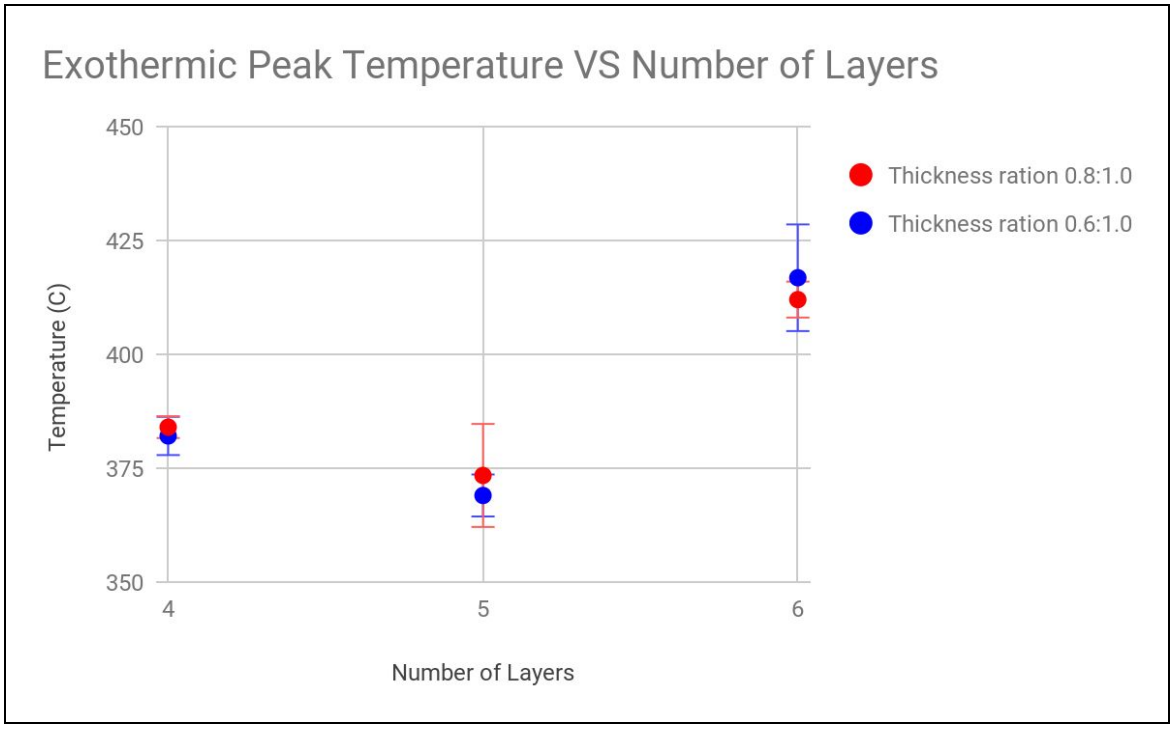

Figure 4.17 EPT for four - six layers with various thickness ratios

Specific Energy Release and Layer Thickness Ratio

The final reaction characteristic to be examined is the energy released per gram of reactant, shown in Figure 4.18. Due to the difficult nature of determining this reaction characteristic resulting in high degrees of error, there are no statistically significant findings in terms of if the layer thickness ratio affects the energy release per gram of reactant.

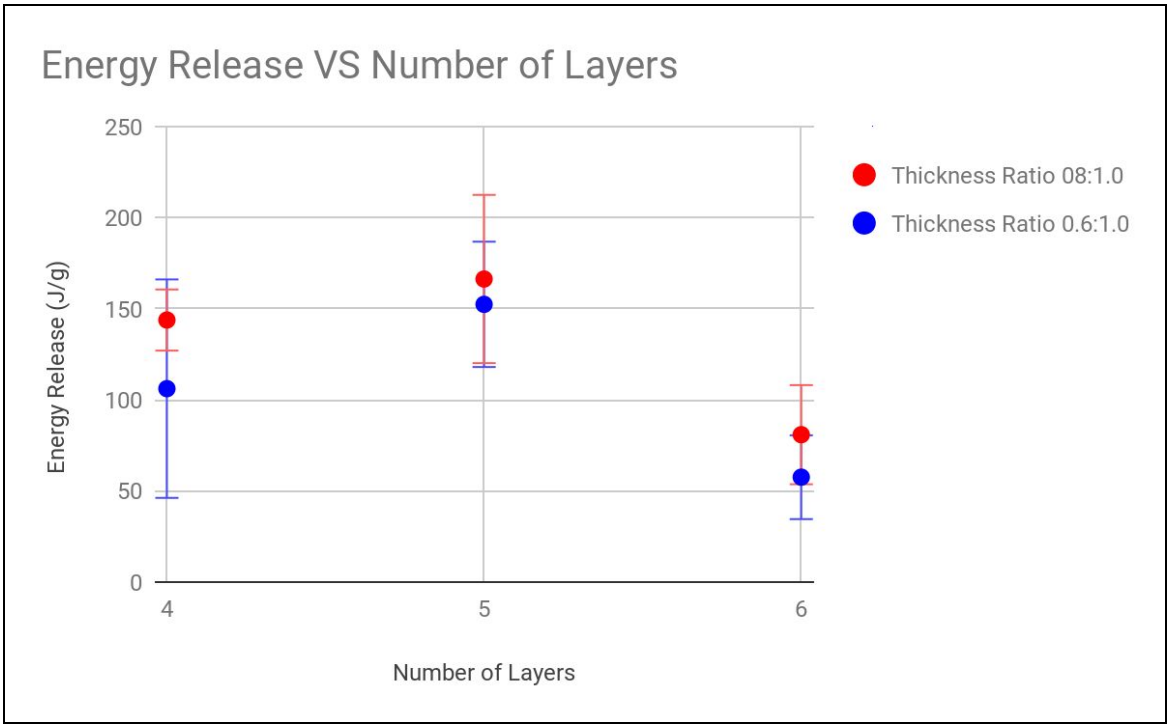

Figure 4.18 Specific Energy Release for four - six layers with various thickness ratios

4.4.2 Second Thermal Event

The second event is indicated by the onset of aluminum-melting (660 °C), with endothermic and/or exothermic peaks occurring between 575 - 700 °C. This indicates that as Al melting begins (which is typically an endothermic peak), the interfacial area between components increases and this increase results in a second exothermic energy release. This second thermal event is only significant in the two- and three-layer samples, as well as the four- and five- layer samples with a thickness ratio of 0.8:1.0 (Al:Cu_2O). This indicates that these samples have an excess amount of Al that is left unreacted from the first thermal event. As the sample continues to be heated following the first thermal event, the Al layer(s) experiences melting and the structure of nano-laminate becomes amorphous. This increases the interfacial area between Al and

Cu_2O, resulting in new exothermic reduction/oxidation reactions in this temperature range. It is shown that all 0.6:1.0 (Al:Cu_2O) except the two- and three-layer samples do not have excess Al after the first thermal event, resulting in no significant reactions throughout the second thermal event.

4.4.3 Third Thermal Event

The final thermal event occurred at approximately 1075 °C, consistent with the melting point of Cu_2O. Endothermic peaks were visible in all samples with a thickness ratio of 0.6:1.0 (Al:Cu_2O), except for the two- and three- layer samples. There was no third event recorded for the four- or five-layer samples with a thickness ratio of 0.8:1.0 (Al:Cu_2O), however there was an endothermic peak found for the six-layer sample. This indicates that there is unreacted Cu_2O remaining in the samples displaying this endothermic peak. Table 4.2 summarizes the nature of peaks present in each sample.

Table 4.2 Summary of Thermal Events

Sample	Thickness ratio	First Event	Second Event	Third Event
2	0.6:1.0	exo	exo	none
3	0.6:1.0	exo	endo/exo	none
4a	0.6:1.0	exo	exo	endo
4b	0.8:1.0	exo	endo	none
5a	0.6:1.0	exo	exo	endo
5b	0.8:1.0	exo	none	endo
6a	0.6:1.0	exo	exo	endo
6b	0.8:1.0	exo	none	endo
7	0.6:1.0	exo/endo	none	endo
8	0.6:1.0	exo/endo	none	endo
9	0.6:1.0	exo/endo	none	endo
10	0.6:1.0	exo/endo	none	endo

In order to optimize the ignition and reaction characteristics per gram of material, it is ideal to have the entire nanothermite react within the bounds of the first event, resulting in no excess Al or Cu_2O within the system, and thus no reactions in the bounds of the second or third events. With this knowledge, it is clear that none of the samples tested were completely optimized, and the structural characteristics can be further enhanced. Suggestions to improve the nano-laminate structure to optimize the ignition and reaction characteristics are found in Section 6.3.

4.4.4 Effect of Substrate

In many applications, it can be useful to have static nanothermite material that can not be easily moved such as in microfluidic channels where the nanothermite must remain in place while resisting the movement of fluids within the channel. One way to

achieve this is the use of a substrate. As previously discussed in Section 2.6.5, nanolaminates lend themselves very well to the use of substrates because of the sputtering fabrication method. If substrates are used in these applications, it is critical to understand the effects that these substrates may have on the ignition and reaction characteristics of the thermite.

In this thesis, two commonly used substrates were selected for testing: glass and quartz. Plain, precleaned VWR soda lime glass microscope slides from VWR American and Alfa Aesar fused quartz microscope slides were cleaned and placed into the AJA sputtering machine to be directly sputtered upon (details included in Appendix III). The fabricated samples consisted of two, four, and six layers and had a constant thickness ratio of 0.6:1.0 (Al:Cu_2O), with a constant thickness of approximately 355 nm. The slides were cut into pieces using a diamond knife in order to fit into the DSC crucible, as described in Section 4.4.

4.4.4.1 Glass Substrate Effects

A major issue encountered with the glass substrate was its softening at 720 °C. This limited the temperature range at which we could test the samples (the substrate-free samples were tested up to 1200 °C). This issue prevented the possibility of recording thermal events that could have occurred between 800 - 1200 °C. Although not ideal, it was still possible to perform DSC/TGA tests under this limited temperature range and investigate the effect of a glass substrate on ignition and reaction characteristics.

Glass Substrate Effects on Ignition Onset Temperature

The presence of the glass substrate significantly increased the ignition onset temperature (150 °C+) than the substrate-free samples. Because of its low electrical conductivity, the glass acted as a heat sink and absorbed heat from the environment and from the nano-laminate material. This heat sink effect prevented the buildup and dispersion of heat throughout the layers, resulting in a significant delay in Cu_2O decomposition and therefore ignition onset.

The ignition onset temperatures for the two- and four-layer glass samples were very similar, mirroring the trend of the two- and four-layer substrate-free samples. The six-layer sample on glass had a lower ignition onset, which is opposite from the trend discovered for the substrate-free sample. Figure 4.19 shows the IOT for the two-, four- and six-layer samples, with and without a glass substrate.

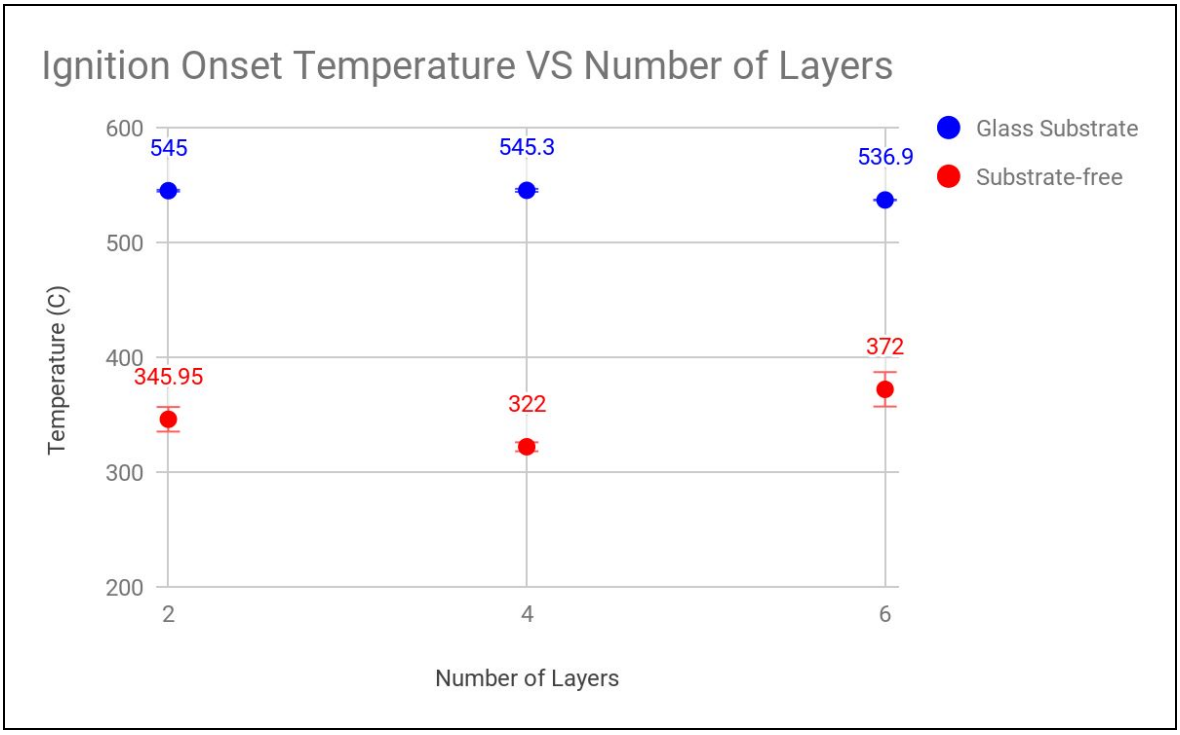

Figure 4.19 IOT for two-, four-, and six-layers with and without glass substrate

Glass Substrate Effects on Exothermic Peak Temperature

The exothermic peak temperatures were significantly (100 °C+) higher for all samples with the glass substrate than their substrate-free counterparts. There was a linearly decreasing trend from the two-layer (574 °C) to the six-layer (554 °C) peak temperatures. Figure 4.20 shows the EPT for the two-, four- and six-layer samples, with and without a glass substrate.

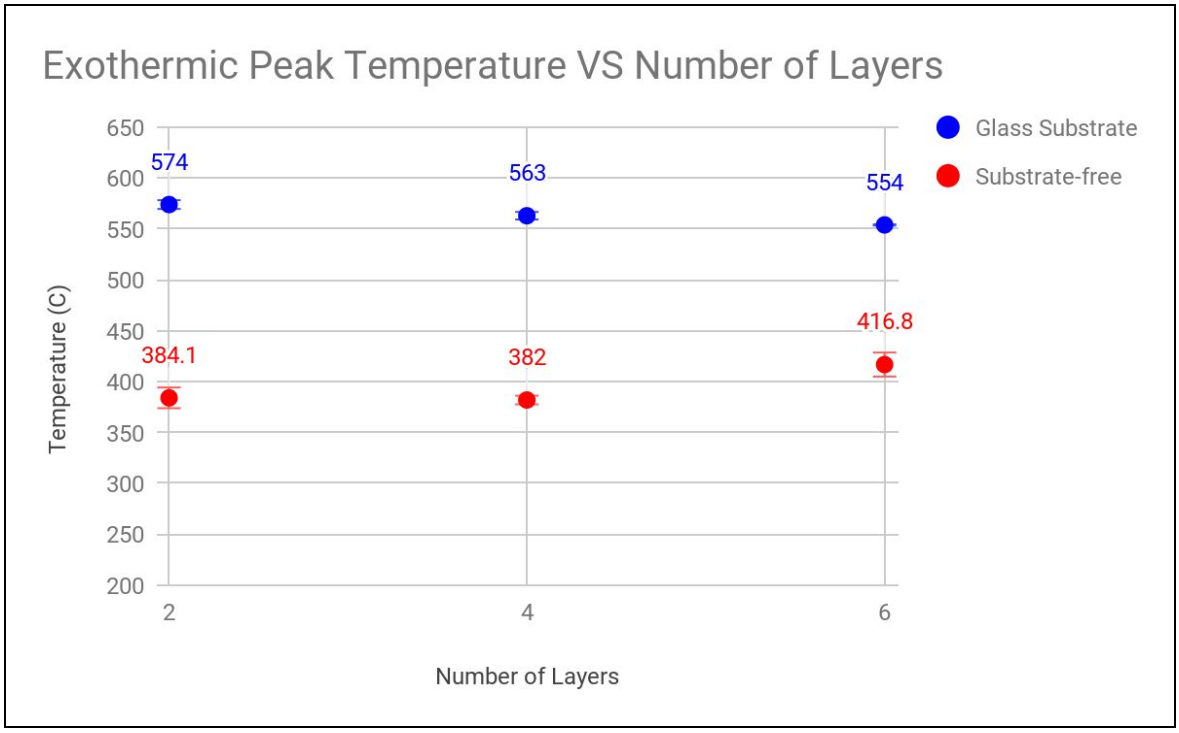

Figure 4.20 EPT for two-, four-, and six-layer samples with and without glass substrate

Glass Substrate Effects on Specific Energy Release

The specific energy release is significantly lower than the substrate free samples because the mass used in the calculation was the mass of both the glass piece and nano-laminate layers. This resulted in masses in the range of 25 mg, as opposed to the 5-10 mg masses used in the substrate-free cases. With this in mind, trends can still be assessed. The specific energy release increases linearly from the two-layer (1.56 J/g) to the six-layer (1.68 J/g) samples. This shows that the six-layer glass sample undergoes a more complete reaction. Figure 4.21 shows the EPT for the two-, four- and six-layer samples, with and without a glass substrate.

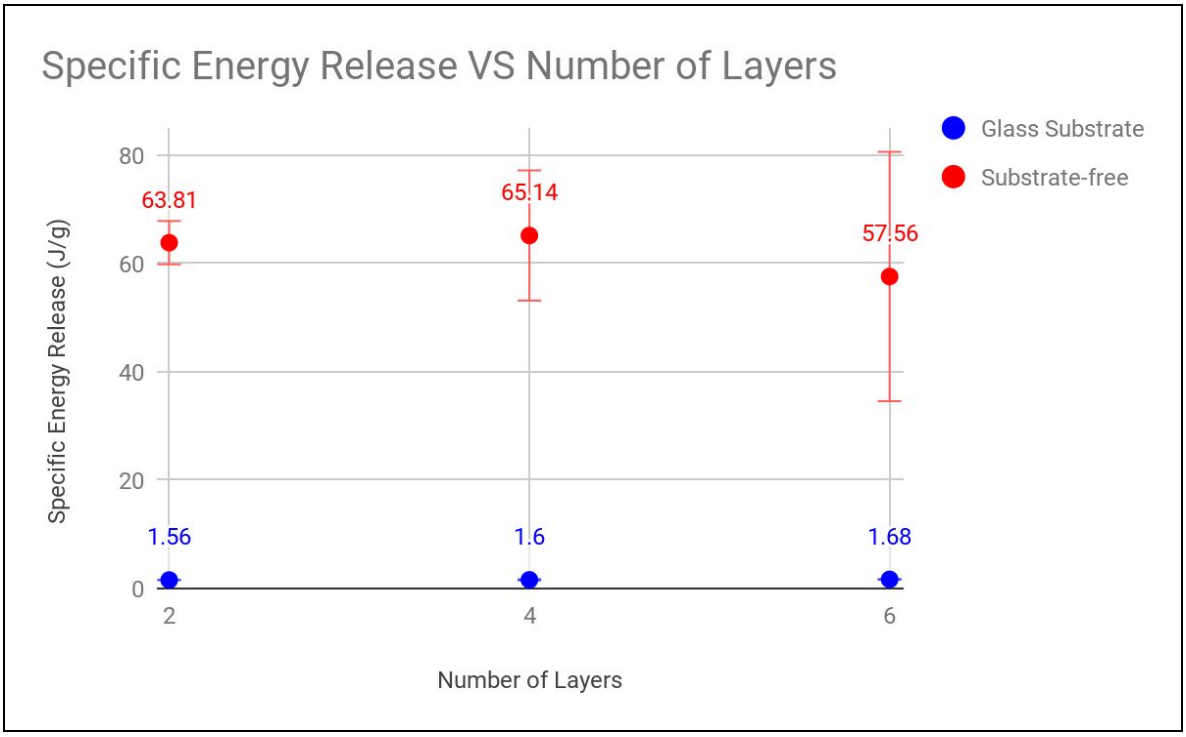

Figure 4.21 Specific Energy Release for two-, four-, and six-layers with and without glass substrate

It is clear that the glass substrate significantly limits the nano-laminate thermite ignition and reaction characteristics by elevating the IOT and EPT while lowering the specific energy release. The samples on the glass substrate also have smaller ranges of error, showing their reliability. These controlled attributes may make a glass-substrate appropriate for certain applications where a lower ignition onset temperature is to be avoided to mitigate the risk of unwanted ignition.

4.4.4.2 Quartz Substrate Effects

The quartz substrate was chosen due to its high purity and high melting point, however when tested in the DSC/TGA from room temperature to 1200 °C there were no

exothermic or endothermic peaks in any of the samples. This indicates that there were no Al/Cu_2O interactions of any sort. The highly insulating quality of the quartz slide is responsible for preventing the heating of the sample, and thus preventing any reactions from occuring.

4.5 Sources of Error

There are some critical sources of error to consider while evaluating the results found in the above studies. The first originates from the fabrication process used to create the substrate-free flakes. This fabrication process involved the spin coating of Su8-2005 on a substrate which was then sputtered upon, then dissolved in an acetone bath. There is a possibility that the substrate-free flakes may have Su8-2005 residue that did not properly separate from the sample. This could affect the DSC/TGA results for these substrate-free samples. Figure 4.22 and Figure 4.23 shows the TGA and DSC results for Su8 photoresist, respectively.

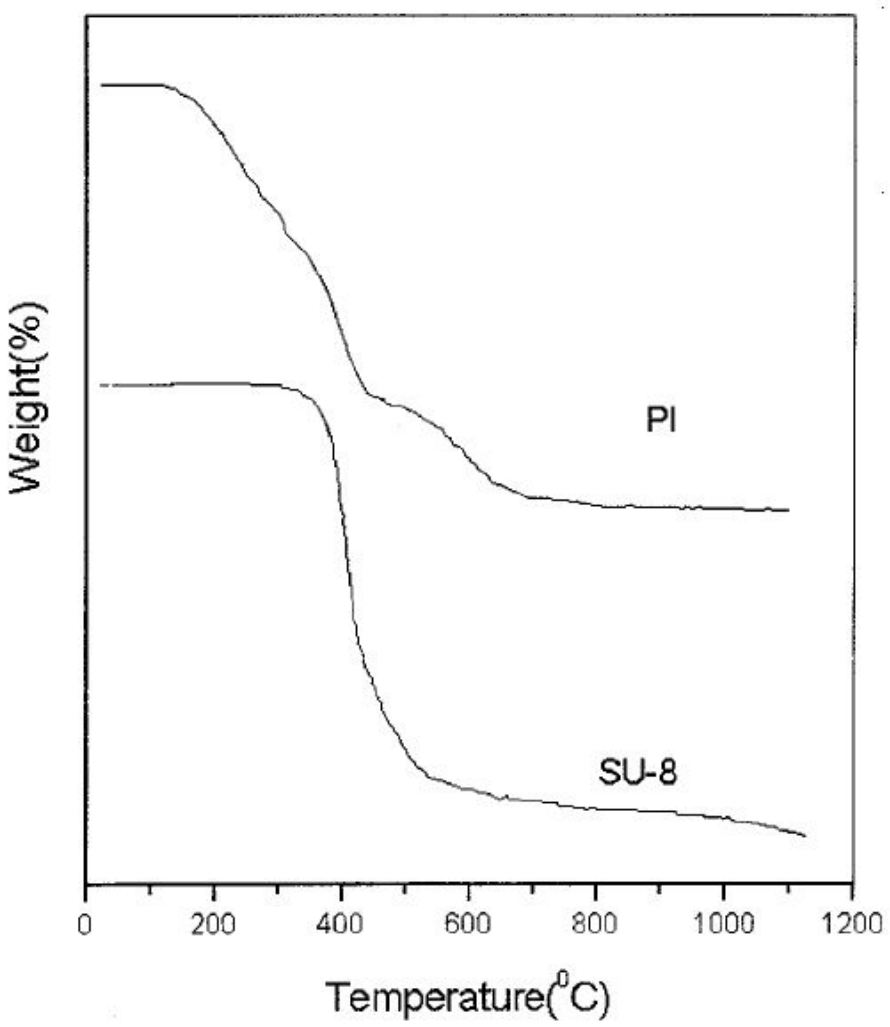

Figure 4.22 TGA of Su-8 displaying large mass changes at approximately 400°C [71]

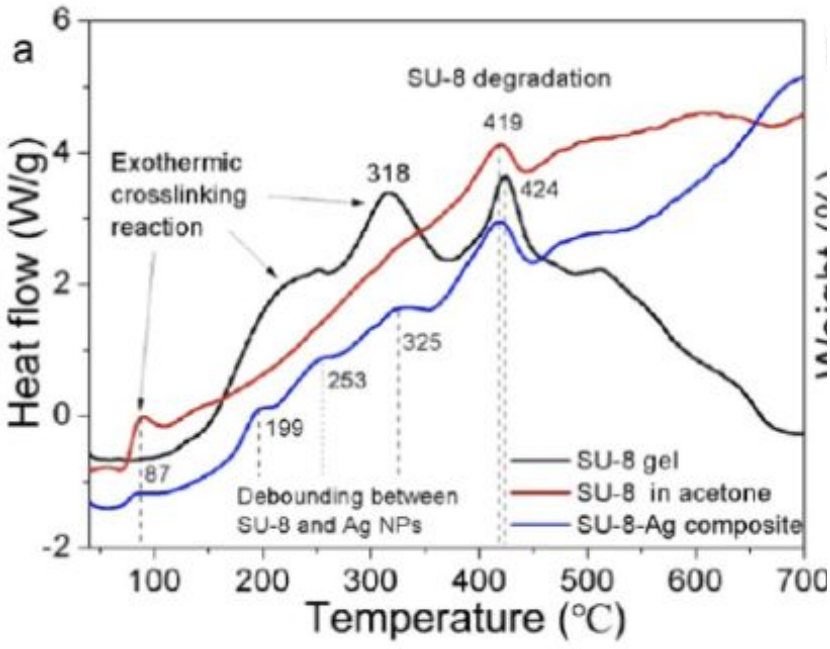

Figure 4.23 DSC curve of Su-8 photoresist showing exothermic energy release during heating [71]

The DSC data for the photoresist shows an exothermic energy at 318°C and 424°C. This directly corresponds to the first thermal event in the samples, and could significantly alter the results and conclusions drawn in this thesis. As discussed in Section 4.2.2.1, it is advised that further chemical characterization in the form of XPS be done following the substrate separation procedure to ensure that all of the photoresist has been removed from the sample. If it is found that there is significant photoresist residue on the samples, a new procedure for the separation of the substrate-free flakes from the substrate may be required.

The second major source of error for this section originates from the quality of results from the DSC/TGA machine. Due to the sensitive nature of this machine, it can

be difficult to achieve accurate, repeatable results. In order to mitigate these issues, steps were taken including using a constant mass of approximately 6 mg for the trials of substrate-free flakes, tests were repeated at least three times to ensure accuracy, and the calibration procedure as described in Section 4.3 was performed prior to testing.

4.6 Summary

In this study, the effects of the number of layers, layer thickness ratio, and presence of a substrate on the ignition and reaction characteristics of Al/Cu_2O nano-laminate thermite were studied. The characteristics examined included the percentage mass loss, ignition onset temperature, exothermic peak temperature, reaction speed, and specific energy release.

The reaction profiles for each sample were developed and analyzed. Three separate thermal events were defined and conclusions were drawn regarding how the absence or presence of these events indicated the complete-ness of the reaction. It was shown that the optimization of the number of layers and layer thicknesses is challenging and complex.

It was shown that the three-layer sample presented a unique reaction profile with two exothermic peaks during the first thermal event, while all other samples presented only one. Further testing is required to confirm the components and reaction mechanism(s) involved in these two exothermic reactions.

Clear correlations were made between the number of layers and the various energetic characteristics studied. It was determined that there were two distinct characteristics limiting the reaction based on the number of layers: samples with

two-five layers were limited by the heat dispersion through the layers, while samples with six-ten layers were limited by the oxygen transport to the interface. These limiting factors affected the trends for the IOT, EPT, reaction speed and specific energy release characteristics.

Two distinct layer thickness ratios were examined using four-, five-, and six-layer samples. It was shown that the higher thickness ratio improved only the IOT, while the EPT and the specific energy release remained constant. This supported the findings of the above study.

Finally, the effects of glass and quartz substrates were examined. It was shown that the glass substrate drastically increased the IOT and EPT, while lowering the specific energy release. The quartz substrate did not present any reactions due to its highly insulating nature.

5. Investigation of Various Ignition Methods of Al/Cu_2O Nano-Laminate Thermite

5.1 Motivation

As previously discussed, nano-thermite materials are uniquely appropriate for many micro-scale applications including microjoining, micropropulsion and for use in MEMs in roles such as pressure pulse generators, initiators, spot-heaters, and micro-actuators.

With an increased interest in the integration of nano-thermite into MEMs, an interesting issue of ignition methods is introduced. Traditional ignition methods including convective and radiative bulk heating results in the heating of a large area, potentially resulting in damages to sensitive components in MEMs due to their small size, leaving the MEMs incapable of performing the desired tasks. Conductive heating may have the ability to heat only the small, desired portion of the system, however the direct contact it requires is often incompatible with the system design [67] and poses dangers for the overheating of near-by sensitive components.

Alternative ignition methods for nano-thermite are an emerging area of research with recent developments including laser ignition [24] and microwave-induced ignition of Al-based nanothermite materials [66]. These methods of ignition could fill a gap regarding an effective, efficient, non-contact ignition method which is easily implemented for use in a variety of micro-electro-mechanical systems.

5.1.1 Laser Studies Motivations

Laser ignition in particular is of great interest in the MEMs space due to the small size and sensitivity of components often surrounding the nanothermite in the system. Unlike conventional conductive or convective heating methods which are difficult to control and heat the entire device, laser ignition allows precise application of heat and effectively avoids distributing this heat throughout the device. Laser ignition offers advantages over traditional ignition methods due to the tunability of the wavelengths, power densities and spot sizes through focussing. Finally, laser ignition utilizes a high power density over a very small area (often less than 1 mm in diameter) resulting in efficient ignition of the thermite sample without damage to surrounding components.

A critical characteristic of laser ignition is the ignition delay, defined as the time delay between the initiation of laser power and the onset of ignition. This parameter characterizes the ease of ignition for various samples using a laser ignition source.

5.1.2 Microwave Studies Motivations

The use of microwaves as an ignition source for nanothermite materials presents an opportunity to expand the use of nanothermites in MEMs. Small-scale microwave generators are commonly used in MEMs in an array of capacities including phase shifters, tunable microwave surfaces, reconfigurable leaky-wave antennas, multi-stable switches, and tunable capacitors [67]. Due to their common applications in MEMs, the ease of integration is a clear advantage over other ignition methods. Furthermore, the integration of the microwave generator directly into the system significantly improves the

ease and reliability of ignition when compared to a laser which needs to be positioned very specifically.

5.2 Laser Ignition Studies

To investigate the ignition mechanism of Al and Cu_2O nanothermite laminates with varying layer thicknesses, samples were ignited under atmospheric conditions with a low-power laser diode. The ignition delay was measured experimentally by both a photodiode and a high-speed camera.

5.2.1 Laser Ignition Methods

The following laser ignition studies took place at the Defence Research and Development Canada (DRDC) Valcartier research center.

5.2.1.1 Experimental Setup

A diagram of the experimental setup is shown in Figure 5.1. A diode laser (3 W power, 200 ms pulse duration, 808 nm wavelength) was used to ignite the samples contained in a small crucible. The laser beam was focused at 760 W/cm^2. A photodiode (Osram SFH206K) was used to record the light intensity, and a high speed camera (Photron Fastcam SA1.1) operated at 100,000 fps recorded the flame plume during the combustion [26 in paper]. The experimental setup was operated via LabView.

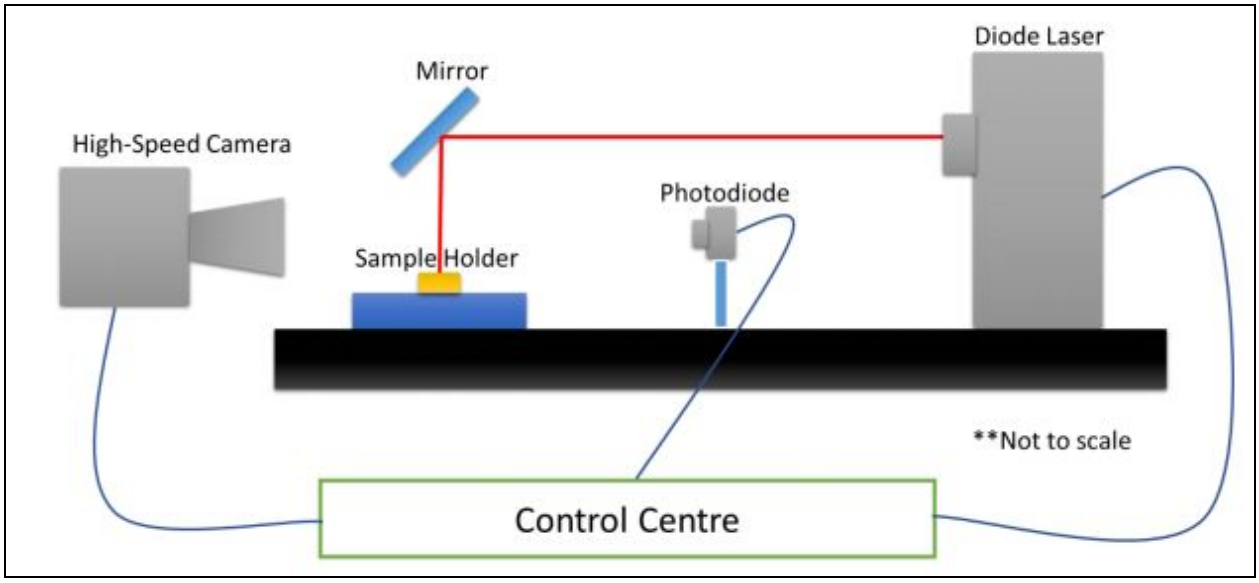

Figure 5.1 Experimental setup for laser studies [24]

In this study, four- and five-layer nanolaminate thermites were used. The four-layer samples had two distinct geometries:

1) Cu_2O layer thickness varying from 10 to 110 nm with constant Al layer thickness of 45 nm
2) Al layer thickness varying from 15 to 90 nm with constant Cu_2O layer thickness of 54 nm

The five-layer sample consisted of constant Al layer thicknesses of 45 nm, and Cu_2O layers varying from 10-80 nm thicknesses. In all geometries, the thicknesses were consistent in all layers of its kind throughout that sample. These geometries were chosen based off of previous work completed by Sacleanu et al. [39].

5.2.1.2 Data Analysis

The ignition delay was determined from the photodiode signal, which captured the emissions from laser initiation and sample ignition above a predefined threshold level. The initiation of the laser illumination appeared as a small peak in the photodiode measurement, followed by a linear signal (the ignition delay) until the reaction initiates and there is a very sharp increase in the photodiode signal. Figure 5.2 shows an example of a typical photodiode signal showing ignition delay.

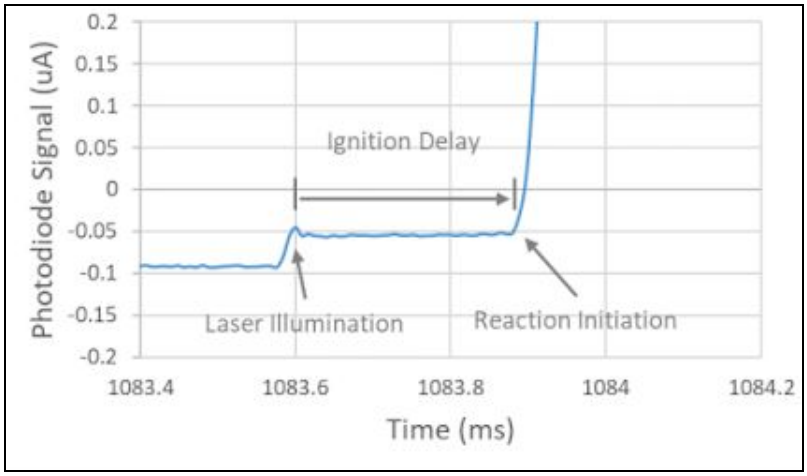

Figure 5.2 Typical photodiode signal showing ignition delay [24]

5.2.2 Laser Studies Results and Discussion

5.3.1.1 Effects of Altering Al and CU_2O Layer Thicknesses in a Four-Layer Sample

In order to determine the effects of altering the layer thicknesses on ignition delay for the four layer samples, the Al and Cu_2O layer thicknesses were varied separately. Figure 5.3 shows the correlation between ignition delay and Cu_2O layer thicknesses.

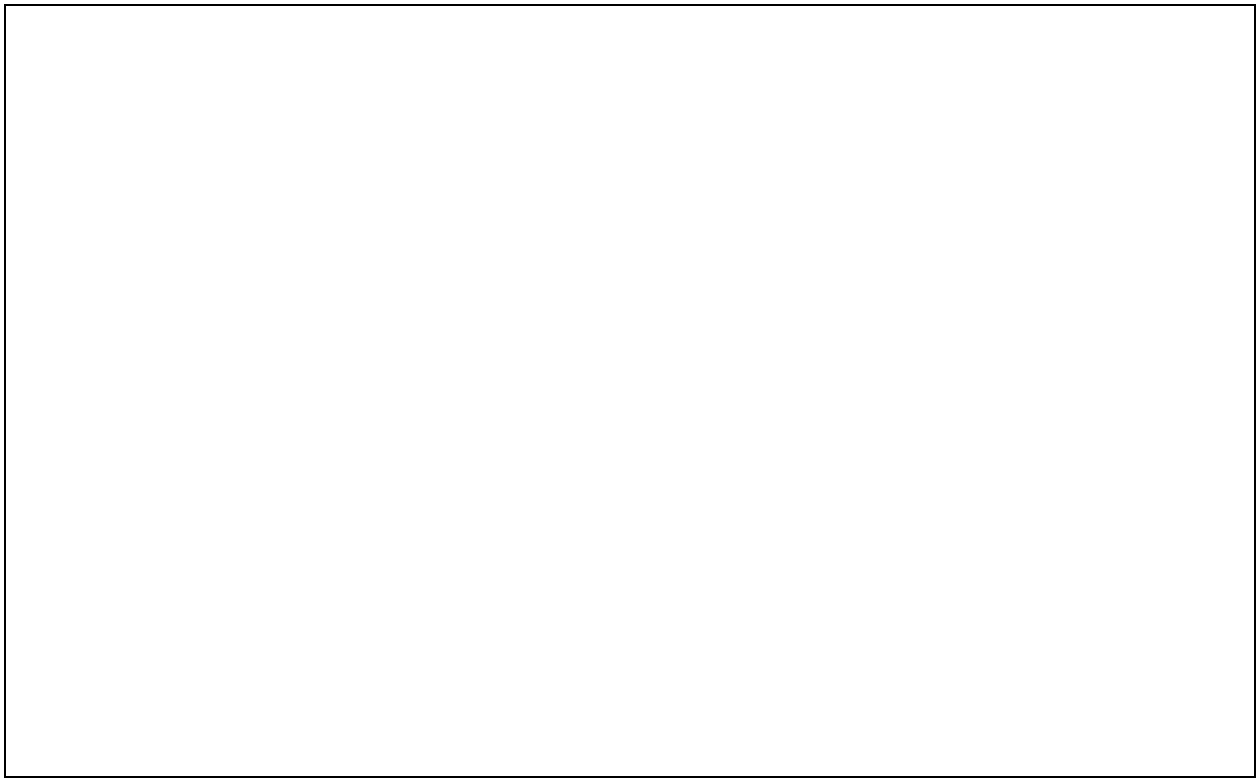

Figure 5.3 Ignition Delay and varying Cu_2O thicknesses with Al thickness of 45 nm in a four-layer sample

In the case of the first geometry, where the Al layers are constant and the Cu_2O layers are varied in the four layer structure, the figure above clearly shows that the ignition delay is minimized for the sample with 54 nm Cu_2O layers. The concave trend, with higher ignition delays at both low and high thicknesses indicates that there are two interacting mechanisms affecting the ignition delay. As previously discussed in section 2.8, the initiation of ignition requires sufficient heat (energy absorption) for the Cu_2O to decompose, as well as oxygen transport to the interface. The thicker Cu_2O layers absorb more energy (which decreases the ignition delay), however the released oxygen atoms must travel longer distances to reach the reactive interface, increasing the ignition delay. Therefore, the ignition delay of the samples with less than 50-60 nm layer

thicknesses are controlled by the oxygen transport requirement, while the samples with higher than 50-60 nm layer thicknesses are controlled by the heat absorption ability of the Cu_2O layers.

The second geometry of the four layer structure studied the effects of varying the Al layers while the Cu_2O remains constant. It is shown in Figure 5.4 that the ignition delay is independent of the Al layer thickness. The supports the conclusion that the ignition delay is controlled by the energy absorption and oxygen transport.

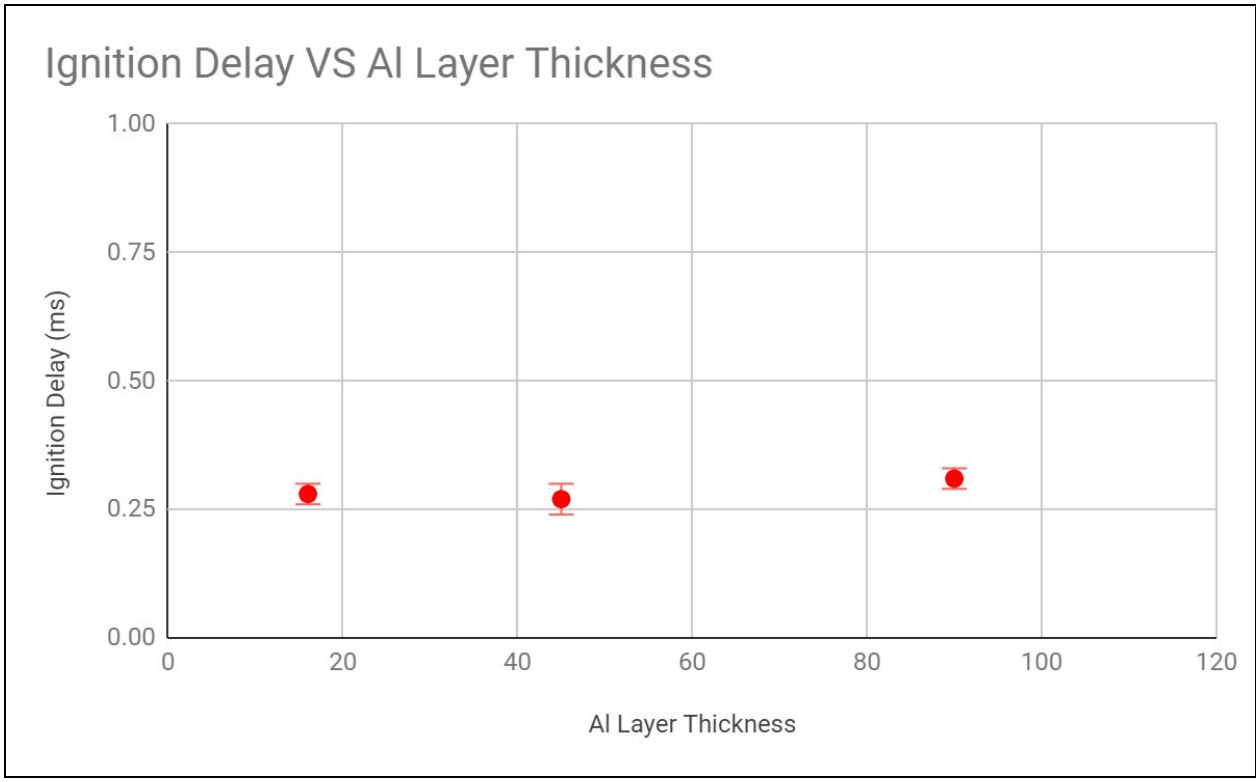

Figure 5.4 Ignition Delay and varying Al thicknesses with Cu_2O thickness of 54 nm in a four-layer sample

5.3.1.2 Effects of Altering CU_2O Layer Thickness in a Five-Layer Sample

In order to confirm the results found for the four-layer sample, a five layer sample with the same layer thicknesses was tested. Figure 5.5 shows that the 54 nm Cu_2O thickness in the five-layer samples also resulted in the lowest ignition delay.

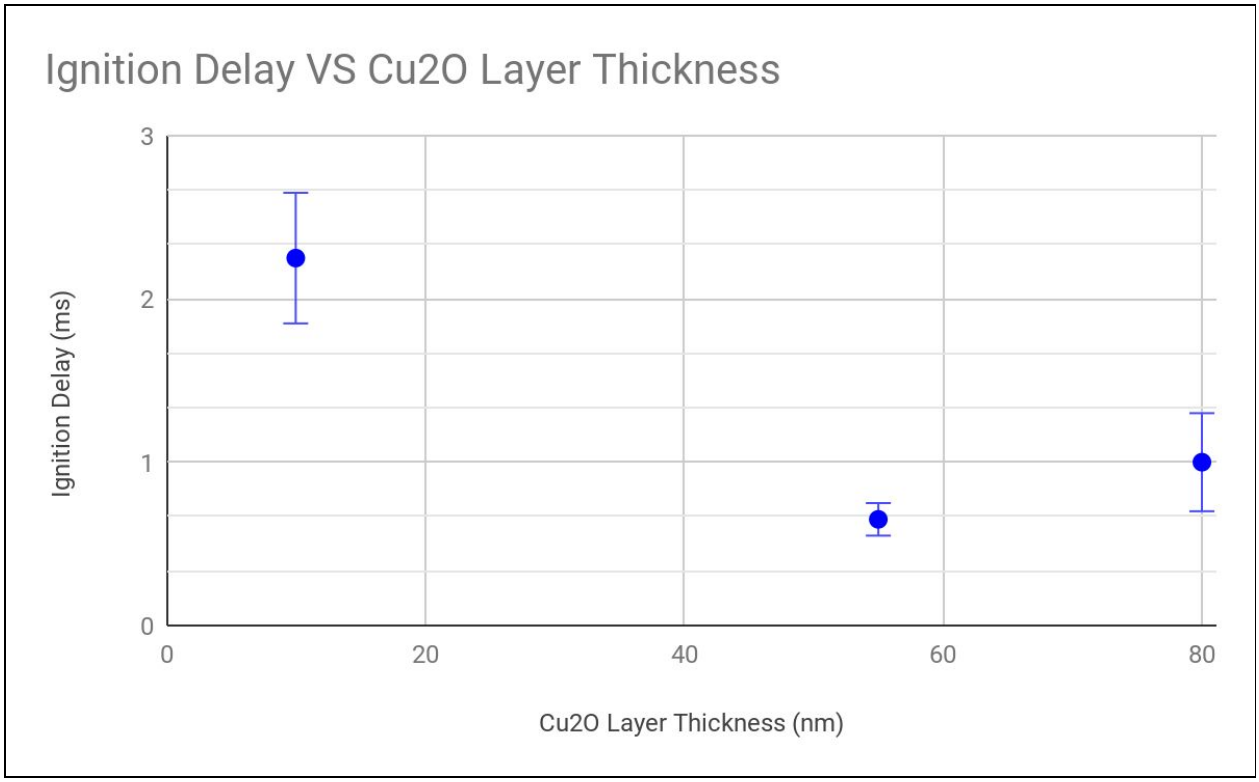

Figure 5.5 Ignition Delay and varying Cu_2O layer thicknesses with Al thicknesses of 45 nm in the five-layer sample

Interestingly, the ignition delay for the four-layer sample is less than that of the five-layer sample. This is a unique phenomenon which disagrees with the ignition onset temperature findings for DSC/TGA testing in Section 4.4.1.1.5. This highlights the importance of understanding the effects of the methods of ignition have on the ignition and reaction characteristics, prior to use in applications. The laser ignition source is

directed on only the top surface of the nano-laminate, and thus heats the structure from top to bottom. This ignition method relies on the heat absorption in the top layer to ignite the topmost interface, which then contributes heat to the remaining interfaces. In contrast, the DSC experiments studied in Chapter Four utilizes bulk heating from all sides of the sample, resulting in a build-up of heat throughout the sample prior to ignition, which accounts for the different trends in terms of ignition delay and ignition onset temperature.

5.3 Microwave Ignition Studies

Microwaves as an energy source is a promising development for the ignition of thermite and nano-thermite materials. Unlike traditional heating methods, microwaves can be tuned to the resonant frequency of the material, resulting in the heating of only the thermite. This is especially beneficial in MEMs, reducing the possibility of damage to other sensitive components in the system. Microwaves have been shown to successfully ignite thermite powder using direct injection methods with a power source of 100 W [67], as well as ignite thermite powder underwater with a power source of 1000 W [3]. Due to the various energetic improvements from traditional to nano-thermite structures, it is reasonable to assume that microwaves are a viable ignition option for nano-laminate thermite.

5.3.1 Microwave Ignition Methods

5.3.1.1 Generation of Microwaves on a Chip

The ideal setup for nano-laminate thermite application in a MEMs is on a system chip with an embedded microwave generator in order to achieve reliable ignition, and maintain simplicity in the chip.

In order to test the possibility of ignition with a microwave source, multiple trials were run with a HMC-T2100 Hittie frequency generator in air. The maximum power was limited to 0.5 W. The resonance frequency of 2.47 gHz was determined through experimental testing. 5-10 mg of the four-, six-, and eight-layer samples were then tested by being placed directly on the microwave generator chip, and applying the 0.5 W power.

5.3.1.2 Conventional Microwave Oven

A conventional microwave oven (with a volume of 2.0 cubic feet) was chosen to test the plausibility of high-powered Al/Cu_2O nano-laminate ignition. Four- and six-layer samples were tested with and without a glass substrate. The substrate-free samples were placed into a ceramic crucible, as used in the DSC/TGA testing in Section 4.4. All samples were placed in the microwave oven for 10 seconds under 1000 W.

5.3.2 Microwave Ignition Results and Discussion

5.3.2.1 Microwave Ignition on a Chip Results

Due to the low power generated, ignition was not achieved for any of the trials on the MEMs chip. However, a slight temperature increase was detected. This indicates that although there was not enough power to ignite the system, the nano-laminate thermite was heated by the microwaves. This is a promising development because it indicates that the same system with a higher power may be able to successfully ignite the Al/Cu_2O nano-laminate thermite.

5.3.2.2 Microwave Ignition in a Conventional Microwave Oven Results

All samples were unsuccessful in achieving ignition in the high-powered microwave oven. It was concluded that the size of the oven caused a dispersion of microwaves resulting in a lower amount of power being directly applied to the nano-laminate thermite material. Furthermore, the microwave oven is not tunable to the resonant frequency of the nano-laminate thermite material.

6. Conclusions, Contributions and Future Work

6.1 Conclusions

Extensive work was completed in this thesis to research the ignition and reaction characteristics of the Al/Cu_2O nano-laminate thermite system under varying conditions. This knowledge will provide critical information required to tailor the nano-laminate structure in order to successfully meet the needs of a variety of applications. It is important to note that the results presented in this thesis may be greatly affected by the procedure to remove the substrate-free samples from the photoresist/substrate using acetone. Photoresist contamination would greatly impact both DSC/TGA and laser ignition testing. Further testing is critical to assess the validity of this thesis, as explained in Section 6.3.

6.1.1 Conclusions of the Structural Characteristics on Ignition and Reaction Characteristics

In this section, the reaction mechanism of the Al/Cu_2O nano-laminate thermite system was studied extensively, and the effects of the structural characteristics on the ignition and reaction properties were shown. It was confirmed that there were two main conditions required to be met in order to initiate and sustain the thermite reaction: sufficient energy absorption and sufficient oxygen transport. It was shown that varying the number of nano-laminate layers directly influenced which of the two factors were limiting. For structures with less than six layers, the energy absorption of the material was limiting, while structures with six or more layers experience oxygen transport as the limiting factor.

The effects of layer thickness ratios and the use of substrates were also examined. Fuel-rich thickness ratios resulted in a lower ignition onset temperature in the six layer sample, which supports the hypothesis that this reaction is limited by the oxygen transport. It was shown that the glass substrate significantly increased the ignition onset temperature and exothermic peak temperature, while decreasing the specific energy release. It was also discovered that the quartz slide prevented any nano-laminate thermite ignition.

6.1.1 Conclusions of Ignition Methods Study

In this section, it was shown that laser ignition is achievable for a variety of nano-laminate structures. This study examined both four- and five-layer structures, and showed that in the four- and five-layer samples, the ignition delay was minimized with an optimum Cu_2O layer thickness of 54 nm. It was also proven that the Al layer thickness had no effect on the ignition delay.

Microwave ignition was investigated at both a micro- and macro-scale, but under the applied conditions was unsuccessful. It was determined that a high power, direct contact microwave source would be ideal to instigate nano-laminate thermite ignition.

6.2 Contributions

Significant contributions were made in this thesis to address current gaps in the research. Most notably a full, in depth examination of the ignition and reaction characteristics of the Al/Cu_2O nano-laminate thermite for a catalogue of layer numbers was completed. This work presented a theory for a two-factor limiting reaction mechanism, dependent on the layer number. An in depth examination on laser and

microwave-ignition sources were also completed, and although the microwave source was unsuccessful, groundwork has been laid to be built upon in order to develop this method.

6.3 Future Work

There are many promising aspects of this thesis that should continue to be studied in order to capitalize on these developments. Most notably, the three-layer sample that displayed two distinct exothermic peaks in the first thermal event needs to be characterized fully. This can be done by terminating DSC tests in between the first and second peak, as well as following the second peak, and these products should be examined using XRD analysis in order to determine the chemical composition and crystalline structure. The detailed understanding of this unique structure will provide further insight into the reaction mechanisms for similar structures with less than six layers.

As discussed in Section 4.5, there is a significant source of error originating from dissolving Su-8 photoresist during the preparation of the substrate-free samples. It is critical to understand the chemical composition of the substrate-free samples after separation from the substrate in order to accurately evaluate the quality of the DSC/TGA results. XPS testing must be done to ensure that there is no Su8-2005 photoresist residue on the substrate-free flakes as this could greatly affect the results. If residue is found, a new preparation method for the substrate-free flakes must be developed.

Finally, there are promising developments in microwave generation as an ignition source for Al/Cu_2O nano-laminate thermite. Future work should include the use of a high-power frequency generator (100+ watts) on a MEMs chip in direct contact with the nano-laminate thermite. This would validate microwaves as an ignition source and greatly contribute to the use of nano-thermite in MEMs.

References

[1] S, B. Chemistry And Physics Of Energetic Materials; Springer Netherlands: Dordrecht, 1990.

[2] Piercy, D. G., Klaptotke, T. M. Nanoscale Aluminum - Metal Oxide (Thermite) Reactions for Application in Energetic Materials. Central European Journal of Energetic Materials 2010, 7, 2, 115-129.

[3] Y. Meir and E. Jerby, "Underwater microwave ignition of hydrophobic thermite powder enabled by the bubble-marble effect," Appl. Phys. Lett., vol. 107, no. 5, p. 054101, 2015.

[4] F. Alvarez, A. Delgado, J. Frias, M. Rubio, C. White, S. Narayana, E. Shafirovich, F. Alvarez. Combustion of Thermites in Reduced Gravity for Space Applications, Journal of Thermodynamics and Heat Transfer. 27(3) (2013) 576-583.

[5] W. Gutkowski, T.A. Kowalewski, Mechanics of the 21st Century, 2004.

[6] C. Bodsworth, The extraction and refining of metals, New York: Boca Raton, FL, 1994.

[7] J.R. Luman, B. Wehrman, K.K. Kuo, R.A. Yetter, N.M. Masoud, T.G. Manning, L.E. Harris, H.A. Bruck, Development and characterization of high performance solid propellants containing nano-sized energetic ingredients, Proc. Combust. Inst. 31(2) (2007) 2089-2096.

[8] M.W. Beckstead, K. Puduppakkam, P. Thakre, V. Yang, Modeling of combustion and ignition of solid-propellant ingredients, Prog. Energy Combust. Sci. 33(6) (2007) 497-551.

[9] C. Rossi, D. Esteve, C. Mingues, Pyrotechnic actuator: a new generation of Si integrated actuator, Sens. Actuators 74 (1999) 211-215.

[10] C. Rossi, K. Zhang, D. Esteve, P. Alphonse, P. Tailhades, C. Vahlas, Nanoenergetic
materials for MEMS: A review, J. Microelectromech. Syst. 16(4) (2007) 919-931.

[11] P. Pennarun, C. Rossi, D. Estève, D. Bourrier, Design, fabrication and characterization of a MEMS safe pyrotechnical igniter integrating arming, disarming and sterilization functions, J. Micromech. Microeng. 16(1) (2006) 92-100.

[12] C. Rossi, D. Esteve, C. Mingues, Pyrotechnic actuator: a new generation of Si integrated actuator, Sens. Actuators 74 (1999) 211-215.

[13] J.W. Choi, C.H. Ahn, A functional on-chip pressure generator using solid chemical propellant for disposable lab-on-a-chip, (2003).

[14] T. Troianello, Precision foil resistors used as electro-pyrotechnic initiators, Electronic Components and Technology Conference, 2001.

[15] H.H. DiBiaso, B.A. English, M.G. Allen, Solid-phase conductive fuels for chemical microactuators, Sensors and Actuators A: Physical 111(2-3) (2004) 260-266.

[16] Y. Lin, A.A. Nepapushev, P.J. McGinn, A.S. Rogachev, A.S. Mukasyan, Combustion joining of carbon/carbon composites by a reactive mixture of titanium and mechanically activated nickel/aluminum powders, Ceram. Int. 39(7) (2013) 7499-7505.

[17] J.D.E. White, A.H. Simpson, A.S. Shteinberg, A.S. Mukasyan, Combustion joining of refractory materials: Carbon–carbon composites, J. Mater. Res. 23(01) (2011) 160-169.

[18] G. Feng, Z. Li, R. Liu, S. Feng, Effects of Joining Conditions on Microstructure and Mechanical Properties of Cf/Al Composites and TiAl Alloy Combustion Synthesis Joints, Acta Metall. Sin. (Engl. Lett.) 28(4) (2015) 405-413.

[19] C. Rossi, B. Larangot, D. Lagrange, A. Chaalane, Final characterizations of MEMS based pyrotechnical microthrusters, Sensors and Actuators A: Physical 121(2) (2005) 508-514.

[20] D.W. Youngner, S.T. Lu, E. Choueiri, J.B. Neidert, R.E. Black, K.J. Graham, D. Fahey, R. Lucus, X. Zhu, MEMS Mega-pixel Micro-thruster Arrays for Small Satellite Stationkeeping, 14th Annual/USU Conference on Small Satellites.

[21] D.H.L. Jr., S.W. Janson, R.B. Cohen, E.K. Antonsson, Digital MicroPropulsion, Sensors and Actuators A, Physical 80(2) (2000) 143-154.

[22] C. Rossi, D. Briand, M. Dumonteuil, T. Camps, P.Q. Pham, N.F.d. Rooij, Matrix of 10×10 addressed solid propellant microthrusters: Review of the technologies, Sensors and Actuators A: Physical 126(1) (2006) 241-252.

[23] S. J. Apperson, A. V. Bezmelnitsyn, R. Thiruvengadathan, K. Gangopadhyay, S. Gangopadhyay, W. A. Balas, P. E. Anderson and S. M. Nicolich, "Characterization of nanothermite materials for solidfuel microthruster applications," J. Propul. Power, vol. 25, no. 5, pp. 1086-1091, 2009.

[24] L. LeSergent (2018). Tailoring the Ignition and Reaction Properties of Cu2O Thermite Nanolaminates. UWSpace. http://hdl.handle.net/10012/13739

[25] E.L. Dreizin, Metal-based reactive nanomaterials, Prog. Energy Combust. Sci. 35(2) (2009) 141-167.

[26] C. Rossi, K. Zhang, D. Esteve, P. Alphonse, P. Tailhades, C. Vahlas, Nanoenergetic
materials for MEMS: A review, J. Microelectromech. Syst. 16(4) (2007) 919-931.
[27] L.L. Wang, Z.A. Munir, Y.M. Maximov, Review Thermite reactions: their utilization in the synthesis and processing of materials, J. Mater. Sci. 28 (1993) 3693-3708.
[28] Routh, E. Engineering Reactivity In Thermite Reactive Nano-Laminates; NC: North Carolina State University: Raleigh, 2018.
[29] L. Joseph, D. Davis, S. Kalay, Strengthening the track structure for heavy axle loads: 195 strengthening track infrastructure provides another method of dealing with ever-increasing car capacities. TTCI R&D, 2002.
[30] L. Galfetti, L.T.D. Luca, F. Severini, L. Meda, G. Marra, M. Marchetti, M. Regi, S. Bellucci, Nanoparticles for solid rocket propulsion, J. Phys.: Condens. Matter 18(33) (2006) 208 S1991-S2005.
[31] D. S. Hacker and P. Lieberman, "Thermodynamic performance evaluation of a hydroduct using a thermite fuel," J. Hydronautics, vol. 3, no. 3, pp. 139-144, 1969.
[32] Pantoya, M.; Granier, J. Combustion Behavior Of Highly Energetic Thermites: Nano Versus Micron Composites. Propellants, Explosives, Pyrotechnics 2005, 30, 53-62.
[33] X. Zhou, M. Torabi, J. Lu, R. Shen and K. Zhang, "Nanostructured energetic composites: synthesis, ignition/combustion modeling, and applications," ACS Appl. Mater. Interfaces, vol. 6, pp. 30583074, 2014

[34] V.E. Sanders, B.W. Asay, T.J. Foley, B.C. Tappan, A.N. Pacheco, S.F. Son, Reaction Propagation of Four Nanoscale Energetic Composites (Al/MoO3, Al/WO3, Al/CuO, and Bi2O3), J. Propul. Power 23(4) (2007) 707-714.

[35] K.C. Walter, D.R. Pesiri, D.E. Wilson, Manufacturing and Performance of Nanometric Al/MoO3 Energetic Materials, J. Propul. Power 23(4) (2007) 645-650.

[36] W.L. Perry, B.L. Smith, C.J. Bulian, J.R. Busse, C.S. Macomber, R.C. Dye, S.F. Son, Nano-Scale Tungsten Oxides for Metastable Intermolecular Composites, Propellants, Explosives, Pyrotechnics 29(2) (2004) 99-105.

[37] H. Sui (2019). Investigation on Reaction Mechanisms of Nano-energetic Materials and Application in Joining. UWSpace. http://hdl.handle.net/10012/14402

[38] J. Wang, A. Hu, J. Persic, J.Z. Wen, Y. Norman Zhou, Thermal stability and reaction
properties of passivated Al/CuO nano-thermite, J. Phys. Chem. Solids 72(6) (2011) 620-625.

[39] F. Saceleanu (2019). Heterogeneous Reactions of Micro and Nano Aluminum Particles with Various Oxidizers. UWSpace.

[40] Y. Zhang (2019). Fabrication and energetic characterization of micro and nano sized Al/CuO core-shell particles. UWSpace.

[41] Govinda Rao, B.; Mukherjee, D.; Reddy, B. Novel approaches for preparation of nanoparticles; Nanostructures for Novel Therapy: Synthesis, Characterization and Applications 2017, 1-36.

[42] Lawrence W. Hrubesh, Aerogel applications, Journal of Non-Crystalline Solids, Volume 225, 1998, Pages 335-342, ISSN 0022-3093,

[43] V.A. Babuk, V.A. Vasilyev, Model of Aluminum Agglomerate Evolution in Combustion Products of Solid Rocket Propellant, J. Propul. Power 18(4) (2002) 814-823.

[44] J.R. Luman, B. Wehrman, K.K. Kuo, R.A. Yetter, N.M. Masoud, T.G. Manning, L.E. Harris, H.A. Bruck, Development and characterization of high performance solid propellants containing nano-sized energetic ingredients, Proc. Combust. Inst. 31(2) (2007) 2089-2096

[45] P. Martin. (2010). Handbook of Deposition Technologies for Films and Coatings - Science, Applications and Technology (3rd Edition). William Andrew Publishing.

[46] H. Seim, M. Nieminen, L. Niinisto, H. Fjellvag, L.-S. Johansson, Growth of LaCoO3 thin films from b-diketonate precursors, Appl. Surf. Sci. 112 (1997) 243-250.

[47] P. Tagtstrom, P. Martensson, U. Jansson, J.O. Carlsson, Atomic Layer Epitaxy of Tungsten Oxide Films Using Oxyfluorides as Metal Precursors, J. Electrochem. Soc. 146(8) (1999) 3139-3143.

[48] T.S. Yang, W. Cho, M. Kim, K.-S. An, T.-M. Chung, C.G. Kim, Y. Kim, Atomic layer deposition of nickel oxide films using Ni (dmamp) 2 and water, Journal of Vacuum Science & Technology A: Vacuum, Surfaces, and Films 23(4) (2005) 1238.

[49] S Swann 1988 *Physics in Technology* 19 67

https://doi.org/10.1088/0305-4624/19/2/304

[50] I. Abdallah, J. Zapata, G. Lahiner, B. Warot-Fonrose, J. Cure, Y. Chabal, A. Estève and C. Rossi, "Structure and chemical characterization at the atomic level of reactions in Al/CuO multilayers," ACS Appl. Energy Mater., vol. 1, no. 4, pp. 1762-1770, 2018.

[51] V. Baijot, L. Glavier, J. -M. Ducéré, M. Djafari-Rouhani, C. Rossi and A. Estève, "Modeling the pressure generation in aluminum based thermites," Propellants Explos. Pyrotech, vol. 40, no. 3, pp. 402-412, 2015.

[52] F. Bensebaa, "Nanoparticle technologies from lab to market," Interface Sci. and Tech., vol. 19, pp. 279-383, 2013.

[53] M. Petrantoni, C. Rossi, L. Salvagnac, C. V., A. Estève, C. Tenailleau, P. Alphonse and Y. J. Chabal, "Multilayered Al/CuO thermite formation by reactive magnetron sputtering: Nano versus micro," J. Appl. Phys., vol. 108, 2010

[54] G. Lahiner, A. Nicollet, J. Zapata, L. Marin, N. Richard, M. Djafari-Rouhani, C. Rossi and A. Estève, "A diffusion-reaction scheme for modeling ignition and self-propagating reactions in Al/CuO multilayered thin-films," J. Appl. Phys., vol. 122, 2017.

[55] A. Nicollet, G. Lahiner, A. Belisario, S. S., M. Djafari-Rouhani, A. Estève and C. Rossi, "Investigation of Al/CuO multilayered thermite ignition," J. Appl. Phys., vol. 121, 2017.

[56] L. Marín, Y. Gao, M. Vallet, I. Abdallah, B. Warot-Fonrose, C. Tenailleau, T. Lucero, J. Kim, A. Esteve, Y. J. Chabal and C. Rossi, "Performance enhancement via incorporation of ZnO nanolayers in energetic Al/CuO multilayers," Langmuir, vol. 33, pp. 11086-11093, 2017.

[57] J. B. DeLisio, F. Yi, D. LaVan and M. R. Zachariah, "High heating rate reaction dynamics of Al/CuO nanolaminates by nanocalorimetry-coupled time-of-flight mass spectroscopy," J. Phys. Chem., vol. 121, pp. 2771-2777, 2017.

[58] L. Marín, N. C. E., J. -F. Veyan, B. Warot-Fonrose, S. Joulie, A. Estève, C. Tenailleau, C. Y. J. and C. Rossi, "Enhancing the reactivity of Al/CuO nanolaminates by Cu incorporation at the interfaces," ACS Appl. Mater. Interfaces, vol. 7, pp. 11713-11718, 2015.

[59] Y. Li, Y. Gao, X. Jia, B. Zhou and R. -Q. Shen, "Fabrication and performances of Al/CuO nano composite films for ignition application," Mater. Sci. Eng., vol. 87, p. 012102, 2015.

[60] G. C. Egan, E. J. Mily, J. -P. Maria and M. R. Zachariah, "Probing the reaction dynamics of thermite nanolaminates," J. Phys. Chem. C. , vol. 119, pp. 20401-20408, 2015.

[61] M. Bahrami, G. Taton, V. Conédéra, L. Salvagnac, C. Tenailleau, P. Alphonse and C. Rossi, "Magnetron sputtered Al-CuO nanolaminates: effect of stoichiometry and layers thickness on energy release and burning rate," Propellants Explos. Pyrotech. , vol. 39, pp. 365-373, 2014.

[62] J. Kwon, J. M. Ducéré, P. Alphonse, M. Bahrami, M. Petrantoni, J. -F. Veyan, C. Tenailleau, A. Estève, C. Rossi and Y. J. Chabal, "Interfacial chemistry in Al/CuO reactive nanomaterials and its role in exothermic reaction," ACS Appl. Mater. Interfaces, vol. 5, pp. 605-613, 2013.

[63] P. Zhu, R. Shen, Y. Ye, X. Zhou and Y. Hu, "Energetic igniters realized by integrating Al/CuO reactive multilayer films with Cr films," J. Appl. Phys., vol. 110, p. 074513, 2011.

[64] N. A. Manesh, S. Basu and R. Kumar, "Experimental flame speed in multi-layered nano-energetic materials," Combust. Flame, vol. 157, pp. 476-480, 2010.

[65] Mid-IR Imaging and Multivariate Analysis of Dynamic Processes in Pharmaceutically Relevant Microparticles - Scientific Figure on ResearchGate. Available from: https://www.researchgate.net/figure/Illustration-of-a-SEM-instrument-showing-the-main-components-adapted-from-23_fig20_328253173 [accessed 14 Sept, 2020]

[66] Yehuda Meir, Eli Jerby,Thermite powder ignition by localized microwaves, Combustion and Flame, Volume 159, Issue 7,2012, Pages 2474-2479, https://doi.org/10.1016/j.combustflame.2012.02.015

[67] Sterner, Mikael & Somjit, Nutapong & Shah, Syed Umer Abbas & Dudorov, Sergey & Chicherin, Dmitry & Raisanen, Antti & Oberhammer, J.. (2011). Microwave MEMS devices designed for process robustness and operational reliability. International Journal of Microwave and Wireless Technologies. 3. 547 - 563. 10.1017/S1759078711000845.

[68] Sarkar P., De D., Uchikochi T., Besra L. (2012) Electrophoretic Deposition (EPD): Fundamentals and Novel Applications in Fabrication of Advanced Ceramic Microstructures. In: Dickerson J., Boccaccini A. (eds) Electrophoretic Deposition of Nanomaterials. Nanostructure Science and Technology. Springer, New York, NY.

[69] Thermo Fisher Scientific Inc., "Copper," Thermo Scientific , 2018. [Online]. Available: https://xpssimplified.com/elements/copper.php. [Accessed 17 December 2019].

[70] Singh, A., Jayaram, J., Madou, M., Akbar, S. (2002). Pyrolysis of Negative Photoresists to Fabricate Carbon Structures for Microelectromechanical Systems and Electrochemical Applications. Journal of Electrochemical Society. 149(3). doi: 10.1149/1.1436085

[71] Zhang, D., Choi, W., Yazawa, K., Numata, K., Tateishi, A., Cho, S., Lin, H., Kuen Li, Y., Ito, Y., Sugioka, Y. (2018). Two Birds with One Stone: Spontaneous Size Separation and Growth Inhibition of Femtosecond Laser-Generated Surfactant-Free Metallic Nanoparticles via ex Situ SU-8 Functionalization. ACS Omega *3* (9), 10953-10966 doi: 10.1021/acsomega.8b01250

Appendices

Appendix I - Fabrication Plan

# of samples	Substrate	Number of Layers	Al Layer Thickness (nm)	Cu2O Layer Thicknesses (nm)	Bilayer thickness ratio
1	Glass	2	135	220	0.6
1	Glass	4	65	110	0.6
1	Glass	6	110	75	0.6
1	Quartz	2	135	220	0.6
1	Quartz	4	65	110	0.6
1	Quartz	6	45	75	0.6
1	Su-8 2005 coated Si	2	130	225	0.6
1	Su-8 2005 coated Si	3	85	135	0.6
1	Su-8 2005 coated Si	4a	65	110	0.6
1	Su-8 2005 coated Si	4b	45	54	0.8
1	Su-8 2005 coated Si	5a	50	85	0.6
1	Su-8 2005 coated Si	5b	45	54	0.8
1	Su-8 2005 coated Si	6a	45	75	0.6
1	Su-8 2005 coated Si	6b	45	54	0.8
1	Su-8 2005 coated Si	7	37	61	0.6
1	Su-8 2005 coated Si	8	35	65	0.5
1	Su-8 2005 coated Si	9	30	48	0.6
1	Su-8 2005 coated Si	10	25	35	0.7

Appendix II - DSC/TGA Results

All testing was performed in Argon with a heating rate of 20 K/min, Ar gas flow of 20 mL/min. For specific sample specifications, refer to Appendix I. Error bars were generated using the standard deviation of three results for each sample.

Substrate-Free 2 Layer

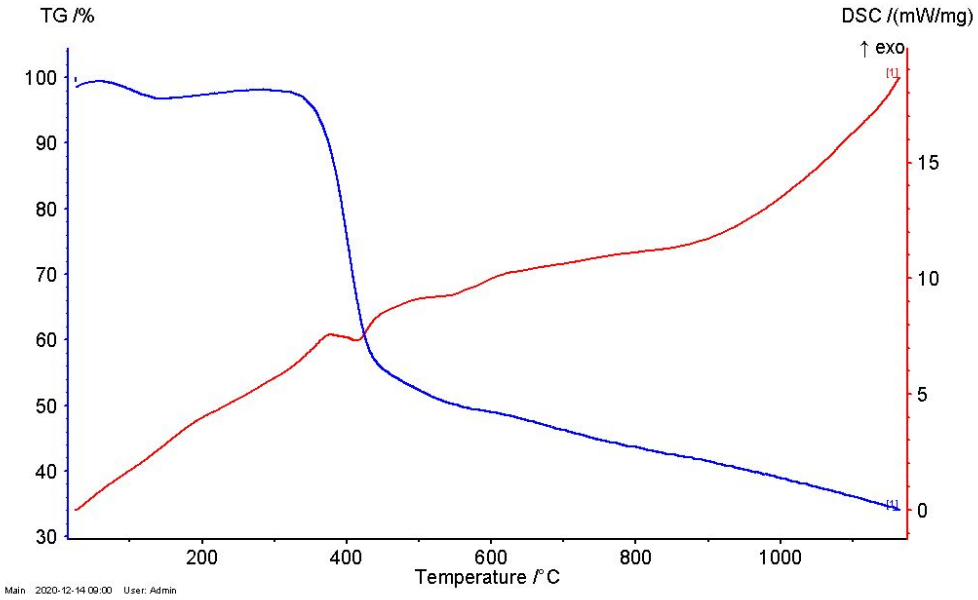

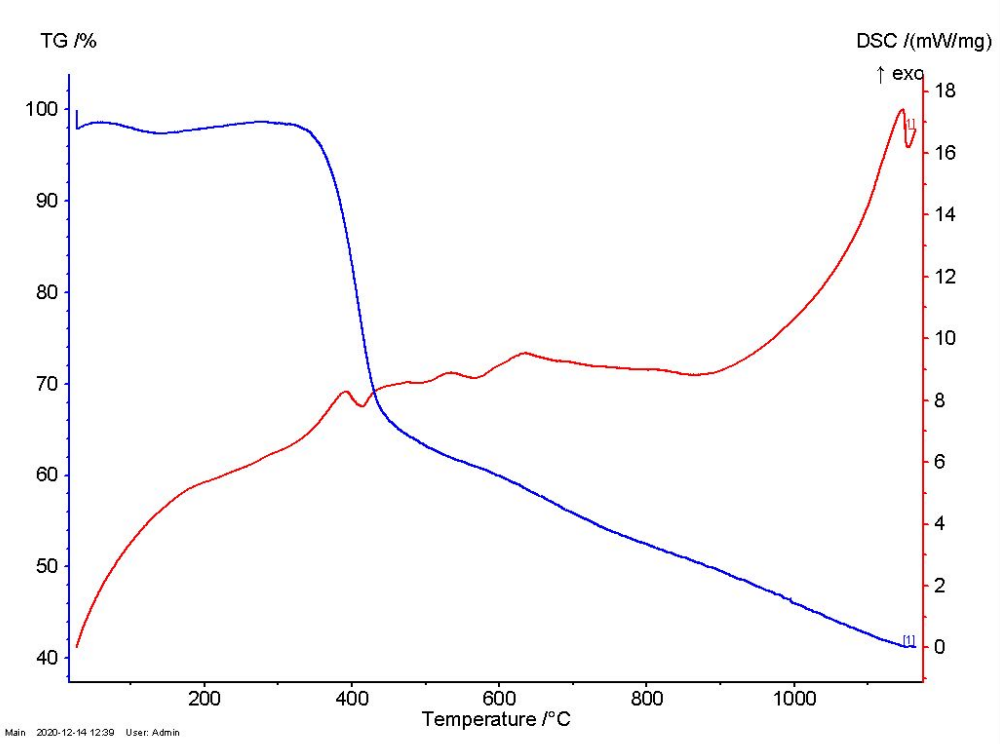
TG /%
DSC /(mW/mg)
↑ exo
100
90
80
70
60
50
40
18
16
14
12
10
8
6
4
2
0
200
400
600
800
1000
Temperature /°C
Main 2020-12-14 12:39 User: Admin

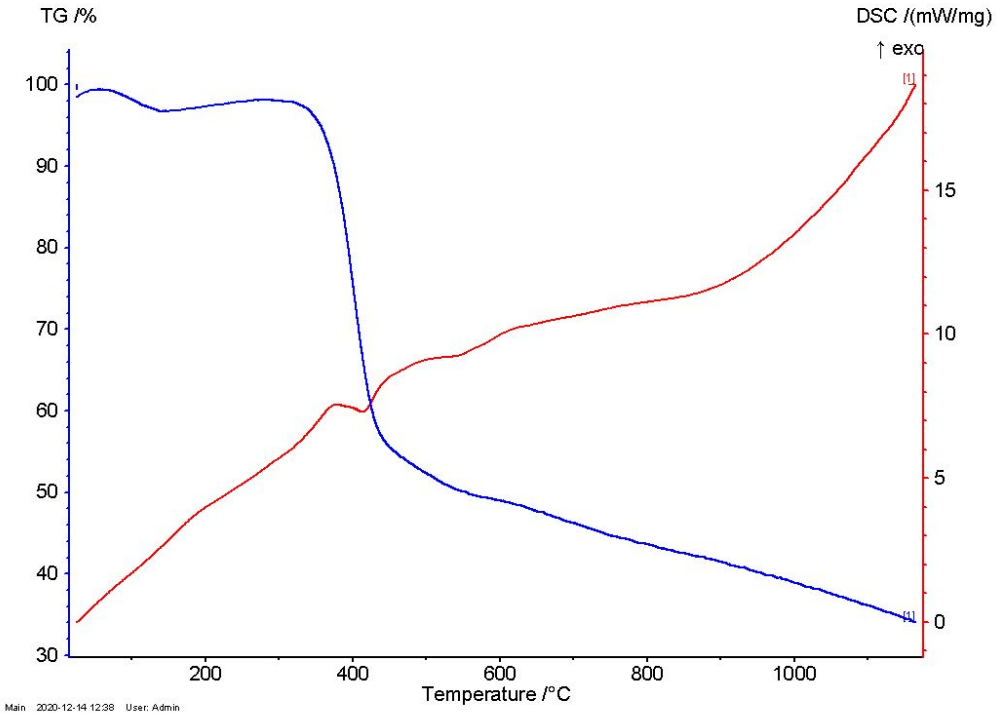
TG /%
DSC /(mW/mg)
↑ exo
100
90
80
70
60
50
40
30
15
10
5
0
200
400
600
800
1000
Temperature /°C
Main 2020-12-14 12:38 User: Admin

Substrate-Free 3 Layer

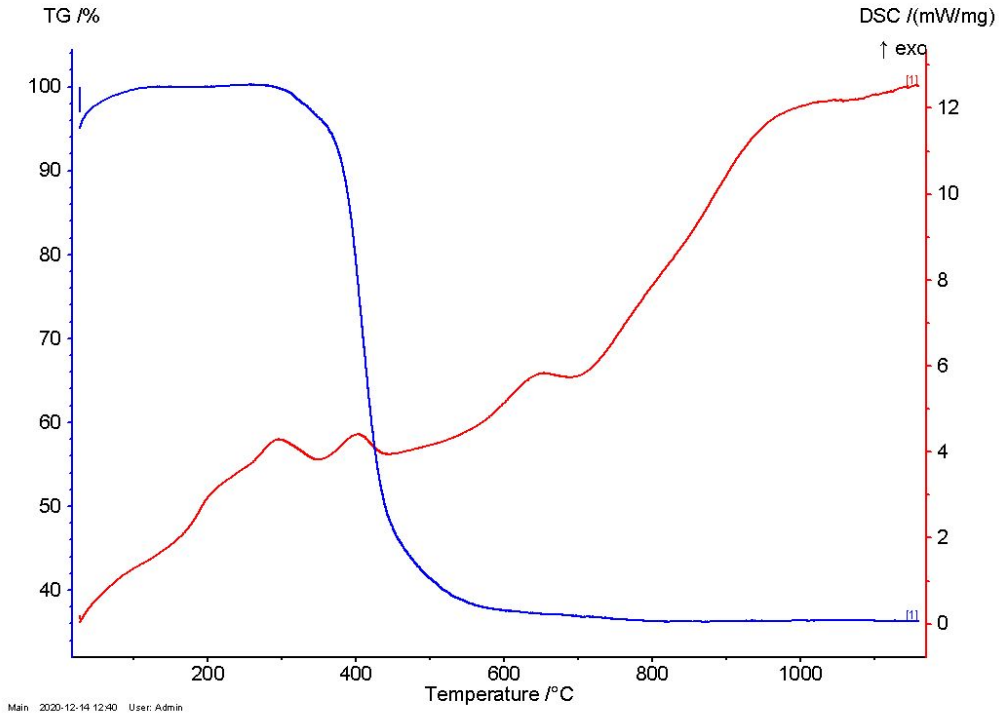

Substrate-Free 4a Layer

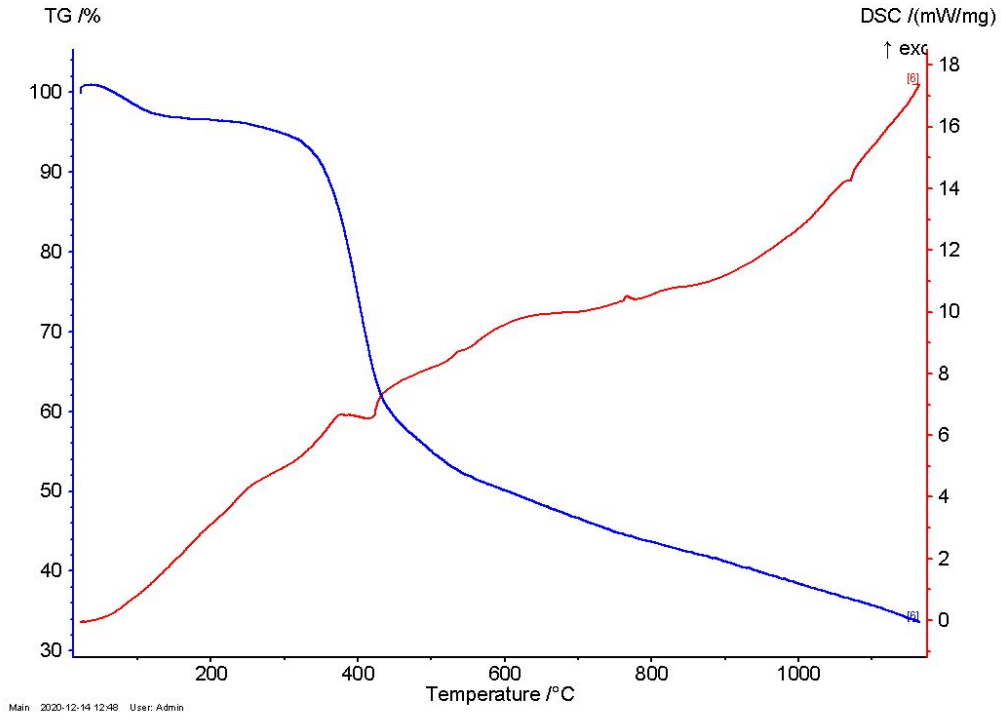

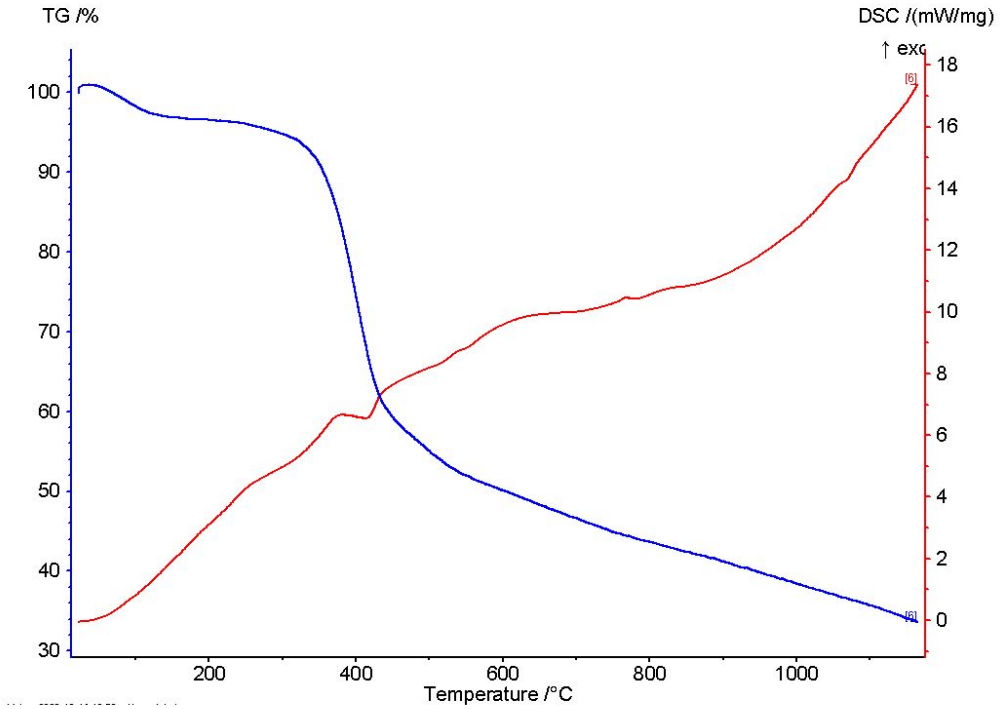
TG /%
DSC /(mW/mg)
↑ exo
100
90
80
70
60
50
40
30
18
16
14
12
10
8
6
4
2
0
200
400
600
800
1000
Temperature /°C

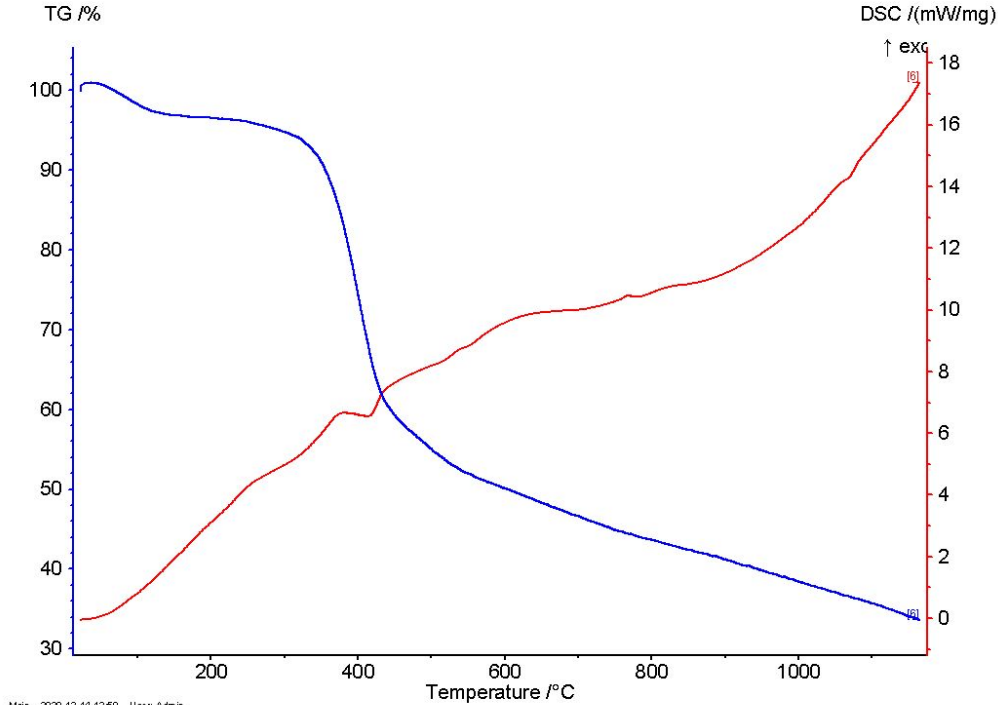
TG /%
DSC /(mW/mg)
↑ exo
100
90
80
70
60
50
40
30
18
16
14
12
10
8
6
4
2
0
200
400
600
800
1000
Temperature /°C

Substrate-Free 4b Layer

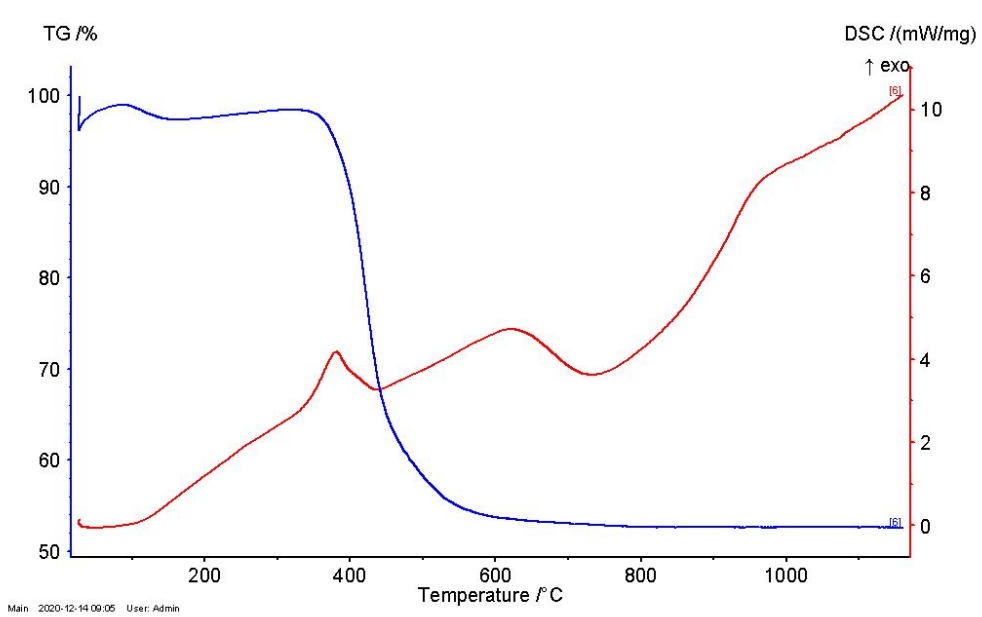

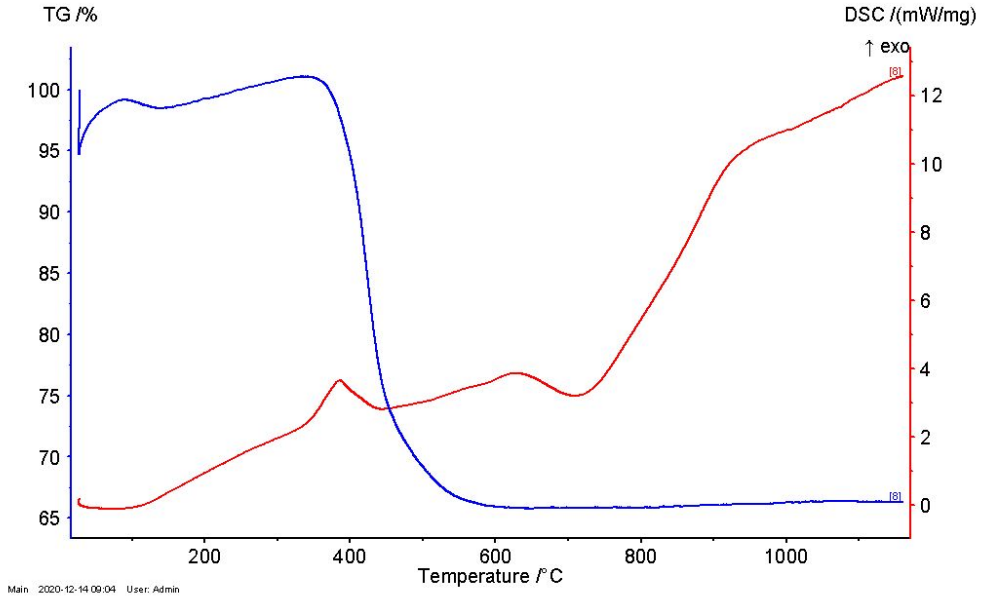

Substrate-Free 5a Layer

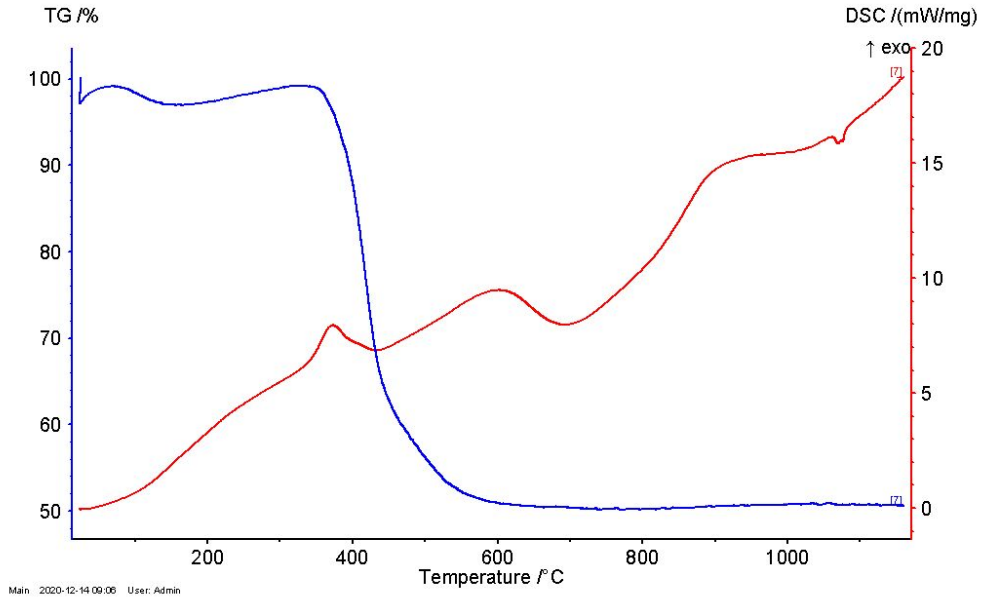

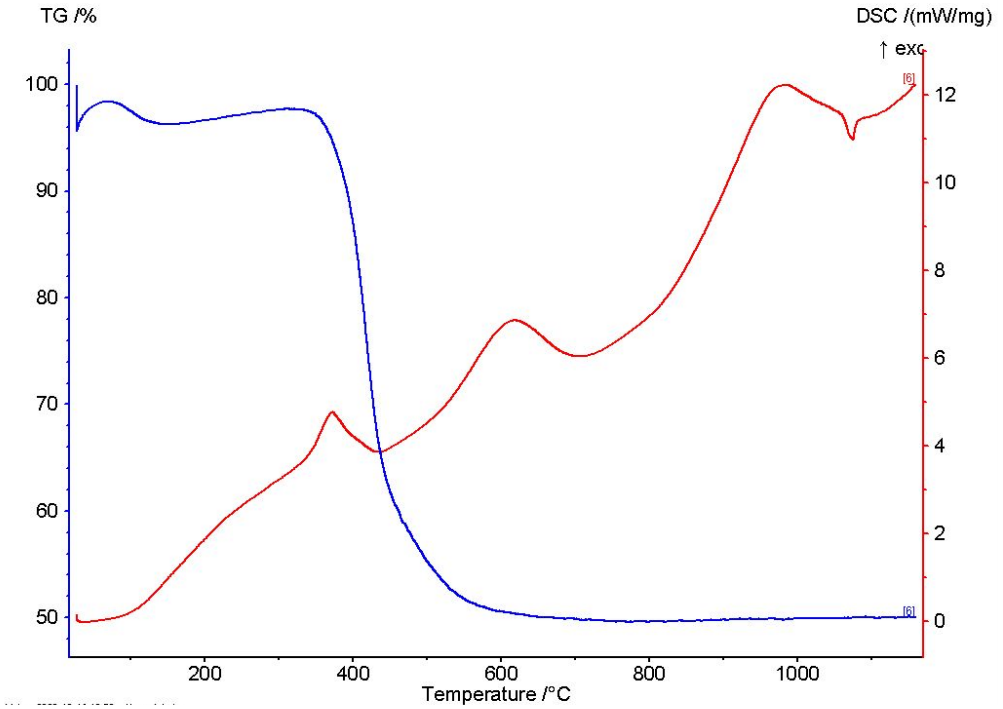
TG /%
DSC /(mW/mg)
↑ exo
100
90
80
70
60
50
12
10
8
6
4
2
0
200
400
600
800
1000
Temperature /°C

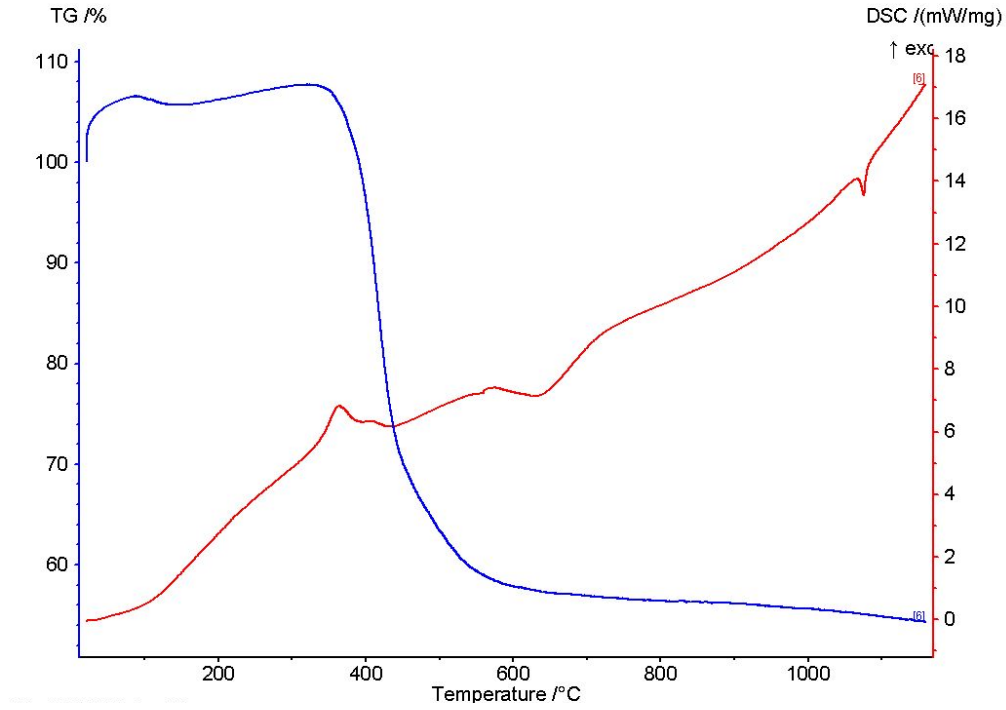
TG /%
DSC /(mW/mg)
↑ exo
110
100
90
80
70
60
18
16
14
12
10
8
6
4
2
0
200
400
600
800
1000
Temperature /°C

Substrate-Free 5b Layer

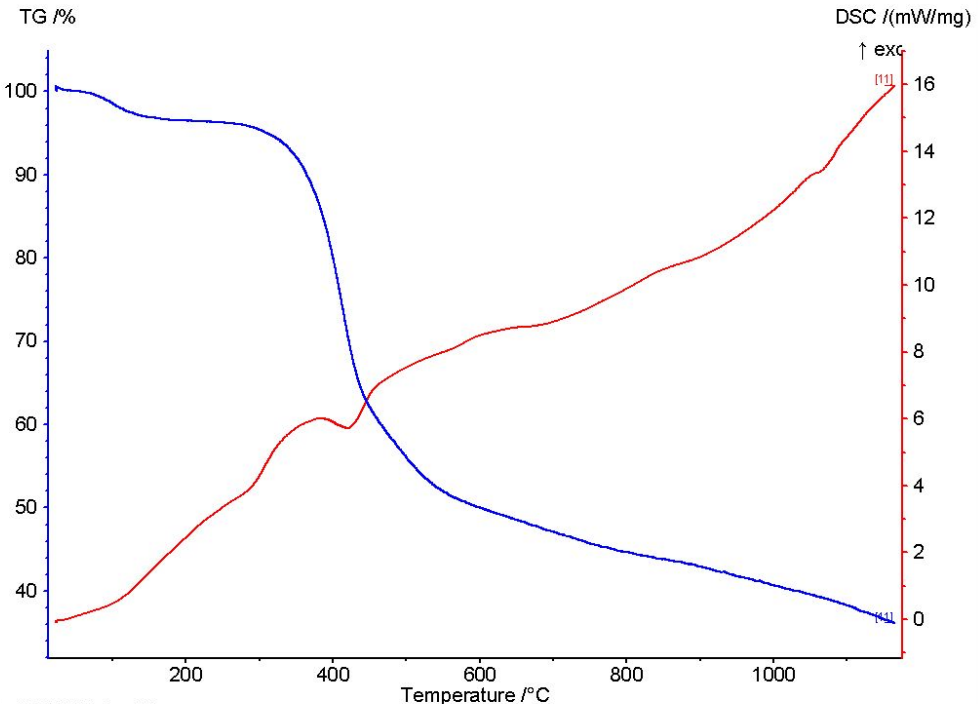

Substrate-Free 6a Layer

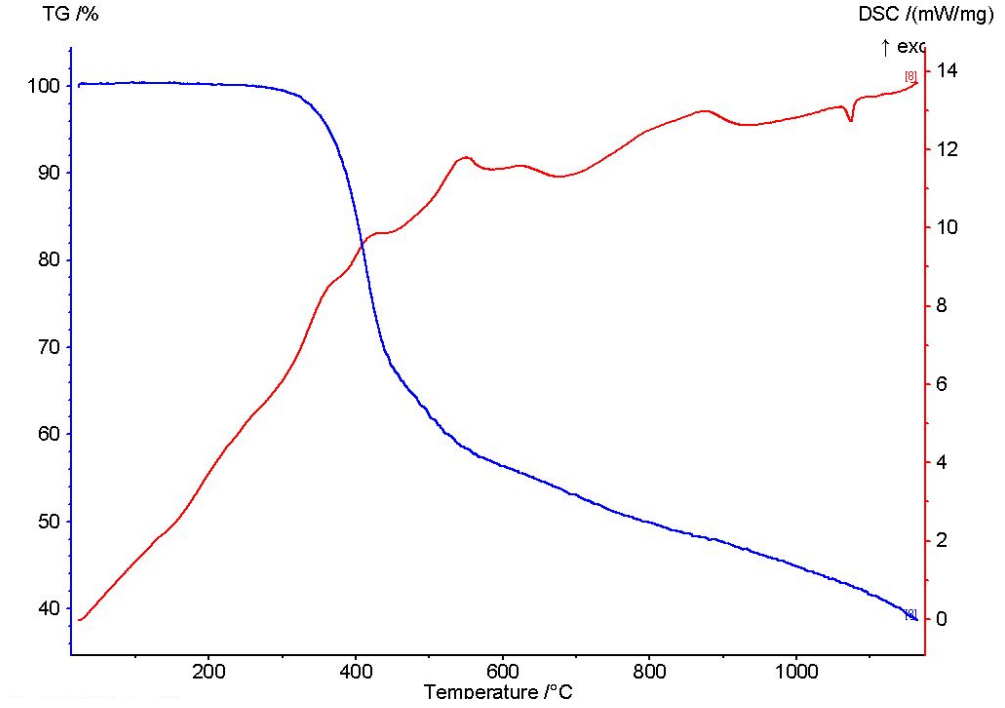

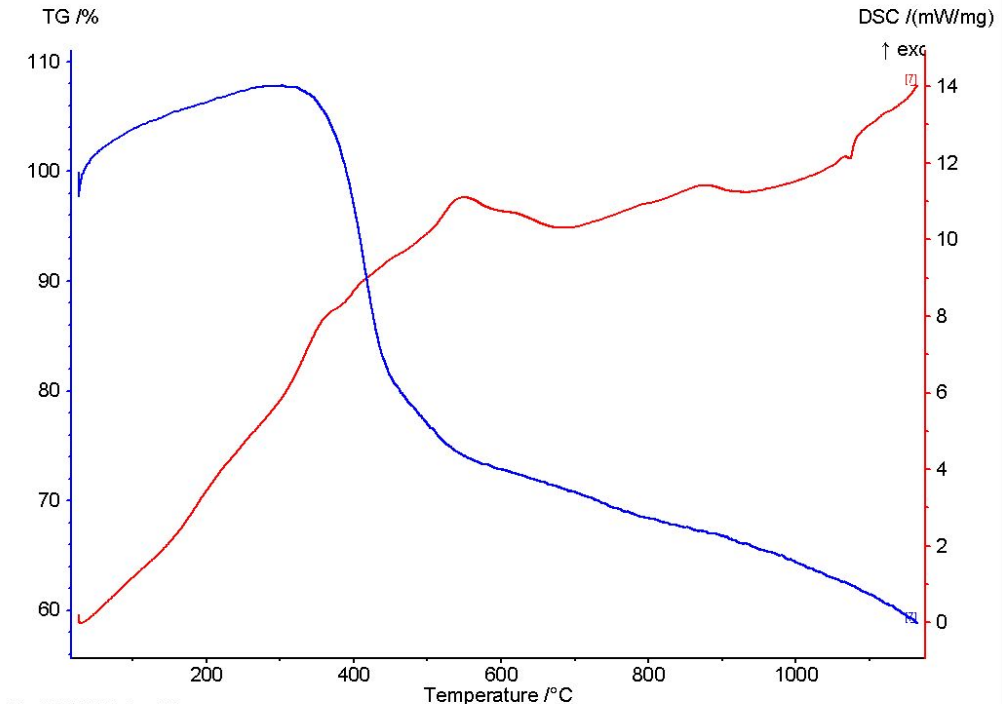

Substrate-Free 6b Layer

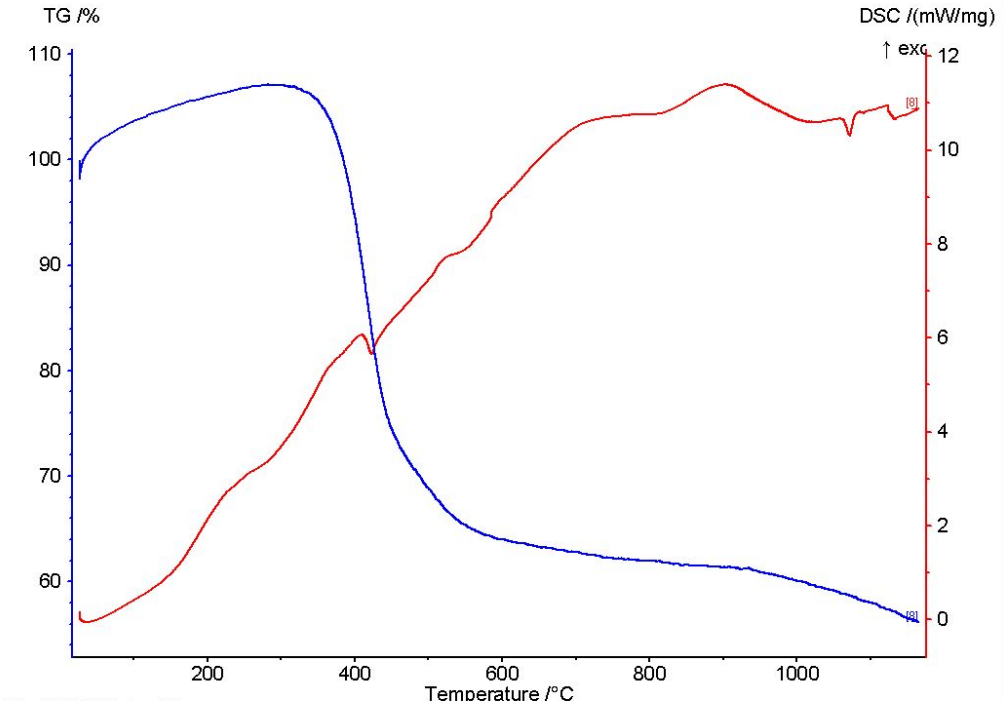
TG /%
DSC /(mW/mg)
↑ exo
110
100
90
80
70
60
12
10
8
6
4
2
0
200
400
600
800
1000
Temperature /°C

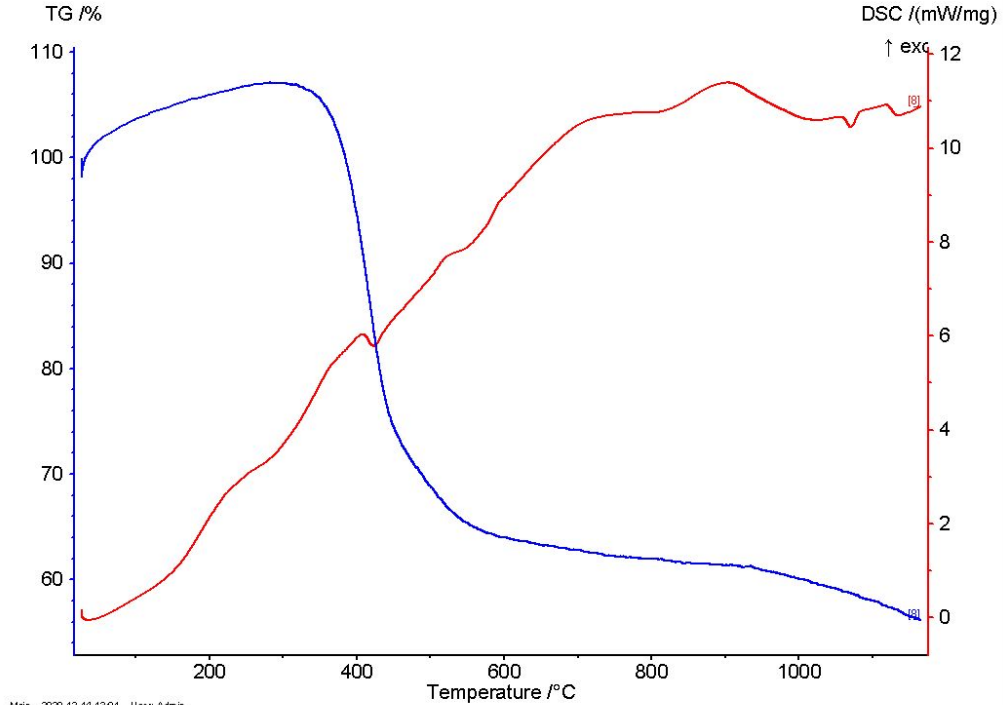
TG /%
DSC /(mW/mg)
↑ exo
110
100
90
80
70
60
12
10
8
6
4
2
0
200
400
600
800
1000
Temperature /°C

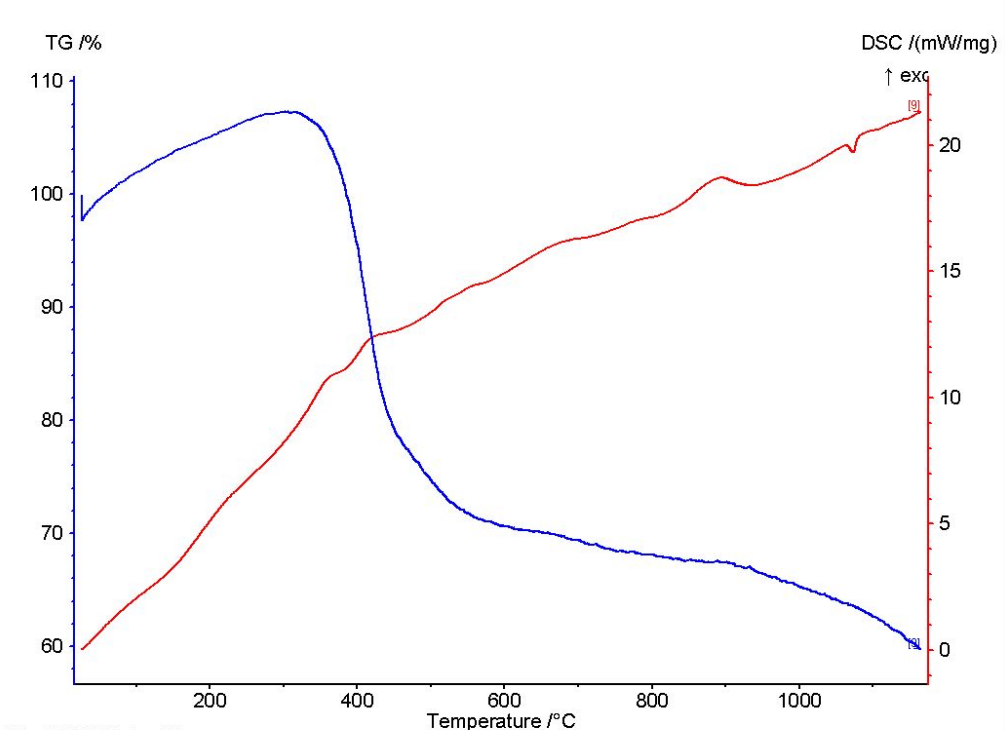

Substrate-Free 7 Layer

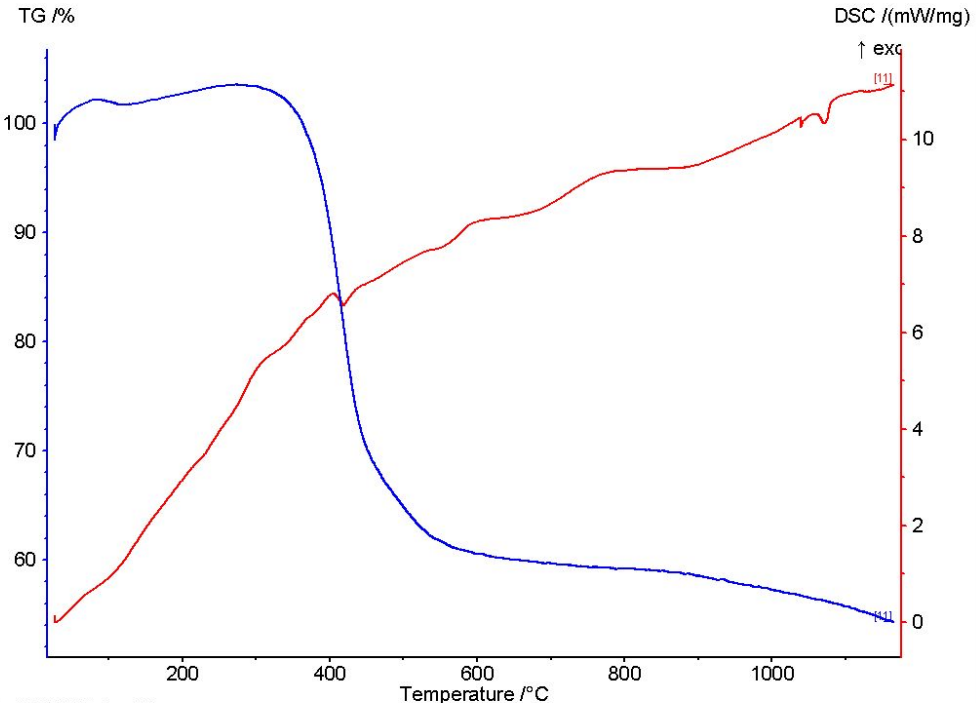
TG /%
DSC /(mW/mg)
↑ exo
[11]
[11]
100
90
80
70
60
10
8
6
4
2
0
200
400
600
800
1000
Temperature /°C

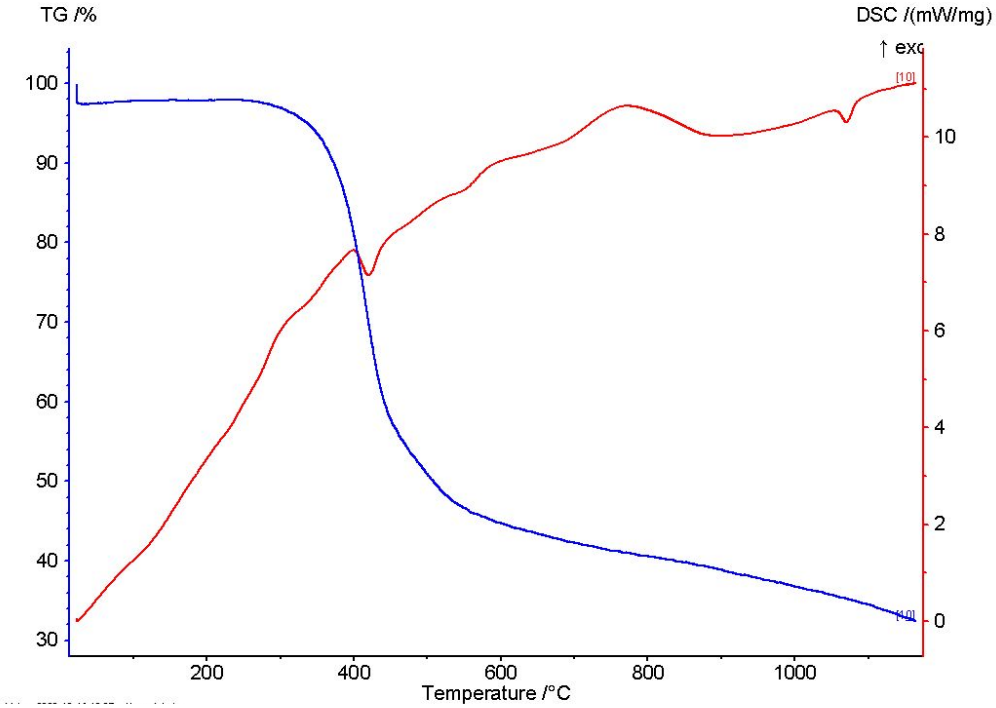
TG /%
DSC /(mW/mg)
↑ exo
[10]
[10]
100
90
80
70
60
50
40
30
10
8
6
4
2
0
200
400
600
800
1000
Temperature /°C

Substrate-Free 8 Layer

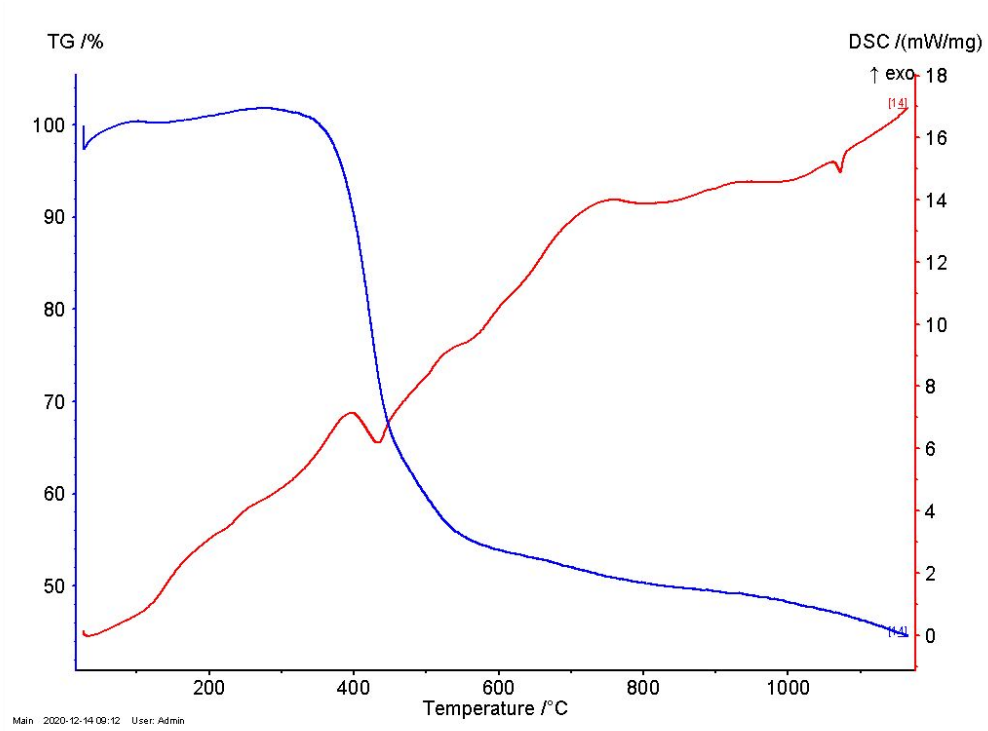

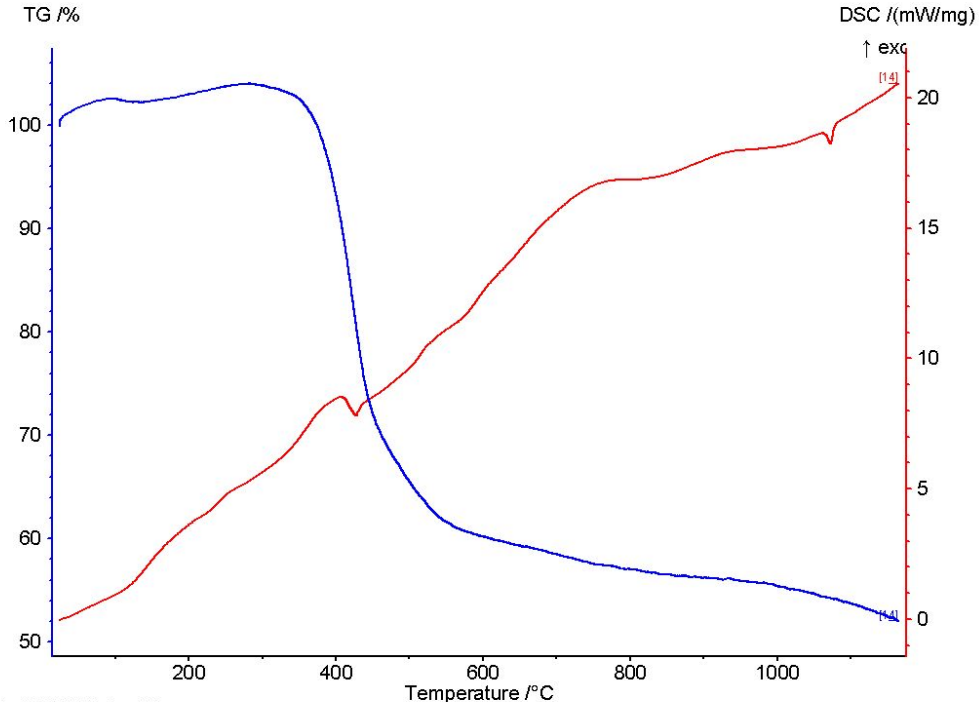

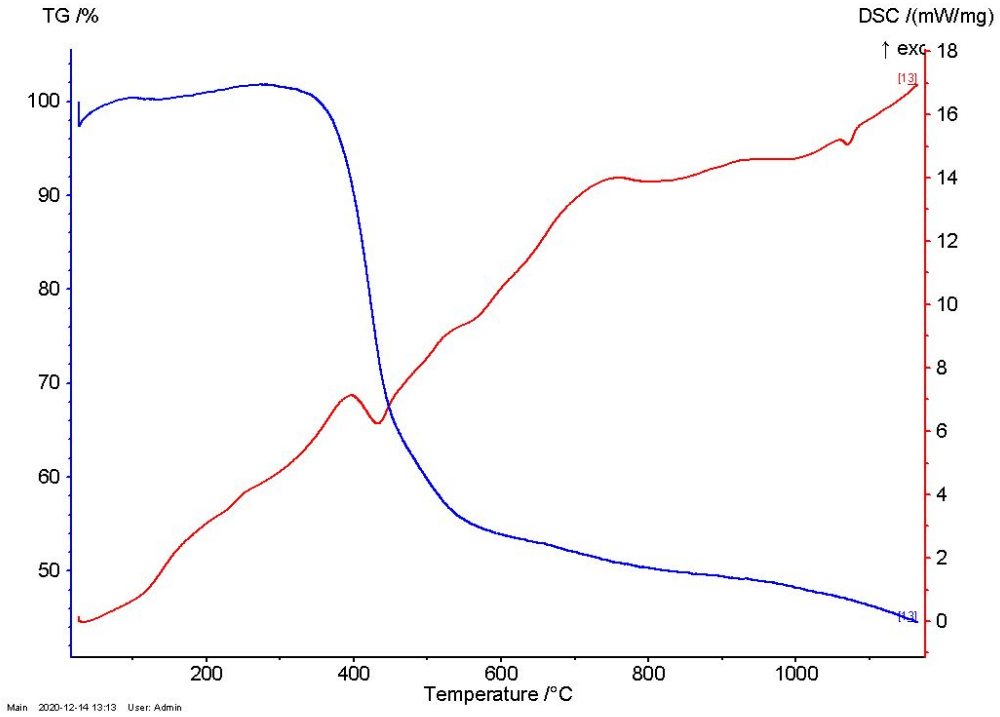

Substrate-Free 9 Layer

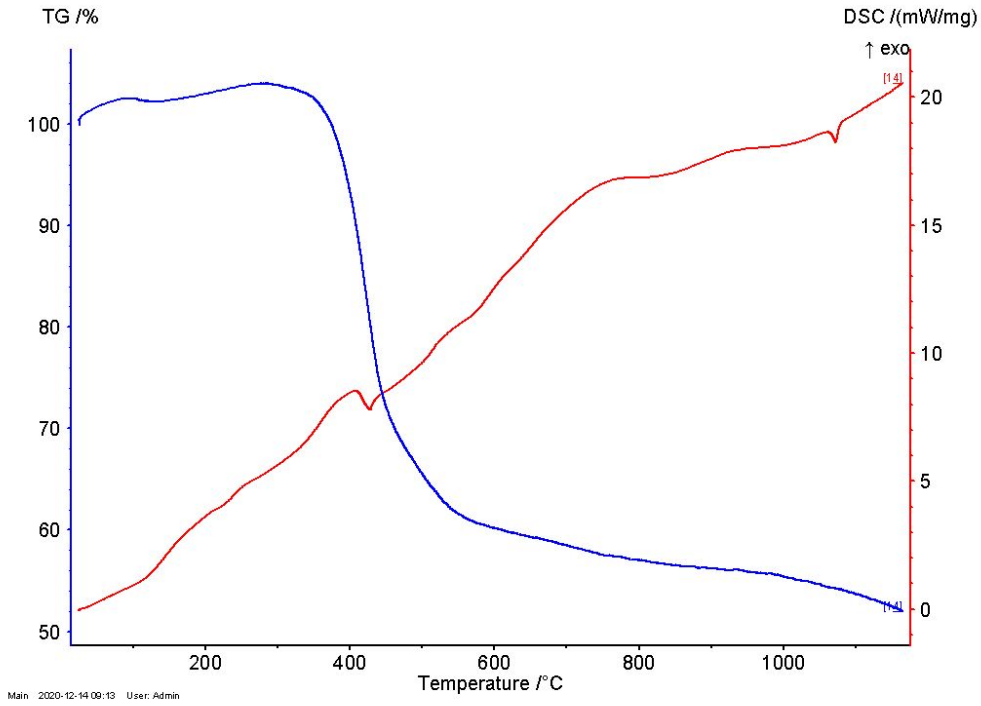

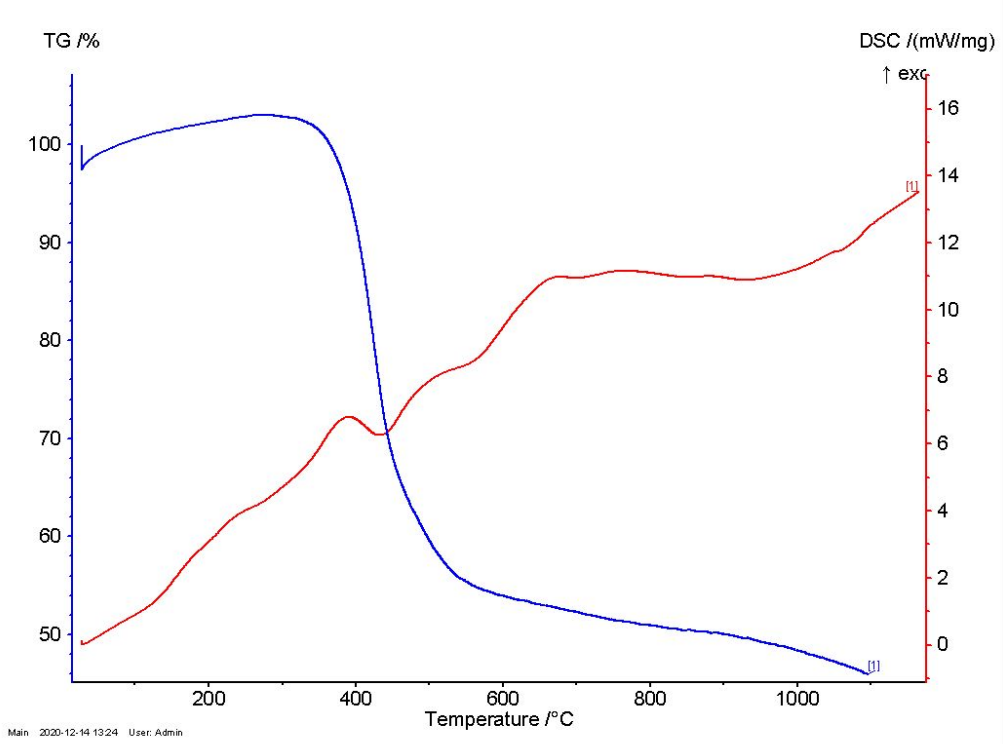
TG /%
DSC /(mW/mg)
↑ exo
100
90
80
70
60
50
16
14
12
10
8
6
4
2
0
200
400
600
800
1000
Temperature /°C
[1]
[1]
Main 2020-12-14 13:24 User: Admin

Substrate-Free 10 Layer

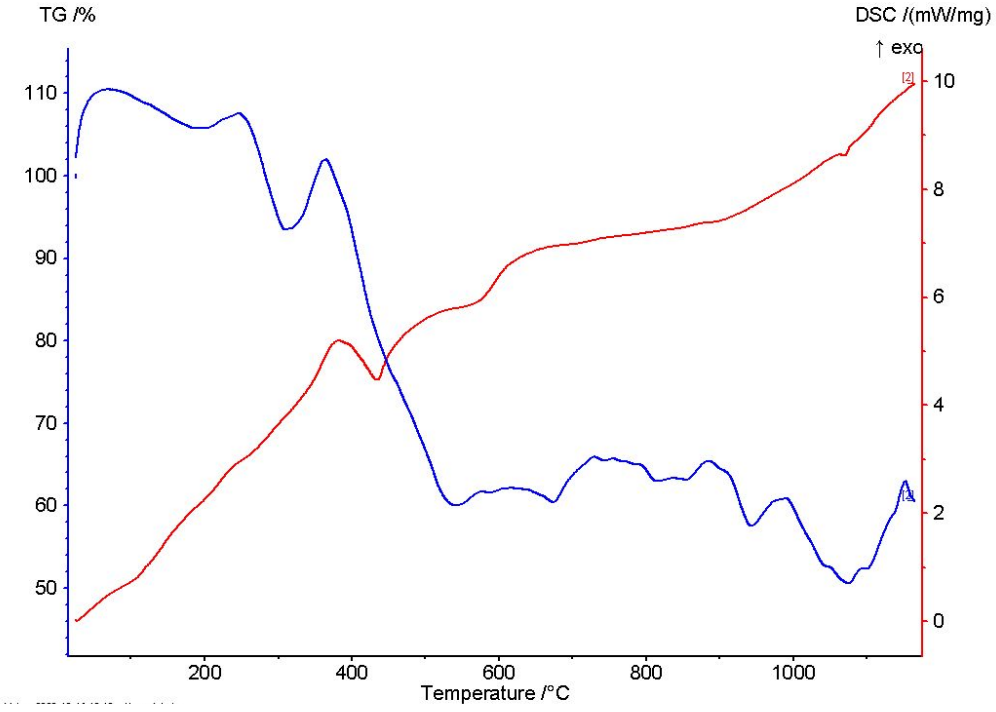

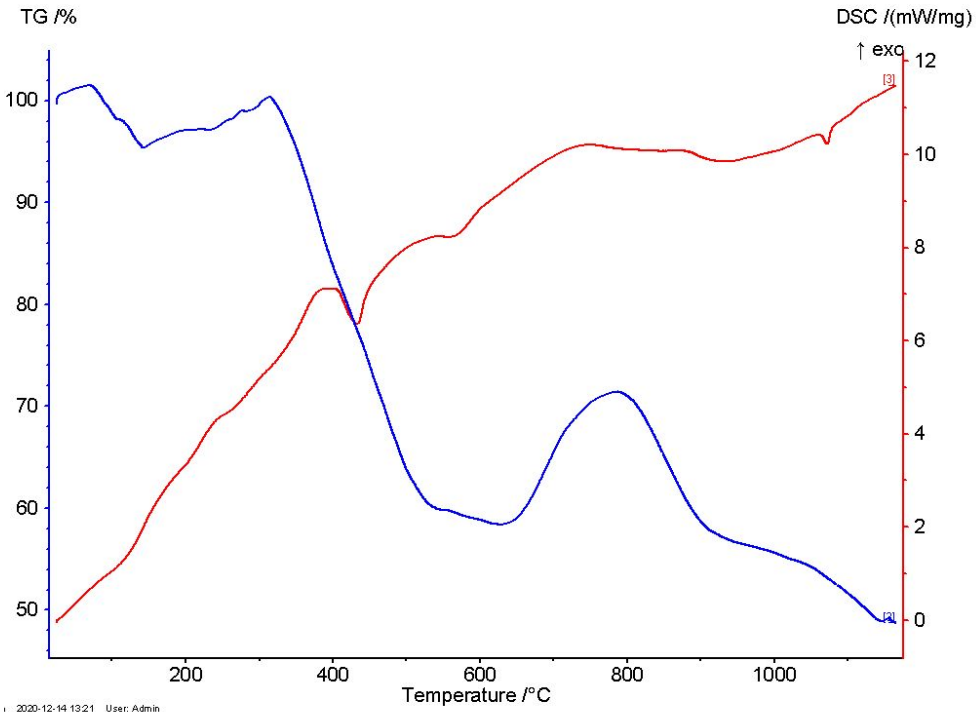
TG /%
DSC /(mW/mg)
↑ exo
100
90
80
70
60
50
12
10
8
6
4
2
0
200
400
600
800
1000
Temperature /°C
2020-12-14 13:21 User: Admin

Data Analysis for Substrate-free Samples

Number of layers	AVG IOT	st dev.	IOT(°C)	AVG EPT	st. dev	EPT(°C)	AVG SE	st. dev	Specific Energy (J/g)
	345.91	10.68	353.50	383.70	7.23	391.30	63.81	4.23	60.82
			338.40			376.90			66.80
2.00			345.82			382.90			63.80
	244.37	2.90	242.40	294.85	0.78	294.30	124.21	0.75	123.68
			246.50			295.40			124.74
3.00			244.20			294.60			124.09
	336.53	9.98	347.50	383.97	2.40	385.30	143.80	16.77	160.10
			334.10			381.20			144.70
4b			328.00			385.40			126.60
	322.03	3.86	319.10	382.07	4.21	385.80	65.14	12.47	52.10
			326.40			377.50			76.94
4a			320.60			382.90			66.37
	295.63	4.46	293.90	373.37	12.48	370.90	175.27	39.78	163.90
			292.30			362.30			142.42
5b			300.70			386.90			219.50
	313.93	6.87	309.10	368.97	4.56	371.50	152.40	34.42	131.00
			321.80			371.70			192.10
5a			310.90			363.70			134.10
	372.00	15.01	389.00	416.80	11.78	410.00	57.56	23.00	84.04
			360.60			410.00			46.06
6a			366.40			430.40			42.58
	336.27	12.56	324.00	412.03	3.95	408.10	80.88	27.27	110.40
			349.10			416.00			56.64
6b			335.70			412.00			75.60
	352.27	13.60	345.70	408.57	10.66	400.00	71.01	23.48	79.04
			343.20			405.20			89.42
7.00			367.90			420.50			44.57
	339.33	0.35	338.90	401.57	6.36	400.30	155.20	11.47	153.30
			339.30			397.70			167.50
8.00			339.80			406.70			144.80
	315.30	3.97	318.60	393.50	3.70	397.60	187.33	9.97	178.60
			310.90			390.40			198.20
9.00			316.40			392.50			185.20
	308.43	1.53	309.60	385.00	3.63	385.90	194.53	22.60	217.20
			309.00			381.00			172.00
10.00			306.70			388.10			194.40

Glass Substrate 2 Layer

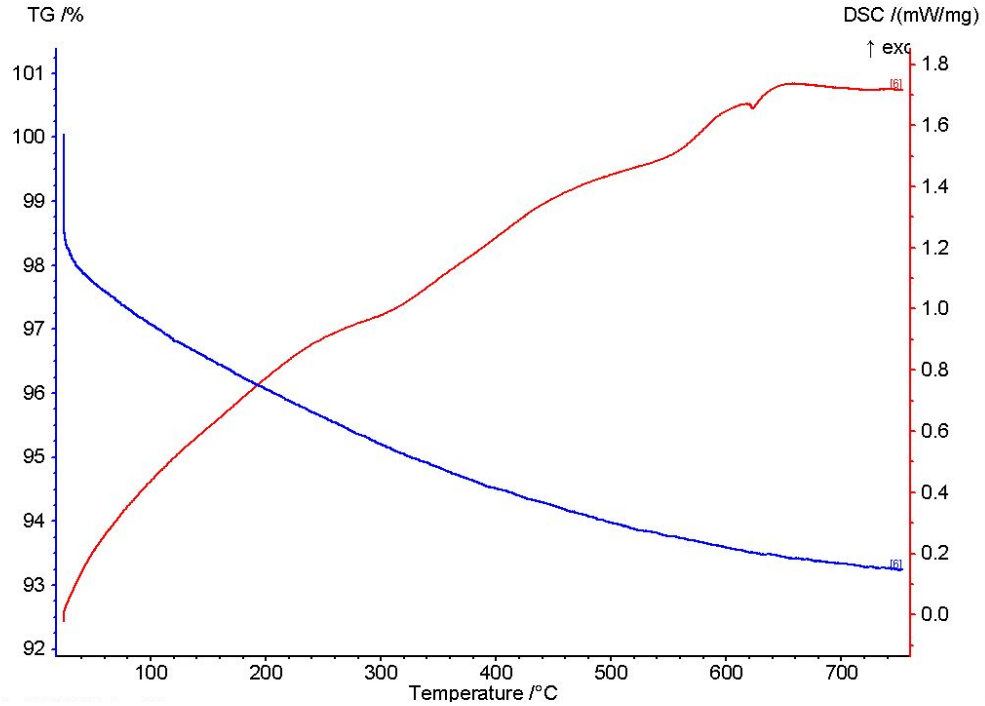

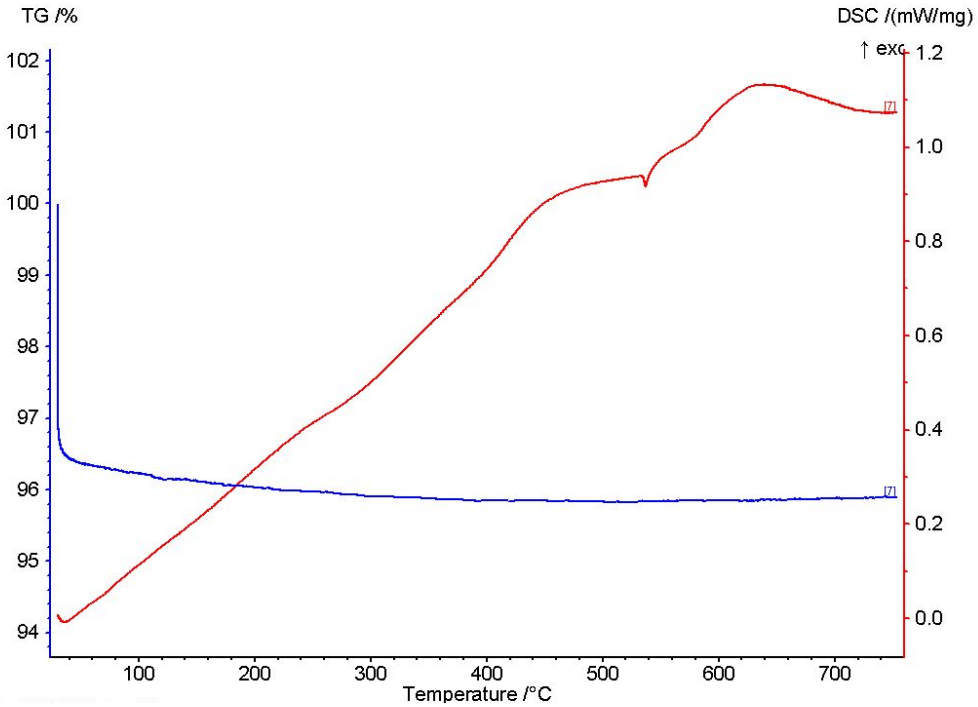

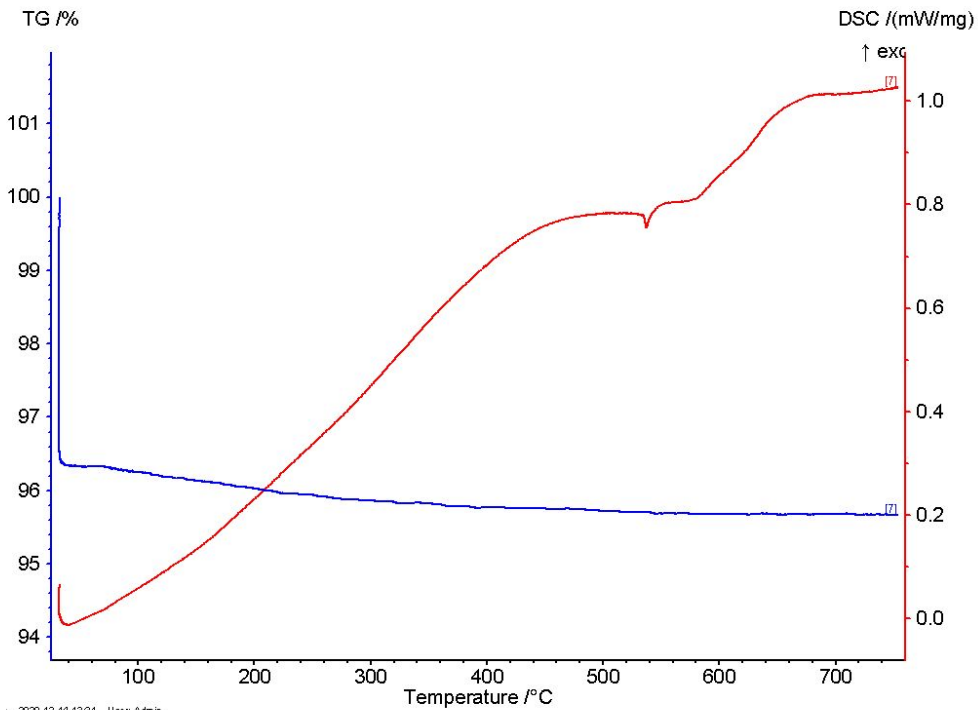

Glass Substrate 4 Layer

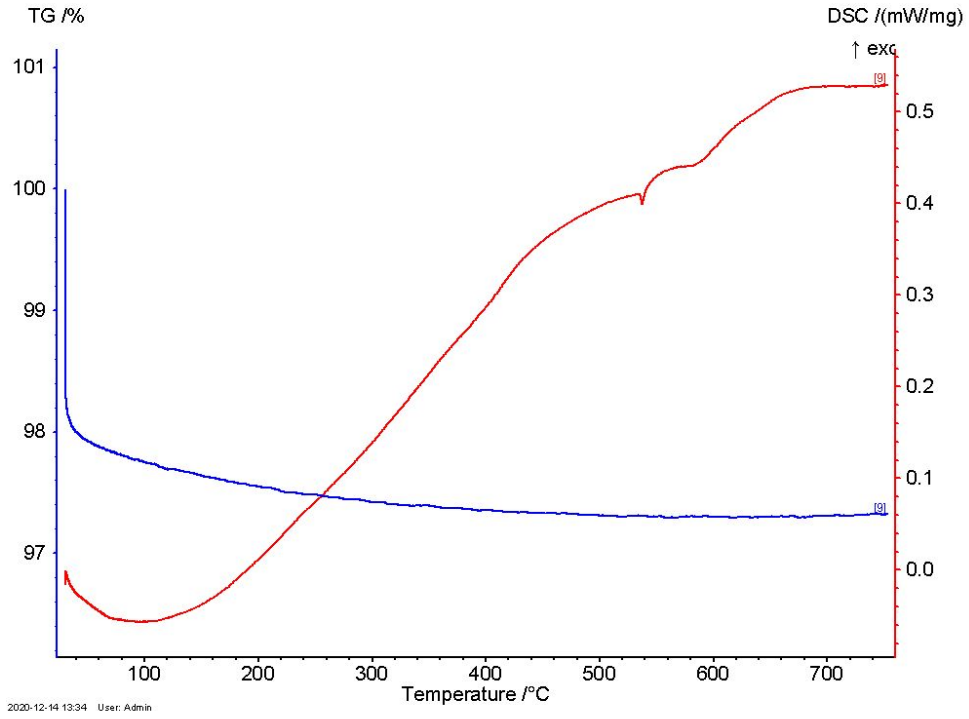

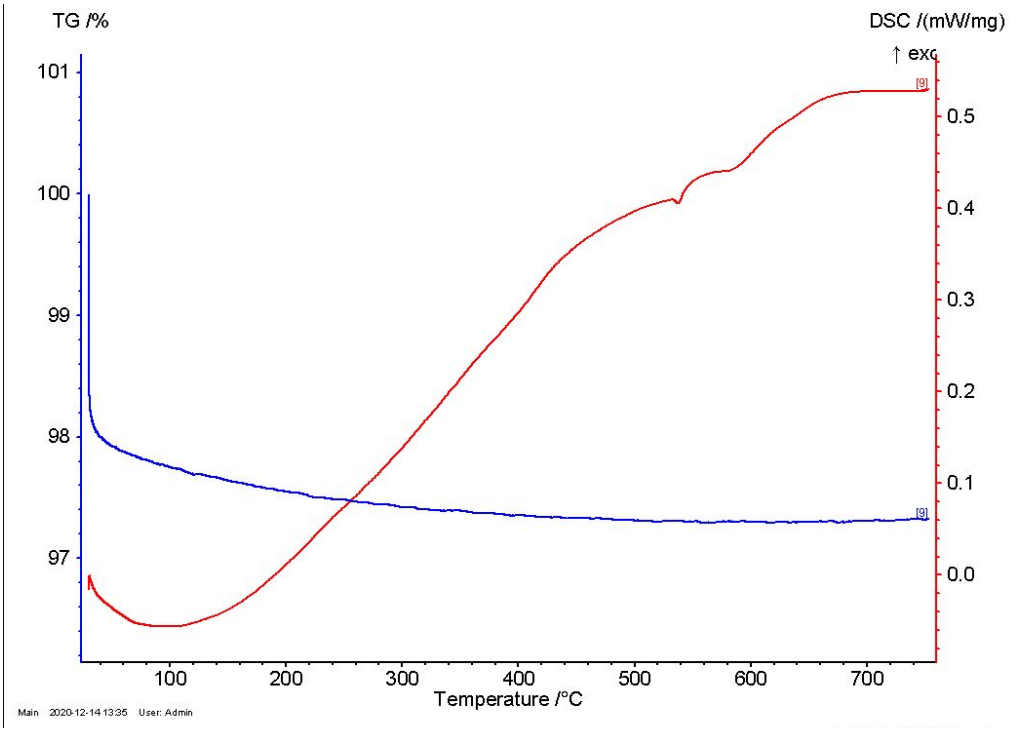
TG /%
DSC /(mW/mg)
↑ exo
101
100
99
98
97
0.5
0.4
0.3
0.2
0.1
0.0
[9]
[9]
100
200
300
400
500
600
700
Temperature /°C
Main 2020-12-14 13:35 User: Admin

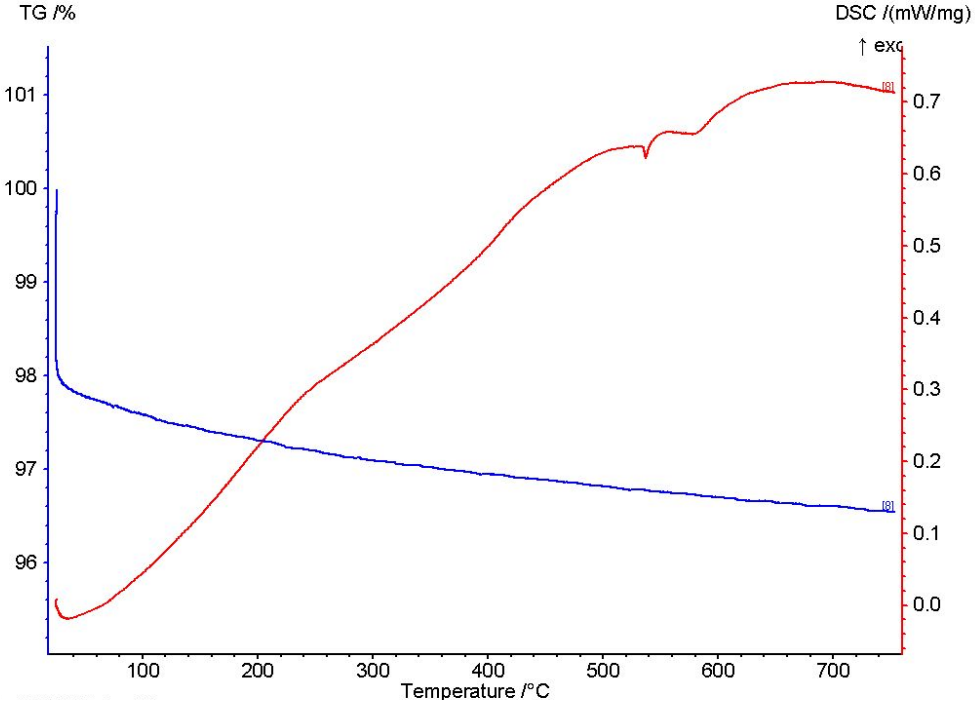
TG /%
DSC /(mW/mg)
↑ exo
101
100
99
98
97
96
0.7
0.6
0.5
0.4
0.3
0.2
0.1
0.0
[8]
[8]
100
200
300
400
500
600
700
Temperature /°C

Glass Substrate 6 Layer

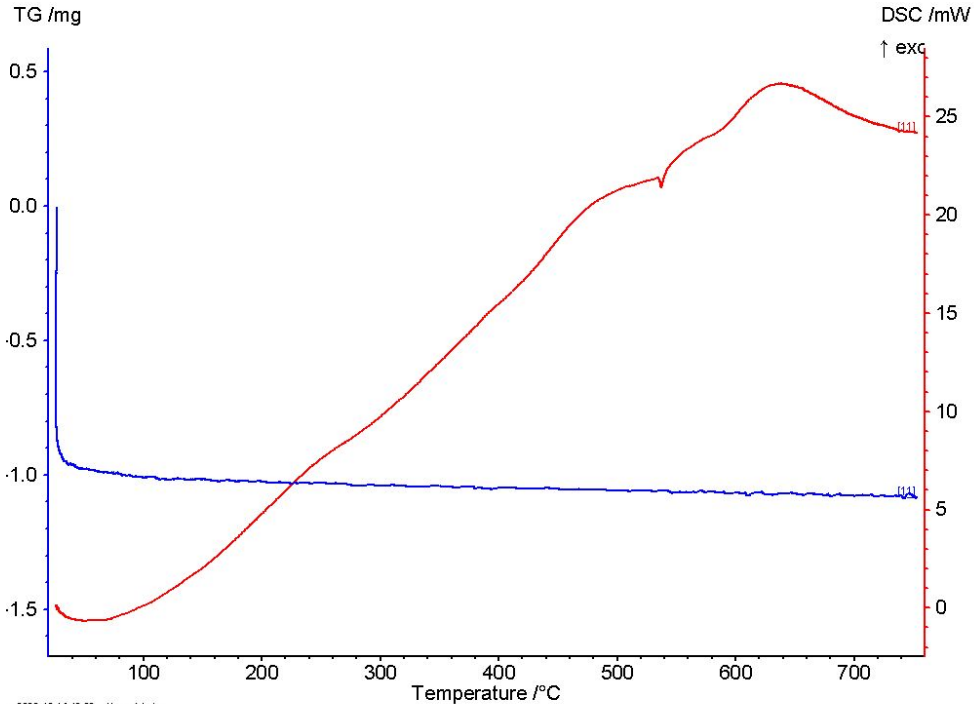

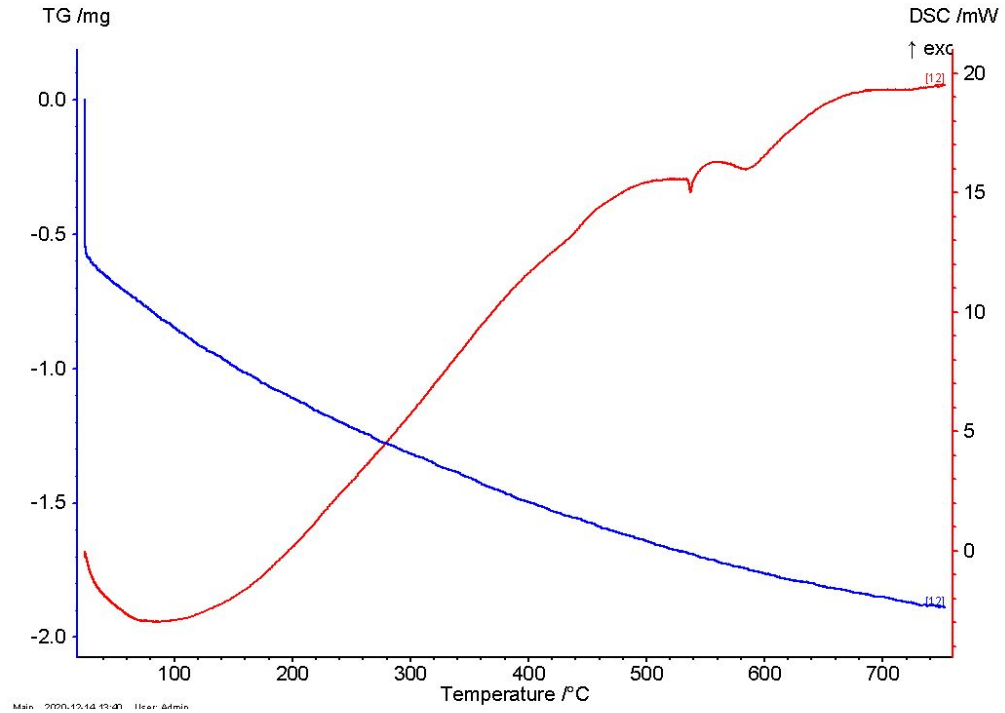

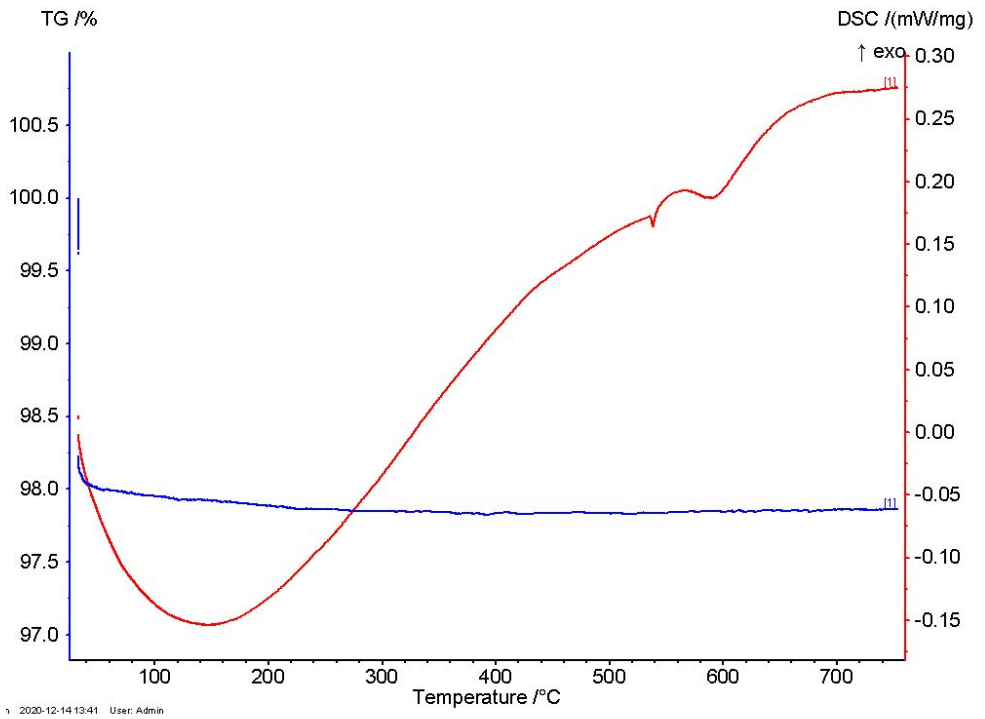

Data Analysis for Glass-Substrate Samples

Number of Layers	Avg IOT	st dev	IOT (°C)	Avg EPT	st dev	EPT (°C)	avg energy release	st dev	energy release (J/g)
2.00	544.93	0.78	544.30	573.53	4.26	570.10	1.56	0.07	1.61
			544.70			578.30			1.59
			545.80			572.20			1.49
4.00	545.30	1.35	546.70	562.73	3.68	565.90	1.58	0.09	1.69
			544.00			558.70			1.54
			545.20			563.60			1.52
6.00	536.87	0.31	537.20	554.83	0.61	555.50	1.68	0.07	1.62
			536.80			554.30			1.67
			536.60			554.70			1.76

Appendix III - XPS Reference

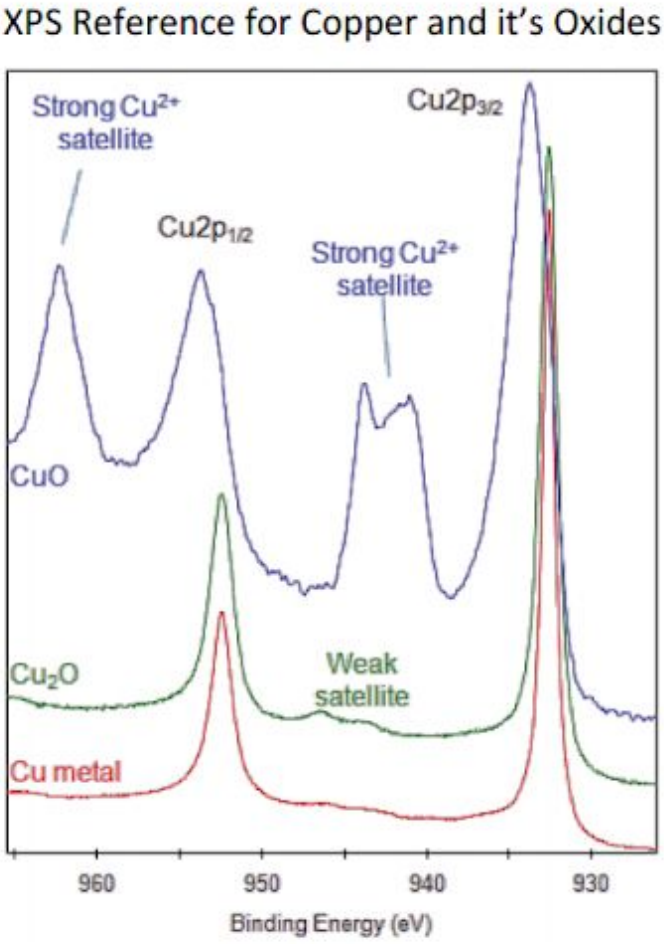

Image from Thermo Fisher Scientific Inc. [69]

Appendix IV - Detailed Procedures

Glass Slide Specifications

Typical chemical composition of soda lime glass microscope slides

Compound	Wt%
SiO2	72.2
Na2O	14.3
CaO	6.4
MgO	4.3
Al2O3	1.2
K2O	1.2
SO3	0.03
Fe2O3	0.03
TiO2	0.01

Typical physical properties of soda lime glass microscope slides

Parameter	Value/unit
Light transmission, total solar	91.5%
Refractive index	1.517 at 546.07nm
Density	2.48 g/cm3
Hardness	6 Mohs scale
Coefficient of expansion	90.6 x 10-7 °C
Poission's ratio	0.2
Strain Point	494°C
Annealing temperature	545°C
Softening temperature	720°C
Melting temperature	1675°C

Applying Photoresist to Substrate

1. Heat substrate to 95C on hot plate
2. Turn on spin-coater and input settings (500 rpm, 30 sec)
3. Remove from hot plate and allow to cool under aluminum foil dome
4. Place clean substrate on the sample holder and turn on vacuum pump
5. Using dispensing tube, apply photoresist (Su-8 2005) to coat the substrate surface
6. Close the lid to the spin coater and run the program set in step two
7. Once the program is complete, remove substrate from spin-coater and place on hot plate (95C) for 5 minutes to cure
8. Remove substrate from hot plate and allow to cool under aluminum foil (10 minutes)

9. Shut down spin coater and clean
10. Once cool, the substrate is ready for use. If not used immediately, store under vacuum

AJA Sample Loading

1. Vent Load Lock chamber (vacuum pump switch down)
2. Remove sample holder and mount substrate
3. Reinstall sample holder (arrow facing forwards)
4. Pump Chamber (turn on vacuum switch)
    - 1500 Hz and 2.0x10^-5 mbar before loading
5. Crank open gate valve
6. Slide in sample
7. Align Propeller shaft with sample holder, raise from 25 to 35, watching to make any position adjustments as needed
8. Rotate shaft to lock into place
9. Lower mount
10. Check rotation
11. Retract transfer arm
12. Close gate valve (hear a click)

AJA Sample Settings

Al: Al Target,

Cu2O: Cu2O Target,

AJA Sample Unloading

1. Open gate valve
2. Extend transfer arm
3. –Raise from 25 to 35
4. Unlock shaft (counter clockwise)
5. Lower from 35 to 25
6. Retract transfer arm and lock gate valve
7. Vent and open load lock chamber
8. Take out sample and reinstall sample holder, close vacuum lock

Removing Sample from Photoresist-Coated Substrate

1. Soak sputtered sample with substrate in acetone, cover and leave for 24 hours
2. Gently spray sample with acetone to remove any stuck on flakes
3. Remove flakes from acetone bath using tweezers, place on filter paper and dry in oven (two minutes)
4. Place flakes in bag and vacuum seal to ensure quality until testing

DSC/TGA System Setup

- Turn on DSC/TGA System and Cooling System
- Ensure Cooling System is activated to 25.00 °C
- Clean crucible in ultrasonic cleaner with ethanol for 5 minutes or until clean
- Dry crucible in oven for 2 minutes
- Weigh dried crucible, record and zero the scale
- Cut sample into small piece and place inside crucible

- Weigh crucible with sample inside, record
- Carefully place lid on the crucible and place on the stage in the DSC/TGA
- Lower lid and open vent to the chamber
- Turn on vacuum and slowly open the vacuum nozzle at the chamber entrance. Continue until vacuum reaches 96%
- Close vacuum nozzle and turn off vacuum system
- Open valve on Argon gas tank, allowing Argon to flow. Slowly open the Argon valve at the chamber entrance. Allow Argon to flow until 'OVERPRESSURE' is shown on the system monitor.
- Repeat vacuum and argon flow steps once more to reduce the possibility of air inside the chamber

DSC/TGA Settings

System: STA 449 F3 Jupiter

Purge 1 Flow: Argon 20 ml/min

Purge 2 Flow: None

Protective Flow: Argon 20 ml/min

DSC Calibration

Temperature and Sensitivity calibrations were performed to ensure the accuracy of measurements taken using the DSC for 10 K/min and 20 K/min heating rates

Measurement

- Al2O3 crucibles used

- Performed heating/cooling cycles on the following substances at heating rates of 10 K/min and 20 K/min
    - Indium (In)
    - Tin (Sn)
    - Bismuth (Bi)
    - Zinc (Zn)
    - Aluminum (Al)
    - Gold (Au)
- Each heating segment involved heating the substance through its melting point to achieve a complete melting peak
- Cooling segments involved cooling the substance to about 100 degrees below the melting point
- A total of three heating segments and two cooling segments were performed for each run
- Purge 1 and Protective gases set at a flow of 20 ml/min

Analysis

- The onset temperature of the melting peak and area above the melting curve were determined for each melting peak observed, these values were then averaged to determine the average onset temperature and area
- A new Temperature/Sensitivity Calibration File was created